Università degli Studi di Ferrara

DOTTORATO DI RICERCA IN
"FARMACOLOGIA ED ONCOLOGIA MOLECOLARE"

CICLO XXVI

COORDINATORE Prof. Antonio Cuneo

Dental implants osseointegration: in vitro, preclinical and clinical research results.

Settore Scientifico Disciplinare MED/04

Dottorando
Dott. Sivolella Stefano

Tutore
Dott. Rimessi Alessandro

Anni 2014/2015

TABLE OF CONTENTS

ABSTRACT

Osseointegration is described as the close contact between bone and an implant surface, and the interest on surface engineering has to be understood as an important and natural trend. The biological fixation between the dental implant surfaces and jaw bones should be considered a prerequisite for the long-term success of implant-supported prostheses. In this context, the implant surface modifications gained an important and decisive place in implant research over the last years. The bone response, which means rate, quantity and quality, are related to implant surface properties. For example, the composition and charges are critical for protein adsorption and cell attachment. Hydrophilic surfaces seem to favor the interactions with biological fluids and cells when compared to the hydrophobic ones, and hydrophilicity is affected by the surface chemical composition. Various techniques of surface treatments have been studied and applied to improve biological surface properties, which favors the mechanism of osseointegration. This strategy aims at promoting the mechanism of osseointegration with faster and stronger bone formation, to confer better stability during the healing process, thus allowing earlier loading of the implant. Some of the objectives for the development of implant surface modifications are to improve the clinical performance in anatomical sites characterized by poor quantity or quality of bone, to accelerate the bone healing and thereby allowing immediate or early loading protocols and also stimulating bone growth in order to permit implant placement in sites that lack sufficient residual alveolar ridge, thus providing them a jumping gap ability, for example. Implant morphology influences bone metabolism: rougher surfaces stimulate differentiation, growth and attachment of bone cells, and increase mineralization; furthermore, the degree of roughness is important. Implants may have "smooth" (machined) or rough surfaces. The main methods that are reported in the literature to create implant roughness are acid etching, sandblasting, titanium plasma spraying and hydroxyapatite (HA) coating. A current tendency is the manufacturing of implants with micro and submicro (nano) topography. Furthermore, the bio-functionalization of implants surfaces, by adding different substances to improve its biological characteristics, has also been recently investigated.

In this contex, aim of the present project has been focused on dental implant

surface modifications in order to improve the clinical performance in areas with poor quantity or quality of bone.

In detail this aim has been reached trough 3 steps:

1. in vitro studies:

a) in vitro studies of osteoproperties of glass and titanium surfaces grafted with fibronectin sequence motif for integrin binding (Arg-Gly-Asp, RGD)/ human vitronectin protein (HVP)

b) development of an in vitro model to evaluate the degree of implants osteointegration by passing in vivo test.

2. in vivo studies, in big animal model, dogs, of osteointegrative properties of implants with different degree of surface modification.

3. clinical research on short implants, to underline the effect of surface modifications on dental implant survival in the long term in the clinic.

As final results of these studies, we can conclude that there are a huge number of types of implant surfaces in the market, from different implant manufacturers, all of them claiming to have better clinical results. It is important that the clinician choose the surface that have shown the best results in the scientific literature.

The majority of currently available in vitro and in vivo studies seem to indicate that implant surfaces with micro and submicro (nano) topography bring forward benefits to the process of interaction between bone cells and implant surfaces, accelerating and increasing the quality of bone-to-implant-contact (BIC).

Finally, based on the state of the art of implant development, it is possible to predict that, within some time, implant surfaces coated with substances with biomimetic capacity will be available for clinical use. This process of implant bio-functionalization aims at modulating new bone formation around implants, and it represents the next step in implant development.

1. INTRODUCTION

1.1 Dental Implant Osseointegration

A dental implant (also known as an endosseous implant or fixture) is a surgical device that interfaces with the alveolar bone of the jaws (or skull) to support a dental prosthesis such as a crown, bridge, denture, facial prosthesis, or to act as an orthodontic anchor (Fig. 1). The basis for modern dental implants is a biologic process called osseointegration where materials, such as titanium, form an intimate bond to bone. Osseointegration derives from the Greek osteon, bone, and the Latin integrare, to make whole. The term refers to the direct structural and functional connection between living bone and the surface of a load-bearing artificial implant. Osseointegration is also defined as: "the formation of a direct interface between an implant and bone, without intervening soft tissue" (1, 2).
The osseointegration rate of titanium dental implants is related to their composition and surface roughness (fig. 2 and 3). Rough-surfaced implants favor both bone anchoring and biomechanical stability. Osteoconductive calcium phosphate coatings promote bone healing and apposition, leading to the rapid biological fixation of implants. Different methods have been used for increasing surface roughness or applying osteoconductive coatings to titanium dental implants. Surface treatments, such as titanium plasma-spraying, grit-blasting, acid-etching, anodization or calcium phosphate coatings, and their corresponding surface morphologies and properties have been studied. Most of these surfaces are commercially available and have proven clinical efficacy (>95% over 5 years) (3). A huge number of the experimental investigations have demonstrated that the bone response was influenced by the implant surface topography (evaluated using S_a value, that is the arithmetic average of the 3D roughness); smooth (S_a<0.5 μm) and minimally rough (S_a 0.5–1 μm) surfaces showed less strong bone responses than rougher surfaces. Moderately rough (S_a>1–2 μm) surfaces showed stronger bone responses than rough (S_a>2 μm) in some studies (4) (figs. 5-12).

Finally, osseointegration is the growth action of bone tissue, as it assimilates surgically implanted devices or prostheses to be used as either replacement parts (e.g., hip) or as anchors (e.g., endosseous dental implants).The direct contact of bone and implant surface can be verified microscopically. Osseointegration has

enhanced the science of medical bone and joint replacement techniques as well as dental implants and improving prosthetics for amputees.

As recently described by Terheyden H et al (2012) (5) the healing of an osseous wound around a dental implant is a coordinated and sequentially organized repair mechanism of the organism (6). The main players in this process are cells. Cells communicate with each other via exchange of molecules which are read by specific receptors on the cell surface. The different cell types appear in a chronological sequence with a certain overlap. This sequence is known as the four phases of wound healing, a concept that originates from the observation of soft tissue healing (7). However, this concept can be transferred to bone healing and, in particular, to intraoral bone healing of an implant wound – haemostasis, the inflammatory phase, the proliferative phase and finally the remodelling phase. In a physiological soft tissue wound, the haemostasis takes minutes to hours, the inflammatory phase hours to days, the proliferative phase days to weeks and the remodelling phase begins at approximately 3 weeks and lasts for years (7).

The temporal sequence of bone healing around dental implants has been investigated histologically in animals (dogs) (8, 9) and in humans (10, 11). In the animal study, the first biopsy showing erythrocytes and inflammatory cells was taken after 2 h at the transition between haemostasis and inflammatory phase. The second biopsy was taken after 4 days and showed new vessels as well as fibroblasts and osteoclasts on the old bone (early proliferative phase). After 1 week, woven bone had appeared (late proliferative phase). After 2 weeks, a load oriented remodelling of the woven bone by osteoclasts was noted in the areas of the tips of the threads (early remodelling phase). After 4 weeks, the remodelling at the tips of the threads was most intense. After 6 weeks, woven bone formation continued and remodelling also took place in the grooves of the implant threads. After 8 and 12 weeks, most woven bone was replaced by lamellar bone. In the human volunteer study, four time points after 1, 2, 4 and 6 weeks were examined. After 1 week in humans, new bone was observed occasionally on the implant surface in humans – comparable to what had been seen in the dog study. After 2 weeks, woven bone formation had increased, but only in the grooves. In contrast to the dog study, no marked osteoclastic activity was observed in humans (proliferative phase). After 4 weeks, bridging between the parent bone and the implant took place in humans. After 6 weeks, first signs of transition to the

remodelling phase were noted, 2 weeks later than in the dog. The direct comparison of the bone-implant contact rates revealed a delay of at least 2 weeks for humans compared with dogs (9). A microarray analysis of the transcriptome of the material of the human volunteer study showed genes associated with inflammation upregulated at day 4, for angiogenesis at day 7 and for skeletogenesis at day 14 (12, 13). Thus, the duration of the phases of bone healing around dental implants in humans approximates the duration of the same phases in physiological soft tissue healing as a biological constant.

For Terheyden H et al (2012) (5) the key players in this process are the different cell types. We observe coordinated action of several cell types and numerous individual cells in the defect. The action of cells is controlled by sequential activation of typical genes, which in turn are activated by soluble cytokines (soluble protein factors), small molecules (e.g. histamine, prostaglandins etc.) or molecules from the extracellular matrix (14). These messenger molecules interact with specific receptors on the surface of the cells. Usually, this causes a change of the conformation of transmembrane receptor proteins which become enzymatically active and start an intracellular second messenger system that amplifies or modifies the information and transports it through the nuclear membrane to the DNA. The cellular response is then initiated by activation of genes and expression of certain proteins, either secretory products or intracellular regulatory proteins.

Adjacent cells can communicate with each other through direct membrane channels. However, over distances, the cells communicate through chemical messenger molecules. The most important classes of messenger molecules are cytokines and hormones. Cytokines are proteins (interleukins, growth and differentiation factors). Hormones are subdivided into peptide hormones (e.g. bradykinin), lipid hormones (e.g. prostaglandins or steroid hormones) and amine hormones (e.g. histamine). Although there is an overlap between the definitions of cytokines and hormones, hormones are usually active in nanomolar concentrations and longer ranges, whereas cytokines can be active in femtomolar concentrations through very specific protein receptors within a more restricted area. In addition, cells receive information through interaction with the extracellular matrix, to which they attach with specific receptors (15). On a very local level, small molecules like nitric oxide or even ions like calcium play a role in signalling.

1.2 Haemostasis

Haemostasis (exudative phase) begins with the surgical trauma exerted by the dental implant drill followed by the insertion of the implant (5). The duration of this phase is minutes to hours. With the bone trauma matrix proteins, growth and differentiation factors which are stored in the bone matrix become soluble and active. Usually stored deep in the bone matrix, the factors are unmasked by the bone trauma and liberated from their heparin binding domains by heparin hydrolases from blood platelets (16). Mechanical crushing of the bone matrix in form of bone debris created by the implant drill may facilitate the liberation of such molecules from the matrix (10). Bleeding from injured blood vessels lays the foundation of the polymerization of fibrinogen to create a first extracellular matrix in the defect. The polymerization of fibrinogen is performed by thrombin and initiated by platelets (extrinsic system) and the intrinsic clotting cascade (Hageman Factor).

Immediately after implantation, the implant surface interacts with water molecules and ions. This can change the charge pattern of the surface, and bivalent ions like calcium can potentially link equally negatively charged partners (a reason for the requirement of calcium ions in blood clotting) (17). Ions are followed by plasma proteins like albumin, globulins or fibrin. The process of protein adsorption is very effective, increasing the concentration of proteins on the surface rapidly by a factor of 1000 compared with the surrounding aqueous solution (18). The first proteins to bind are those that are present at high concentrations in blood such as albumin. These will slowly be replaced by proteins with a lower concentration, but a higher affinity for the surface such as vitronectin or fibronectin. In this process, size and thus mobility of the proteins also play a role (also referred to as Vroman effect) (19). The adsorption of proteins is determined by various factors such as properties of proteins and the solid substrate surface as well as environmental conditions. With respect to the protein properties, the charge, size, stability of the structure, amino acid composition and steric conformation may play a role. Proteins with low internal stability (soft) adsorb mainly based on a gain in conformational entropy as they change their shape. On hydrophobic surfaces, these changes can occur to a great extent and can lead to protein denaturation and loss of protein function, as hydrophobic residues usually hidden in the protein interior are exposed. To a much smaller extent this also applies to very stable (stiff) proteins, but these will only adsorb if there is electrostatic attraction even on

hydrophobic surfaces (20). Overall shape also plays a role, as rod-like proteins with a higher surface to volume ratio will have more interaction sites and thus bind more strongly than globular ones. Thus, hydrophilic titanium surfaces may better preserve the protein conformation and function. Clinically, a faster osseointegration was observed for ultrahydrophilic surfaces compared with standard titanium surfaces (11). On the metal side also, topography and surface energy are important factors. Little is known about spatial distribution of these properties on a nanometre scale. Patterns may bind and select effective proteins more specific than uniform surfaces.

Through protein absorption, cells are able to attach to the titanium surface. The subsequent cell attachment is influenced extensively by this initial coating of the titanium with blood proteins (21). Fibronectin, for example, contains cell binding sites (RGD sequence) that can interact with cellular adhesion proteins (integrins).

At the sites of vascular injury, platelets aggregate and form a white thrombus closing the vascular leak. Bioactive molecules such as thrombin, ADP, collagen, fibrinogen and thrombospondin are generated. Vitronectin bound to the metallic surface can bind platelets. These stimuli activate platelets, converting the major platelet integrin $\alpha_v\beta_3$ from a resting state to an active conformation. Integrin activation refers to the change required to enhance ligand-binding activity. The activated $\alpha_v\beta_3$ interacts with the fibrinogen and links platelets together in an aggregate to form a platelet plug. $\alpha_v\beta_3$ bound to fibrin generates more intracellular signals (outside-in signalling), causing further platelet activation and platelet plug retraction. Platelets also bind to collagen with collagenspecific glycoprotein Ia/IIa receptors. This adhesion is further strengthened by von Willebrand factor, which forms additional links between the platelets glycoprotein Ib/ IX/V and the collagen fibrils. Surface bound fibrin on the metal surface of the implant can bind thrombocytes over the glycoprotein IIb/IIIa receptor to the titanium implant surface. This binding results in activation and degranulation of the thrombocytes. Haemostasis is supported by vasoactive substances from the platelets like serotonin, which results in vasoconstriction. Also, thromboxane from platelets plays a role in the initial vasoconstriction. The release of cytokines from degranulating platelets is the beginning of the inflammatory phase.

1.3 Inflammatory phase

Terheyden H et al (2012) (5) report that the inflammatory phase begins approximately after 10 min and lasts for the first days after surgery. The phase begins with the degranulation of the platelets. The platelets release growth factors like transforming growth factor beta (TGF-b), platelet-derived growth factor (PDGF), Basic fibroblast growth factor (bFGF). Bradykinin from degranulated platelets increases the vascular permeability for fluids, serum proteins and white blood cells. Vasodilative histamine derived from the platelets increases blood flow, decreases the blood stream velocity and induces hyperaemia. The initial vasoconstriction in the haemostatic phase turns into vasodilatation, clinically detectable as swelling and warming of the skin overlying the wound.

In the very early stages of the inflammatory phase, the innate host defence systems are activated (22). The innate immune system is activated by unspecific molecules of bacterial origin, and is not adaptable. It consists of molecular (e.g. complement system) and cellular elements: polymorphonuclear leucocytes (PMN, also called neutrophil granulocytes) and macrophages. The complement system is a group of glycoproteins which form membrane perforating channels (perforins) that damage bacterial cells. Complement C3b binds to bacterial glycoproteins and labels (opsonization) bacteria and other foreign bodies for phagocytosis by the immune cells. The PMN invade the blood clot by amoeboid migration, squeezing through little gaps in the walls of the blood vessels. This process is known as the diapedesis. Diapedesis is initiated by loose adhesion of lectins in the inner lining of blood vessels. These first bindings are reversible. The leucocytes move to the periphery of the blood stream, attach and detach and roll along the inner lining of the blood vessel mediated by adhesion of L-selectin on the leucocyte with E-selectin on the endothelial side. Later, stronger chemical adhesions occur until the cells finally attach. Intercellular adhesion molecule-1 (ICAM-1), ICAM-2 (similar to immune globulins) and the vascular cell adhesion molecule-1 (VCAM-1) catch the granulocyte out of the blood stream, binding to integrins on the leucocyte (22). After adhesion, endothelial cells open a small gap, and the granulocyte migrates in amoeboid fashion through the gap. PMN produce elastase and collagenase which helps them in digesting the basal lamina of the blood vessel and pass beyond the

basal lamina. After the cell has left the blood vessel, its further amoeboid migration is directed by chemotaxis (22).

Chemotactic substances for PMN include: fibrinopeptides from fibrin activation through thrombin, products from fibrinolysis, complement 5a, leucotriene B4 from present PMN, bacterial proteins (N-formyl methionyl peptides), platelet activating factor (PAF), tumour necrosis factor alpha (TNF-alpha), Platelet factor 4 (PF4), PDGF and interleukin8 (IL-8). Some of these factors are produced from PMN or macrophages already present which had antigen contact. If the granulocytes encounter large numbers of bacteria, they recruit more PMN by releasing proinflammatory cytokines (TNF-alpha, IL-8).

Thus, abundance of bacteria prolongs and amplifies the cellular immune response. PMN kill bacteria through reactive radicals (oxygen species and hydroxygroups, chlorine radicals and hypochlorites) which are also toxic for the host cells and the healthy tissue surrounding the wound. Thus, a fulminant neutrophil granulocyte response can induce loss of healthy surrounding tissues (22).

Furthermore, PMN secrete digestive enzymes like collagenase and elastase. These factors can further enhance the tissue damage in the neighbouring tissues. If granulocyte action is prolonged through a high concentration and prolonged presence of bacteria in the wound, a toxic wound environment can develop. In a toxic wound environment, concentrations of proinflammatory cytokines and toxic radicals are high. An elevated activity of the urokinase-type plasminogen activator uPA results in plasmin activity, fibrinolysis and degradation of the extracellular matrix (23). The fibrin network can dissolve. Under these conditions, the concentrations of protective extracellular matrix glycoproteins and proteoglycans such as fibronectin and decorin are low. These proteins normally can bind and protect growth factors from the digesting proteolytic enzymes. A high concentration of these digesting enzymes therefore is typical for a toxic wound environment. If the number or virulence of bacteria further increases, the tissues can be liquified and pus is formed. The early inflammatory phase within the first 3 h is rather decisive for the further fate of the wound. High numbers of bacteria enhance inflammation. Contaminated foreign bodies in the wound, which unlike living tissue have no own defence mechanisms against bacterial colonisation, can increase bacterial counts in the wound. To limit the inflammatory phase, the

cleanest possible surgical work with low bacterial inoculation is likewise important as antibacterial measures including antibiosis and local disinfection. Clean conditions help the organism to move as quickly as possible through the inflammatory phase into the proliferative phase.

PMN are relatively short-lived in acute wounds and are replaced by lymphocytes and macrophages. The roll of lymphocytes is not well defined in the repair process, but they appear to assist by secreting cytokines that are mitogens and chemoattractants for fibroblasts, while simultaneously clearing the wound of old neutrophils (7). If bacteria have to be eliminated, the number of macrophages increases. In presence of bacteria, they secrete proinflammatory cytokines, but they can act as a switch to end the inflammatory phase. After having removed tissue debris, macrophages secrete angiogenic and fibrogenic growth factors. The level of the radical nitric oxide (NO) in the wound formed by inducible nitric oxide synthase (iNOS) by macrophages correlates positively with cyclooxygenase activity and prostaglandin production, which is necessary for subsequent fibroblast activation (24, 25). Under the conditions of a healing wound which was successfully cleaned from bacterial contamination these cells secrete TIMPs (tissue inhibitors of metalloproteinases). These molecules antagonize the digesting enzymes of PMN and therefore protect the extracellular matrix proteins like proteoglycans. These in turn can protect growth factors which are stored in the extracellular matrix (26). The concentration of growth factors is further increased by secretion of growth factors like bFGF and PDGF from macrophages. A high concentration of fibronectin allows attachment of fibroblasts via integrin binding sites. These cells can hereupon crawl into the wound. This is the beginning of the proliferative phase.

1.4 Proliferative phase

The transition into the proliferative phase is characterized by the formation of new extracellular matrix and by angiogenesis (5). This newly formed tissue is called granulation tissue. The duration of this phase ranges from a few days to a few weeks.

Stimulated by FGF from macrophages, fibroblasts from the surrounding healthy tissue migrate by amoeboid movement into the blood clot. These cells drill tunnels through the provisional extracellular matrix of the fibrin clot by secreting matrix

metalloproteinases. The metalloproteinases degrade the blood derived fibrin in the clot und uncover integrin binding sites in the fragments. The fibroblasts attach via integrins to the RGD peptides of fibronectin and crawl from attachment to attachment deeper into the wound (27). To replace the degraded provisional clot matrix, they produce insoluble cellular fibronectin and other insoluble proteins of the extracellular matrix like collagens, vitronectin, decorin and other proteoglycans. The movement of the fibroblasts is directed by the concentration gradient of growth factors produced by the macrophages (PDGF, TGF-b, basic FGF, connective tissue growth factor (CTGF)).

In parallel, angiogenesis is stimulated by hypoxia. Hypoxia attracts macrophages (28), which are able to survive under hypoxic conditions by adjusting their metabolism to an oxygen independent generation of ATP. In macrophages, vascular endothelial growth factor (VEGF) expression is stimulated by an intracellular transcription factor called hypoxia inducible factor (HIF-1). The macrophage is able to function under low oxygen tension (29) and releases VEGF, which stimulates the production of endothelial cell precursors and is chemotactic for these cells. Furthermore, end products of lipid oxidation, ω-(2-carboxyethyl) pyrrole (CEP) and other related pyrroles stimulate endothelial cells over the toll like receptor 2 (30). Also, other growth factors like PDGF from platelets and FGF from macrophages act angiogenic.

In response to VEGF, pericytes detach from the outer walls of the vessel. These cells use matrix metalloproteinases to digest the basal lamina around the vessels (31). The pericytes give rise to the new endothelial progenitor cells, which migrate to the place of low oxygen tension where they are chemotactically attracted by the chemokine stromal cell derived factor (SDF-1) which is produced by cells in the wound (32). This process is called homing of endothelial cells. The cells proliferate to form condensed groups and they arrange themselves to form tubes. The room needed for that is created by matrix metallo-proteinases. Finally, these newly formed tubes are connected to an existing blood vessel. A new vascular loop is created and blood can flow through.

Angiogenesis is the prerequisite for osteogenesis. New bone forms only in close connection to blood vessels. The mature bone cell does not survive more than 200 µm away from a blood vessel. First, the blood vessel develops and then the bone

follows, a process called angiogenetic osteogenesis. The formation of new bone needs a mechanically stable environment.

An osteoprogenitor cell attaches to the surface of an implant via integrins. Integrins attach to extracellular matrix proteins such as fibronectin via the RGD motif. An osteoblast does not directly attach to metal, but to the protein layer on top of the implant. The bone precursor cell itself produces insoluble cellular fibronectin needed for cellular attachment to titanium (33). After firm attachment to the surface, the osteoprogenitor cell that becomes secretory active is called osteoblast. As a molecular marker, the osteoblast starts to express osteocalcin and alkaline phosphatase.

Osteoblasts derive from mesenchymal stem cells and there is growing evidence that these stem cells are pericytes in the walls of smallest blood vessels (34). The precursors of pericytes originate from bone marrow cells (35). Bone morphogenetic proteins bind to receptors on the cell surface of the bone precursor cells (36). Binding to preformed complexes of receptors I and II will lead to activation of the Smad pathway, where the activated SMAD protein ultimately binds to DNA and in turn activates SMAD responsive genes like Runx. Bone morphogenic proteins (BMP) may also bind to single receptors, which induces their oligomerization, caveolae-dependent internalization and the activation of non-SMAD pathways such as ERK (extracellular signal regulated kinases) and MAPK (mitogen activated protein kinase). These will activate ATF2, c-jun or c-fos, which regulate BMP target genes like osteopontin, alkaline phosphatase or collagen typeI (37).

It is unclear from where the first BMPs in the wound originate. BMPs are stored in the bone matrix, bound in an inactive form to the glycosaminoglycane heparan sulphate. This allows the organism to store large quantities of active growth readily available and independent of new protein synthesis (16). With bone trauma matrix proteins, growth and differentiation factors which are stored in the bone matrix become soluble and active. Usually stored deep in the bone matrix, the factors are unmasked by the bone trauma and liberated from their heparin binding domains by heparin hydrolases from blood platelets (16). Heparan sulphate binding growth factors (e.g. BMPs, FGF, PDGF, VEGF) can also be released from the matrix by soluble heparin degrading enzymes (heparin hydrolases), which can be released

by platelets, lymphocytes or mast cells. The factors can also be released by competition with heparin, with proteins that bind to the growth factor or with other heparin binding proteins. A number of factors can be released by special proteolytic enzymes, e.g. PDGF-B (thrombin) or VEGF (plasmin) or TGF-b (multiple serin proteases) (16). The growth factors may be also unmasked or synthesized by osteoclasts (38, 39). They are produced by myofibroblasts and osteoblasts. BMPs appear in the bone wound after 3 days. Therefore, new bone forms with a latency.

With implant insertion, a dental implant gains primary stability. The implant is passively stabilized in the bone wound through friction with the primary bone contacts. The denser the host bone is, the more primary bone contacts are available and the higher primary stability of the implant will be. Primary stability implies that the friction holding the implant is higher than the highest dynamic load forces applied. Micromovement caused by load peaks higher than friction hold is critical. Micromovement of the implant can grind and slowly smoothen the bone surface, reducing the interlock between bone and titanium and ultimately resulting in a loss of primary stability. Therefore, it is critical to overload the implant occlusally in the early phase. Primary stability is important during the first days after implant installation. Under normal conditions the first weeks are a vulnerable phase because primary stability can decrease to critical levels before secondary stability has developed.

As early as 1 week after implant, placement new bone formation starts and the primary bone contacts are supplemented by newly formed secondary bone contacts (8). The first bone that forms after an injury is woven bone. Histologically, this bone is characterized by the fact that its collagen fibres are not parallel, but randomly oriented. Woven bone usually grows along the existing bone surfaces and along the dental implant surface towards the groves of the threads. Bone debris created by the implant drill was demonstrated to be important for early bone formation, and is incorporated into the immature trabelculae of woven bone (10). In the beginning, these bone contacts are not load oriented and randomly distributed. In a human volunteer study, new bone apposition amounted to a bone-implant contact of 62% of the intraosseous implant surface after 6 weeks, irrespective whether a SLA (sandblasted large grit and acid etched) or a modified ultrahydrophyllic SLA (SLActive) was used. However, the modified ultrahydrophilic

surface yielded more bone early contacts after 2 and 4 weeks compared with the standard SLA surface (11) (Fig. 8).

New bone formation begins with the secretion of a collagen matrix by osteoblasts. Depending on the process of ossification (endochondral or intramembraneous), this can be collagen type II or type III, which is ultimately replaced by collagen type I. Bone formation within the alveolar process is a process of intramembranous ossification, starting by the secretion of collagen type III. This matrix is subsequently mineralized by hydroxyapatite. The exact mechanism of this process is still widely debated, but in all probability is based on the concept of heterogenous nucleation, where organic or inorganic precursor seeds direct the formation of apatite from soluble inorganic ions (40). Opinions diverge on the nucleation site and the molecular nature of the nucleator: One theory proposes matrix vesicles (small vesicles derived from mineral forming cells such as chondroblasts or osteoblasts) as the site of an initial mineralization prerequisite for the following secondary mineralization of collagen (41). An alternative view proposes direct nucleation of apatite by matrix molecules such as collagen and noncollagenous proteins.

The mineralization process during primary bone formation is rapid, but relatively unorganized and not in close association to collagen (extrafibrillar). During the following remodelling phase, woven bone is removed by osteoclasts and replaced by lamellar bone. Next, in this process nanometre-sized, uniaxially oriented hydroxyapatite crystal plates are formed within the collagen fibres (interfibrillar) (42). This nanostructural architecture gives rise to the unique mechanical and biological properties of bone, making it rigid enough to resist pressure and traction forces while maintaining elasticity.

Removal of the woven bone by osteoclasts is the beginning of remodelling and thus the fourth and last phase.

1.5 Remodelling phase

One of the cellular key players of the remodelling phase is the osteoclast (5). Osteoclasts appear in the wound after a few days. They start to create space for new bone formation and remove primary boneimplant contacts. The remodelling phase can last several years until most woven bone and old bone from the primary

bone contacts is replaced by newly formed and load oriented bone.

Bone being formed after remodelling is called lamellar bone, named after the parallel orientation of its collagen fibres under polarized light. In contrast to woven bone which is oriented parallel to the titanium surface in the grooves of the threads, lamellar bone attaches rather to the tips of the macrothreads. These trabeculae usually attach at the tip of a thread of the implant in a little extended foot plate. The trabeculae distribute the occlusal loads to the surrounding bone and, if present, neighbouring tooth sockets. The new trabecular network is oriented similar to the supporting arches of a gothic church. According to Wolfs Law in bone, such a structure is built as light as possible. Therefore, between the insertion areas of the trabeculae, non-covered titanium surface areas appear on the implant surface. The so-called bone-implant contact can decrease during the remodelling phase and usually balances at approximately two-thirds of the surface after some time (43, 44).

Osteoclasts and osteoblasts act interdependently (45, 46). The so-called bone balance is necessary, because otherwise, the skeleton would become more porous (osteopenic) or denser (osteopetrotic). Both situations can be pathologic. At the beginning, osteoclast action depends on osteoblasts which control osteoclastsogenesis by the balance between RANKL and its counterpart osteoprotegerin, both produced by the osteoblast (47). Osteoblasts secrete RANKL, the ligand of the RANK (receptor activator of nuclear factor kappa beta) receptor which activates osteoclastogenesis together with M-CSF (macrophage colony stimulating factor). RANKL is membrane bound and can be masked by soluble osteoprotegerin which is also synthesized by osteoblasts and is a decoy receptor for RANKL (48). Thus, osteoprotegerin preserves bone by inhibition of osteoclastogenesis. The ratio of RANKL/ osteoprotegerin can be modulated, and the osteoblast is the target for various bone enhancing and inhibiting messenger molecules including IL-11, sclerostin, prostaglandin E2, parathyroid hormone (PTH) related protein, vitamin D and estradiol (39). PTH inhibits osteoprotegerin secretion from the osteoblast and thus increases osteoclast activation and bone degradation (48). In addition, soluble RANKL and the related messenger molecule TNF produced by lymphocytes can upregulate osteoclastogenesis under inflammatory situations (49).

The origin of osteoclasts is blood borne monocytes. They attach to the walls of the blood vessels by SDF-1/CXCR-4 interaction, and SDF-1 is bound to the endothelial cells surface (50). By diapedesis, these cells leave the blood stream. For the transmigration through the collagen of the basal lamina, they secrete matrix metalloproteinase MMP-9 (50). By chemotaxis, the cells are directed towards the bone. Soluble SDF-1 was identified as chemo-attracting molecule for osteoclast precursors (50), but being originally immune cells also, other immunoregulating molecules like IL-8 (cytokine-induced neutrophil chemoattractant; CINC-1) and monocyte chemotactic protein (MCP-1/CCL2) were demonstrated to be chemoattractive for the osteoclast precursor cells. Precursor cells fuse to form multinuclear giant cells. Osteoclast formation requires the presence of RANKLigand and M-CSF (51).

These membrane bound proteins are produced by neighbouring osteoblasts, thus requiring direct contact between these cells and osteoclast precursors. Proinflammatory cytokines like IL-6 or TNF-alpha can intensify this activation (52). There is some evidence that osteoclast precursors, like many other immune cells, need a costimulation via the ITAM receptor (immunoreceptor tyrosine-based activation motifs) (53).

The life span of an osteoclast was calculated to average 12 days in humans (54). The bone lining cells (terminally differentiated osteoblasts) digest remnants of osteoid by collagenases and thereby liberate RGD peptide endings from non-collagenous bone matrix proteins like osteopontin. The lining cells then detach from the bone surface. The so-prepared surface attracts migrating osteoclast precursors. The osteoclasts form a structure comparable to a suction cup on the bone surface, sealing the margin with a ring of integrin attachments. These integrins attach to bone matrix proteins like osteopontin (55). Between the osteoclasts and bone, a secluded space is created – the resorption lacuna – to protect neighbouring cells from acid and aggressive enzymes and to limit the extent of bone resorption. Under the suction cup, the osteoclasts increase the surface of their cell membrane by forming microscopic folds, the so-called ruffled border, a sign of the actively resorbing osteoclast (39). The cell membrane in the folds contains ion pumps that are comparable to gastric ion pumps. Producing hydrochloric acid, the acid demineralizes bone matrix and liberates bone collagen. Special enzymes, one of which is cathepsin K, digest bone collagen.

The coupling of osteoclasts and osteoblast and the molecular mechanism of how osteoclasts control and activate osteoblasts to fill up the bone void after resorption is still unclear in detail (56). As discussed earlier, growthand differentiation factors like BMP, IGF, TGF beta are stored in the bone matrix bound in an inactive form to heparan sulphate. They can be liberated from the bone matrix and activated by cleavage from the glycosaminoglycan by proteolytic enzymes. These enzymes are located on the surface of many cell types including osteoblasts (16). The role of the osteoclast in unmasking these factors by their proteases in the resorption lacuna is unclear. It is unlikely that these growth factors are transferred in intact form through endocytosis and through the osteoclasts cytoplasm. However, it is known that osteoclasts express and secrete BMP-6 and may thereby amplify the BMP signal which they have received from the degraded matrix (38). BMP-6 and the chemokine sphingosine 1 phosphate (S1P) are released on the tissue side by the osteoclast (56). BMP-6 is a coupling factor of bone resorption and refill involved in the osteoblast recruitment (57). BMP-6 differentiates mesenchymal stem cells to osteoblasts to build new bone (58). With other types of messenger molecules like ephrin and cardiotropin, osteoclasts may control the osteoblasts (45, 39). It has been shown that a bidirectional signalling exists between osteoclasts and osteoblasts in direct neighbourhood by the exchange of membrane bound ephrinB2 and EphB4 ligands. According to this theory, the osteoclasts retract themselves and directly differentiate osteoblasts in direct cell contact to fill the void with new bone (59). Osteoblastic precursor cells can sense the surface topography in the resorption lacuna by creating pseudopodia and thus attain information about how much bone is needed to fill the void (39). At this point, there is a scientific parallel to the different osteoconductivity of microand nanostructured titanium implant surfaces, which can also be sensed by the osteoblasts (60).

The formation of new osteons and remodelling of cortical bone is organized in form of so-called cutting cones. This is mainly a vessel loop with multiple osteoclasts on its tip. These groups of osteoclasts dig a tunnel into the old bone. The tube behind the tip of the tunnel is conclusively lined by concentric layers of newly formed lamellar bone. In the final state, the newly formed unit, containing a central blood vessel is called osteone or Haversian system.

Newly formed bone has to be built in a load oriented fashion. Mechanical stimuli

have to be translated into a cytokine signal to control the action of the osteoblast. This so-called mechanotransduction is thought to be a task of the osteocyte. The osteocyte is buried in bone and has tiny cytoplasmatic processes in nanoscale bone channels. According to the fluid shift theory, loading of bone causes interstitial pericellular fluid shifts within these channels (61) which stimulate primary cilia organs in the cell membrane that in turn induce an intracellular signal (62). These signals propagate through cellular junctions to neighbouring osteocytes, a network that is called the osteocyte syncytium (63). This communication process involves ion streams through gap junctions, small messenger molecules like nitric oxide and prostaglandin signalling (64, 65). This signalling precedes a protein signalling. Osteocytes can inhibit osteoblasts through the messenger sclerostin (66), a soluble inhibitor of canonical Wnt signalling which is closely connected to the PTH signal transduction system (66).

1.6 Introduction to the in vitro, preclinical and clinical studies on osseointegration

The influence of implant surface variation, in terms of surface roughness and application of bioactive molecules, is one of the most important field of research in the context of dental implants osseointegration

The features of implant devices and the reactions of bone-derived cells to foreign surfaces determine implant success during osseointegration. In an attempt to better understand the mechanisms underlying osteoblasts attachment and spreading, the first in vitro study was about adhesive peptides containing the fibronectin sequence motif for integrin binding (Arg-Gly-Asp, RGD) or mapping the human vitronectin protein (HVP). They were grafted on glass and titanium surfaces with or without chemically induced controlled immobilization. Several experimental studies have made reference to the role of heparin-binding motives in the selective binding of osteoblasts [67, 68]. With respect to the various extracellular matrix glycoproteins, the FRHRNRKGY peptide mapped on human vitronectin promotes osteoblast-like but not human umbilical vein endothelial cell (HUVEC) adhesion [69]. Heparin-binding sites of vitronectin and fibronectin are adjacent to the tripeptide sequence motif for integrin binding (Arg-Gly-Asp, RGD) and show a pattern of charged groups making contact with integral cell membrane proteins, namely heparan sulfate proteoglycans. Syndecans and glypicans, members of the proteoglycan family, consist of a core protein covalently bound to

long side-chain sulfated (heparan sulfate) glycosaminoglycan (GAG) or non-sulfated (hyaluronic acid) carbohydrates [70]. These membrane structures make contact with the extracellular environment through electrostatic and polar bindings, largely favoured by the hydrophilic layer described on device surfaces during the post-implantation phases. The energy involved in each of these interactions is relatively small. Large numbers of proteoglycan molecules are, however, expressed on the cellular membrane and the simultaneous cooperation of these contacts leads to a strong, even if transient, interaction [71]. Moreover, these dynamic interactions occurring in the time scale of milliseconds are required to elicit the receptor-mediated intracellular signalling involved in the modulation of subsequent cellular adhesion and in the osteoblasts differentiation [72]. Indeed, formation of new mineralized bone is a multistep, temporally and spatially coordinated process requiring membrane adhesive receptors, such as members of the integrin family [72]. The integrin-mediated signalling requires time frames of the order of minutes, a time-lag depending on the low densities of both the receptors and the ligands and on the lack of their appropriate spatial orientation [73]. An ideal implant surface should, therefore, exhibit electrostatic interactions to promote early osteoblasts attachment, preventing contact with other cell populations while ensuring the specific orientation of cellular receptors leading to platform for subsequent long-term cellular binding.

Tissue engineering procedures can be applied for the study of osseointegration in vitro. In vitro experiments can nowadays be based on tissue engineering methods. The use of 3D scaffolds loaded with human adipose-derived stem cells (ADSCs) has been investigated in the field of bone tissue engineering (74, 75). In this context, blocks of hydroxyapatite used as scaffolds provided an excellent porous architecture for ADSC spreading, adhesion, growth, and proliferation. In vitro ADSC osteo-endothelial commitment, which is a prerogative to mimic native bone, was also described (76) The insertion of a dental implant into a natural bone block that can be secondarily seeded with stem cells was considered one of the in vitro strategies to study osseointegration.

As described, the events related to the bone-to implant interface are within the complex phenomena of healing and bone remodeling, leading to new bone formation on the implant surface and to the intimate contact between the two opposing surfaces. The bone formation in vivo can be affected by various factors,

among them, the distance between the bone wall and the implant, in particular towards the buccal, lingual and apical walls.

Bone bridging in hard tissue defects is dependent on the size of the gap (77). This applies to implant dentistry as well and implies that osseointegration may be compromised at implants with marginal gaps >1mm in width between the implant surface and host bone (for review see: 78, 79). In fact, reports from experiments in dogs confirmed this hypothesis (e.g. 80, 81). These studies have demonstrated that the coronal level of bone-to-implant contact was dependent on the size of the gap between the titanium surface and the hard tissue walls of the recipient site. Conversely, other experimental studies showed that also marginal defects >1mm, even >2mm around implants may heal similarly to control sites (78, 82). It was further observed that new bone formed from the parental bone independently of the dimensions of the defects or irrespective of the use of GBR procedures (83, 84, 85, 86). In the studies cited, primary contact between bone and implants was always achieved in order to guarantee primary (mechanical) stability of the implant.

It had previously been demonstrated that defects up to 1mm gave rise to new bone formation and bridging the gap with one “single jump” while, in larger defects, multiple “jumps” were necessary (77). It has been shown in dogs experiments (83, 78; 87) that, in the presence of a marginal defect around implants, bone formation starts from the lateral and apical bony walls, towards the implant surface. However, the front of the newly formed bone does not reach the implant surface in the early phase of healing, leaving a space of about 0.4mm occupied by connective tissue. After 3-4 weeks of healing, osseointegration processes will start from the bottom of the defect, towards the margin of the implant.

An important role in osteogenesis around implants, and consequently osseointegration, is played by primary stability and by the surface characteristics of the implant (88, 89, 90, 4).

Two different patterns of bone formation at implant sites have been described (89, 91) (figs 12-15). Contact osteogenesis implies bone formation in direct contact with the implant surface, and distance osteogenesis implies new bone formation on the surfaces of the parent bone. This may subsequently become attached to the implant surface as well. When a gap results between the bony wall of the implant bed and the implant surface, a series of events occurs (8, 9, 87). A clot will

initially fill the space and will be replaced by a provisional connective matrix that will act as scaffold for woven bone formation. Contact and distance osteogenesis have been described as biological processes that lead to dental implant osseointegration (89, 91, 92). The existence of these processes has been studied in some animal experiments (93, 8, 9, 83, 84, 87). Contact osteogenesis has been described in an experimental study in dogs (9) in which secluded chambers were used. Newly formed woven bone was found attached to the implant surfaces and occasionally not connected with the parent bone. In another experimental study in dogs, marginal defects around implants were used (83). The healing indicated that both processes, contact and distance osteogenesis, may have participated in the closure of the marginal defects.

It should be emphasized that in the above mentioned experimental studies initial bone contact was provided to the implants by the threads of the implant bodies. However, in a rabbit model, implant contact with the parent bone was avoided (93). Without such initial contact, osseointegration was not achieved. It has to be further realized that a turned implant surface was used in that experiment. This fact may have influenced the healing outcomes as well (90, 4). In any case, the Carlsson et al experiment showed that either contact or distance osteogenesis were not completely impossible, even though with very reduced predictability.

In the study mentioned (93), a device was applied to assure primary stability of the implant, since implant instability has been shown to induce a fibrous encapsulation of the implant rather than osseointegration.

The effect of demineralized bovine bone matrix (DBBM) as a bone substitute and filler of marginal defects around implants has been evaluated in several experimental (e.g. 95, 96, 97, 98) and clinical studies (e.g. 99, 100). This biomaterial appeared to be completely integrated in newly formed bone over time, appearing to offer optimal osteoconductivity (96). Nevertheless, the advantages of DBBM in improving osseointegration when applied at marginal defects around implants is still under debate (97, 101, 102, 103, 104, 105).

The influence on osseointegration of the quality and condition of the alveolar bone in relation to the timing of extraction can affect the pattern of bone healing and osseointegration.

A systematic review (106) has documented that implants installed into alveolar sockets immediately after tooth extraction yielded a similar survival rate as implants placed in healed alveolar bony ridges. The results obtained were

maintained for at least 5 year (107). The use of this surgical approach has been scrutinized in several clinical (e.g. 108; 109) and experimental studies (e.g. 102, 103, 110-118). These studies, however, were not able to confirm the maintenance of the vertical and horizontal dimensions of the peri-implant hard tissue, due to the alveolar bone resorption taking place after tooth extraction (119, 110). The buccal plate of the alveolar extraction socket may be compromised as a consequence of the disease process before tooth extraction. As result, a buccal dehiscence may occur after implant installation. Several different procedures have been proposed to improve the outcomes after healing of such compromised sites (e.g. 120, 121, 122, 123). In a controlled clinical study (123), implants were installed into molar alveolar sockets immediately after tooth extraction, and deproteinized bovine bone mineral covered with a collagen membrane was used to fill the residual dehiscence buccal defects (test sites). As control sites, implants installed in healed molar sites were used. The survival rates were similar in both groups (100%), while better results were obtained at the control sites in relation to probing depths and clinical attachment levels. In animal experiments, buccal dehiscences were produced at extraction sockets and different regenerative methods applied (e.g. 124, 125, 126, 127, 128, 129, 130, 112). In a experiment in monkeys (130), dehiscence-type defects, about 4 mm large and 6 mm deep, were filled with rhBMP-2, while the control sites were left untreated. A vertical bone gain of approximately 4 mm was observed in both groups, the difference between test and control group not being statistically significant. Also the positioning of the implants within the extraction sockets has been shown to affect the final outcome. The closer the implant surface was to the outer contour of the bony crest, the higher was the supracrestal exposure of the buccal portion of the implant (117, 118, 112, 131, 132, 133)

The development of implant surfaces, together with a better understanding of the mechanisms the peri-implant bone healing, leads to variation of some clinical paradigms. Among these, the need to use implants with a length not less than 10 mm, especially in case of immediate post extractive implants

Implants installed into alveolar sockets immediately after tooth extraction have been shown to yield predictable outcomes (e.g. 134, 135). Furthermore, a systematic review (106) has established the fact that such implants present with similar survival rates (estimated annual failure rate: 0.82%) as conventionally

placed implants. The use of this procedure reduces the number of surgical sessions and may also reduce the time between surgery and prosthetic delivery (136). This technique, however, cannot prevent the physiological bone resorption that occurs after tooth extraction (108, 137, 106.)

For this placement modality (type 1; Hämmerle et al. 2004) (136), the need for implants that are longer than the remaining extraction sockets has been propagated under the assumption that implant stability may be guaranteed in the area beyond the apex of the extraction socket (138, 139, 140). Because of the presence of anatomical structures such as the maxillary sinus or the inferior alveolar nerve, however, bone may not be available beyond the apex of the socket. Moreover, it was shown in experimental animals that immediate implants became osseointegrated irrespective of their length in relation to the extraction socket (118). In these experimental studies, however, the length of the implants was at least of 10 mm.

Moreover, the use of short implants (6 mm) has been reported with good outcomes (141, 142, 143) and promising results have been published on the installation of short implants in comparison with alveolar bone augmentation techniques (144, 145).

However, the use of short implants (6 mm) in immediate installation has not been studied as yet.

In vitro and preclinical animals studies demonstrate that the development of implant surfaces can influence the clinical utilization in human. In particular, the overall increase of the implant surface that contacts the alveolar bone – bone to implant contact , related to the increase of surface roughness secondary to treatments at micro and nanoscale, may allow the treatment of edentulism associated with severe alveolar bone atrophy with implants of reduced dimensions (eg length of the intraosseous component <10mm).
Osseointegrated implants have become a viable option for replacing missing teeth in totally and partially edentulous patients, as established by systematic reviews, especially in the case of single-tooth gaps (146-149). However, in many clinical situations, placing long implants could prove difficult as a result of limitations such as the location of the mandibular canal, pneumatization of the maxillary sinus, and alveolar ridge deficiencies. In patients with severe alveolar resorption, there are

different surgical procedures available to facilitate future implant placement. More complex implant techniques include the use of bone grafts harvested extraorally or intraorally and placed as inlays or onlays, distraction osteogenesis, zygomatic implants, transposition of the inferior dental nerve, guided bone regeneration (GBR), and maxillary sinus elevation (150-153).

However, these surgical procedures are case sensitive, technically demanding, and time consuming and may increase postoperative morbidity and the total cost and duration of the therapy. Minimally invasive surgical techniques are currently advocated to reduce patients' postoperative discomfort and contain the risk of complications. The use of short implants was introduced as an alternative treatment in patients with limited amounts of bone available. There is no consensus in the dental literature on the definition of a short implant: in various reviews, it has come in lengths of 7, 8, or <10 mm (141, 154). An implant can also be inserted at different levels, so a short implant has also been defined as an implant designed to have an intrabony length of 8 mm (141).

Recent reviews have compared short implants with conventional implants. Kotsovilis et al (155) concluded in their systematic review that short implants (8 or 10 mm) with rough surfaces are no less effective than implants of conventional length (10 mm) with rough surfaces. Romeo et al (156) wrote that the recent literature has demonstrated a similar survival rate (SSR) for shortand standard-length implants. In a systematic review of horizontal and vertical bone augmentation techniques for the purposes of dental implant treatment, Esposito et al (157) concluded that short implants appear to be a better alternative to vertical bone grafting of resorbed jaws. Conversely, when the clinical outcome of short implants was discussed, non-homogeneous SSRs were reported (158-161). probably because the surface treatment of the implants was not always taken into account.

2. AIM OF THE THESIS

Aim of the present thesis has been to focus on dental implant surface modifications in order to improve the clinical performance in areas with poor quantity or quality of bone. To achieve this objective, the thesis has been developed by identifying specific aims for the in vitro, preclinical and clinical studies.

1) In vitro studies:

a) to better understand the mechanisms underlying osteoblasts attachment and spreading, in this study adhesive peptides containing the fibronectin sequence motif for integrin binding (Arg-Gly-Asp, RGD) or mapping the human vitronectin protein (HVP) were grafted on glass and titanium surfaces with or without chemically induced controlled immobilization.

b) to reproduce the osseointegration process in vitro in order to study the dynamic of bone-implant interactions. To this end, a tissue engineering approach was used by positioning dental implants into stem cells seeded 3D bone-derived scaffolds. The final goal was to overcome the limitations concerning in vitro methods, and to complement and eventually replace animal studies in this field.

2) in vivo studies (in big animal model, dogs, of osteointegrative properties of implants with different degree of surface modification).

a) to evaluate the healing at implants with a moderately rough surface placed and stabilized in recipient sites of dimensions deeper and larger than that of the implants to avoid any contact between parent bone and the implant surface.

b) to evaluate the influence on osseointegration of DBBM particles used to fill defects of at least 1mm around implants having no primary contact with bone.

c) to evaluate the influence of bucco-lingual implant positioning into extraction sockets on bone formation at buccal alveolar dehiscence defects.

d) to compare the bone-to-implant contact of 6 mm osseointegrated implants with that of 11 mm long implants installed into sockets immediately after

tooth extraction.

3) clinical research (on short implants, to underline the effect of surface modifications on dental implant survival in the long term in the clinic).

a) to assess the mediumto long-term prognosis of short implants (7 or 8.5 mm in length), with machined (M) and rough (R) surfaces, placed in partially or totally edentulous arches, in a retrospective clinical trial.

3. MATERIALS AND METHODS

3.1 IN VITRO STUDIES

3.1.1 From Brun et al, 2012. Mechanisms underlying the attachment and spreading of human osteoblasts: From transient interactions to focal adhesions on vitronectin-grafted bioactive surfaces

Peptide synthesis and surfaces preparation

The vitronectin peptide is mapped on the human vitronectin protein (HVP, sequence 351-359: FRHRNRKGY). The RGD peptide is a linear sequence of human fibronectin presenting four GRGDSP motifs per chain (RGD, sequence: GRGDSPGRGDSPGRGDSPGRGDSPK). The RAD peptide is the control peptide with respect to RGD (RAD, sequence: GRADSPGRADSPGRADSPGRADSPK). In its sequence the Arg-Gly-Asp motif is substituted with a similar but not adhesive motif, Arg-Ala-Asp. Both peptides were synthesized as C-terminal amides using the Fmoc Chemistry on Applied Biosystems 431A Instrument, a traditional solid-phase technique (162).

Side-chain protected peptides (t-Butyl (tBu), Tyr; 2,2,5,7,8-Pentamethylchromane-6-sulfonyl (Pmc), Arg; Trityl (Trt), His and Asn; t-butoxycarbonyl (Boc), Lys; tBu, Ser) were synthesized using a Sieber Amide resin. The cleavage from the resin was obtained by incubation for 15 min in (1) 1% 2,2,2-trifluoroacetic acid (TFA)/dichloromethane (DCM) for the full side-chain protected sequences and in (2) 10% TFA/DCM for 20 min for the partially deprotected sequences. The deprotection method (2) produced the loss of Boc and Trt for HVP and of Boc for RGD. The products were ascertained by electrospray ionization/time of flight mass spectrometry. To prepare the glass coverslips (1.76 cm2), glasses were washed several times in an ultrasonic bath (acetone, 30% ethanol in MilliQ water) and treated with 1 N NaOH for 1 h. Glasses were washed in MilliQ water, dried at 100 °C for 10 min, washed with acetone and dried under vacuum. The glass coverslips were then immersed in 2% (3-aminopropyl) triethoxysilane (APTES) in acetone solution at 40 "C overnight, washed three times with dichloromethane (DCM), acetone and finally with MilliQ water. After drying for 10 min at 100 °C the

coverslips were randomly divided into two groups to be used for unspecific or specific functionalization. For specific functionalization (sp), silanized glasses were incubated for 4 h in 20 ml N-methyl-2-pyrrolidone (NMP) and 2.5 ml diisopropylethylamine (DIEA) containing 5 mg glutaric anhydride. The glasses were washed three times with NMP and three times with acetone, and then dried under vacuum for 1 h. The reaction with side-chain protected peptides was carried out for 21 h using 8 mol of protected HVP or protected RGD or protected RAD dissolved in 10 ml NMP containing 3.75 mg O-benzotriazole-N,N,N',N'-tetramethyl-uroniumhexafluoro-phosphate (HBTU), 1.34 mg N-hydroxybenzotriazole (HOBt) and 5 µl DIEA. The glasses were washed three times with NMP and three times with ethanol, and finally dried under vacuum for 15 min. The side-chain de-protection was carried out mixing a solution of 10 ml TFA with 0.23 ml MilliQ water, 0.1 ml TES, and 0.25 ml 1,2-ethandithiol (EDT) for 1 h. The glass coverslips were then washed twice in TFA and in acetone, three times in MilliQ water and twice in acetone. They were then dried under vacuum for 15 min. These surfaces carrying specifically immobilized peptides will be hereafter referred to as ‘‘HVPsp’’, ‘‘RGDsp’’ and RAD.

The same protocol was used for unspecific functionalization (unsp). In this case the partially deprotected sequences of RGD and HVP were used. These surfaces carrying unspecifically immobilized peptides will be hereafter referred to as ‘‘HVPunsp’’ and ‘‘RGDunsp’’. Titanium (Ti) surfaces were obtained by cutting commercially pure cylindrical titanium (Ti grade 2) bars. Ti disks (1.76 cm2) were prepared, as described elsewhere (163) and then treated with glutaric anhydride, side-chain protected peptides, and TFA, as described for the glass coverslips. The morphology of titanium disks was analyzed and reported in Bagno et al (163).

Briefly the roughness data for sand-blasted and acid attacked disks estimated by contact profilometry resulted as follows: Sq (Å) = 25,374.44; Sa (µm) = 2.015; Ssk = -0.0675; Sku = 3.06; Sz (Å) = 161,324.8; Sds = (Å-2) = 2.9 x 10-10; Sdr (%) = 329.02. Roughness parameter values measured on silanized or peptide linked surfaces showed no significant difference in surface morphology.

Surface characterization

Radio-labeling procedure

Radio-labeling of silanized glass surfaces was performed separately treating each sample in triplicate with 600 µl of 0.115 mM [14C] formaldehyde and 10 mM NaBH3CN acetonitrile for 4 h at room temperature. The excess radioactive solution was removed, and the glasses were washed 10 times with acetonitrile, water and then dried using N2. The same procedure was used for the control surface obtained by acetylation of silanized samples. Samples were then incubated overnight at room temperature with a mixture of toluene (1 ml), acetic acid anhydride (100 µl) and pyridine (100 µl). The glasses were rinsed with toluene, DCM and ethanol.

The radioactivity of each sample was measured with a Packard Liquid Scintillation Analyzer using 5 ml of scintillation fluid (Packard). Data expressed as counts per minute were converted into pmol through a titration curve.

X-ray photoelectron spectroscopy (XPS) measurements

XPS studies were performed using an instrument of our design equipped with preparation and analysis chambers separated by a gate valve. The analysis chamber consists of a six-degrees-of-freedom manipulator and 150 mm mean radius hemispherical electron analyzer with a five-lens output system combined with a 16-channel detector. Si2p, C1s, O1s and N1s core level signals were recorded. The reaction yield R for peptide immobilization was calculated from the N/Si ratios, as reported by Xiao et al. (164):

R = [(N/Si) sample – (N/Si) control]/(N/Si) controlX1/NpeptX100, where the (N/Si) sample is the measured ratio for HVPsp, HVPunsp, RGDsp or RGDunsp, the (N/Si) control is the measured atomic ratio for a silanized surface and Npept refers to the nitrogen atoms in a

peptide molecule (22 for HVP and 38 for RGD).

Atomic force microscopy (AFM) analyses

Topographical images were obtained by AFM using a commercial Nanoscope IIIa multimode microscope (Digital Instruments, Santa Barbara, CA, USA). The device was equipped with an <E> calibrated scanner, calibrated using the manufacturer's gratings. All samples were observed in tapping mode (TM) using 0.5–2 Ω cm phosphorous n-doped silicon tips mounted on cantilevers with a nominal force constant of 40 N m-1 and a resonant frequency of 300 kHz. The applied force was varied over a range from several nN up to tens of nN in contact mode. The glass

surfaces were examined ex situ after being gently dried. Image analysis was carried out using DI software, version 4.23r6. The images were flattened to remove background slopes. Film roughness was measured on TM images obtained at a scan speed of 1 Hz over scanned areas of 500 x 500 nm2 for a minimum of three separate images for each sample obtained from different regions. The roughness values are expressed in terms of Ra, Rq and Rmax. In particular, Ra expresses the arithmetic average of the absolute values of the surface height deviations measured from the mean plane within the cursor box using $Ra=\frac{1}{n}\sum_{j=1}^{n}|Zj|$. Rq is the standard deviation of the Z values and is calculated as $Rq=\sqrt{\frac{\Sigma(Zi)2}{n}}$ where Zi is the current Z value and n is the number of points within the cursor box. Finally, Rmax is the maximum vertical distance between the highest and lowest data points within the cursor box.

Cell culture and assays

Human osteoblasts were obtained using a trephine bur from mandible alveolar bone of healthy 54-year-old male subject during a standard procedure for implant surgery. The study was approved by the local Ethics Committee (March 2008). The patient gave his informed consent to the experimentation. Osteoblasts were cultured and differentiated as previously described (165). Human foreskin fibroblasts were purchased from the American Tissue Culture Collection (ATCC, Manassas, VA) and cultured in Dulbecco's modified Eagle's medium (DMEM) supplemented with 20% v/v fetal bovine serum, 1% v/v sodium pyruvate, 1% v/v nonessential amino acids and 1% v/v antibiotic–antimycotic solution (all provided by Gibco, Milan, Italy). The culture medium was renewed every three days. Osteoblasts and fibroblasts were detached using Trypsin–EDTA (Gibco) and used between the fifth and tenth passages.

Adhesion study

Cellular adhesion to glass or Ti-grafted surfaces was evaluated, as described elsewhere (163). Briefly, osteoblasts (1 x 105 cells ml-1) were seeded and cultured for 2 h on differently functionalized surfaces. Cellular cultures were then rinsed three times with phosphate buffer saline (PBS) and then incubated with 200

µl of MTT (3-(4,5-dimethylthiazole-2-yl)-2,5-diphenyl tetrazolium bromide) solution (5 mg ml-1 in PBS, Sigma) at 37 °C for 4 h. Reaction was stopped by adding 0.01 N HCl in 10% w/v SDS and optical density was recorded at 620 nm using a microplate reader (Sunrise; Tecan, Milan, Italy). To quantify adherent cells a standard curve was constructed for each experiment. As indicated, human osteoblast monolayers were incubated for 10 min at 22 °C with 50 mg ml-1 heparin (Sigma, Milan, Italy). The cells were then re-suspended in serum-free medium (6 x 105 cells ml-1) and pretreated either for 30 min at 4 °C with anti-αvβ3 integrin antibody (10 µg/1 x 105 cells, Chemicon, Prodotti Gianni, Milan, Italy) or for 3 h at 37 °C with 1 U ml-1 of heparinase I, 0.5 U ml-1 of heparinase II and 0.5 U ml-1 of chondroitinase ABC (all purchased from Sigma Chemical Co., St Louis, MO, USA). Control cells were incubated in serum-free medium. Cell viability was verified by the trypan blue exclusion test and 1 x 105 osteoblasts were seeded on functionalized glass coverslips or Ti dishes.

Imaging assays

Immunocytochemistry

Osteoblast cells were fixed in paraformaldehyde 4% w/v 10 min at room temperature and then washed twice (5 min each) in Trisbuffered saline (TBS). Nonspecific binding sites were blocked by incubation with 2% bovine serum albumin in TBS for 20 min. Samples were then incubated with mouse polyclonal anti-β actin (1 µg ml-1, Sigma) or rabbit polyclonal anti-pospho-FAK-Y397 antibodies (2 µg ml-1, Santa Cruz Biotechnology, Heidelberg, Germany) for 2 h at 22 °C. Following extensive washes, immunocomplexes were detected with goat anti-mouse IgG Alexa Fluo 555-conjugated or goat anti-rabbit IgG Alexa Fluo 488-conjugated (Invitrogen Corporation, Milan, Italy). The nuclei were stained with TOTO-3 iodide (Invitrogen). Negative controls were performed by omission of primary antibodies. The samples were then washed, mounted, analyzed and photographed using a Leica TCSNT/SP2 confocal microscope (x63 objective, x2 zoom). The images were digitally stored using Leica software.

Total internal reflection fluorescence (TIRF) microscopy

Human osteoblasts (1 x 105 cells ml-1) were cultured for 2 h at 37 °C on glass coverslips functionalized with RGD and HVP peptides. The cells were then probed

with FM 1-43 fluorescent dye (Invitrogen, Milan, Italy) specifically binding to membrane lipids and then examined using an inverted microscope equipped with commercial white light TIRF apparatus (Nikon Instruments). The total internal reflection (TIR) at the glass coverslip–water interface was obtained using an objective based approach (CFI Plan Apochromat TIRF 60x/1.45 oil) with a theoretical penetration depth from ~80 to 200 nm. Images were taken starting 1 min after the probe was added using a 2 megpixel CCD camera DS-2MBWc (Nikon Instruments, USA). To ensure optimal conditions, during acquisition cells were kept in a top-stage incubator (Tokai Hit, Japan) with temperature and CO2 levels at 37 °C and 5%, respectively. As described, osteoblast cells seeded onto HVP functionalized surfaces were treated for 1 h at 37 °C with 50 µM ML141, Cdc42 pharmacological inhibitor, before TIRF analysis (166).

Western blotting

Human osteoblasts cultured for 6 h on functionalized glass surfaces were washed with ice-cold PBS and subjected to total protein extraction and Western blot assay as previously described (167).
Phosphorylated FAK was revealed by incubating the PVDF membrane with rabbit polyclonal anti-pospho-FAK-Y397 antibody (2 µg ml-1, Santa Cruz) and with horseradish peroxidase-conjugated goat anti-rabbit (Sigma). Finally, the enzymatic reaction was developed using ECL detection reagents (Santa Cruz Biotechnology) and photographed using a VersaDoc imaging system (Bio-Rad). Anti-β-actin antibody (Sigma) was used as loading control.

RNA isolation and quantitative real time PCR analysis

Human osteoblasts and fibroblasts cultured for 24 h on different functionalized surfaces were subjected to total RNA extraction using the SV Total RNA Isolation System kit (Promega, Milan, Italy) according to the manufacturer's instructions. As described, osteoblasts were treated with 100 µM AG82 (Calbiochem, Milan, Italy), a pharmacological FAK inhibitor, for 1 h at 37 °C. 2 µg of total RNA were retro-transcribed using oligo random hexamers and MuLV reverse transcriptase (Applied Biosystems, Milan, Italy) to generate cDNA. Gene expression was evaluated using quantitative real time RT-PCR using ABI Prism 7700 Sequence

Detection System (Applied Biosystems), the TaqMan qPCR Master Mix (Applied Biosystems), primers and probes from the Universal Probe Library system (UPL, Roche Applied Science, Monza, Italy; Table 1.1). The expression of the target genes was normalized to the endogenous levels of glyceraldehyde-3-phospate dehydrogenase (GADPH). Gene quantification was carried out using a standard curve generated by amplification of 10-fold serial dilutions of the corresponding cDNA subcloned into the pGEM-T Vector System (Promega).

Statistical analysis

Data are reported as mean ± SE. Statistical analysis was performed using the unpaired Student's t-test or the one-way ANOVA test followed by a Bonferroni's multicomparison test, using GraphPad Prism 3.03 (San Diego, California, USA). P values <0.05 were considered statistically significant.

3.1.2 From: A novel in vitro technique to evaluate dental implantosseointegration.

Biomaterials

Dental implant

Customized cylindrical implants 6.6 mm in length and 3.4 mm in diameter (ZirTi®; Zirconium Sand-Blasted Acid-Etched Titanium, Sweden & Martina, Due Carrare, Padova, Italy) were utilized (Figure 2.1a). Implant design was characterized by the presence of a titanium extension on the coronal side having a 2.5 mm diameter and approximately 10mm length, with a screw morphology at its extremity and a polished surface close to the body of the implant. In the middle of the extension, a polished hexagon was present.

Bone matrix

Orthoss® Blocks 2x2x1.3 cm (GeistlichPharma AG, Wolhusen, Switzerland) were used in this study. Orthoss® is a natural carbonated hydroxyapatite of bovine origin. It is a highly osteoconductive material because of its particular structure, very similar to human spongeous bone, with interconnected macropores (100-300

μm), micropores, and nanopores (10-20 μm), resulting in an higher inner surface and excellent hydrophilic property.

Dental implants were inserted in the bone blocks by means of two customized drilling guides (Fig. 2.1b) with a twist drill (FFT3 300, Sweden & Martina) and dedicated drill stops.

For each experiment, one implant on the 2x2 cm side of one bone block was inserted (Fig. 2.1c).

Human stem cells isolation

Human ADSCs were isolated from the adipose tissue of healthy patients (age, 35–58 years) who underwent cosmetic surgery procedures. All the patients gave written consent. The adipose tissues were digested and the cells were isolated, expanded, and seeded following our previous protocol (76). Briefly, the fat was washed with Phosphate Buffered Saline (PBS, EuroClone, Milan, Italy) and digested using a solution of 0.075% collagenase from Clostridium histolyticum type II (Sigma-Aldrich, St. Louis, MO, USA) in Hank's Balanced Salt Solution (HBSS, LonzaS.r.l., Milano, Italy), for 3 h at room temperature and in slow agitation. At the end of the digestion, the collagenase activity was blocked with an equal volume of complete DMEM (cDMEM). cDMEM consisted of Dulbecco's modified Eagle's medium (DMEM, Lonza, Italy) supplemented with 10% Fetal Bovine Serum (FBS, BidachemS.p.A., Milano, Italy) and 1% Penicillin/Streptomycin (P/S, EuroClone). After centrifugation for 4 min at 1200 rpm, the pellet was washed in PBS and filtered with a 70 μM cell strainer (BD Biosciences, Mississauga, Ontario, Canada). The cell suspension was resuspended in cDMEM, transferred to a 25-cm2 tissue culture flask, then incubated at 37°C and 5% CO2 for 3 days.

Cell counting and 3D cultures

The viable cells were counted using the trypan blue exclusion test. At the confluence point, ADSCs were detached from the flasks with a solution of 0.25% trypsin ad 0.02% EDTA (EuroClone). After the addition of cDMEM, the cells were centrifuged for 4 min at 1200 rpm. The pellet was resuspended in cDMEM, then, 20 μl of the suspension were added to 80 μl of trypan blue for each culture. Cell counting was done using a Burker's chamber.

Cells were seeded at density of 106/cm2 on bone matrix blocksaroundthe dental implant in presence of osteo-endothelial differentiation medium (cDMEM supplemented with 10 nM dexamethasone;50 µg/ml L-ascorbic acid; 10 mM β-glycerophosphate; 10 ng/ml di basic Fibroblast Growth Factor; 0.5 ng/ml Vascular Endothelial Growth Factor; and 10 ng/ml Endothelial Growth Factor). All the 3D cultures were incubated at 37°C and 5% CO2 for 30 days, changing the medium every 2 days.

Real-time PCR

Total RNA was extracted from the ADSCs seeded for 30 days on the bone blocks around the dental implant using the TRIzol® Reagent (Invitrogen, Carsbad, CA, USA). The samples were quantified with the NanoDrop spectrophotometer (NanoDrop™ 1000, Thermo Scientific). For the first-strand cDNA synthesis, 500 ng of total RNA was reverse transcribed using M-MLV RT (Moloney Murine Leukemia Virus Reverse Transcriptase, Invitrogen) according to the manufacturer's protocol.

Human primers were selected for each target gene with Primer 3 software (Table 2.1). Real-time PCRs were carried out using the designed primers at a concentration of 300 nM and FastStart SYBR Green Master (Roche Diagnostics, Mannheim, Germany) on a Rotor-Gene 3000 (Corbett Research, Sydney, Australia). Thermal cycling conditions were as follows: 15 min denaturation at 95°C; followed by 40 cycles of 15 s denaturation at 95°C; annealing for 30 s at 60°C; and 20 s elongation at 72°C. Differences in gene expression were evaluated by the 2ΔΔCt method (168) using ADSCs cultured in cDMEM onto tissue culture polystyrene as control.Values were normalized to the expression of the GAPDH internal reference, whose abundance did not change under our experimental conditions. Experiments were performed with 3 different preparations and repeated at least 3 times.

Mechanical pull-out test

The pull-out test measures the force needed to extract an embedded insert from a concrete mass. The test was performed in quadruplicate and in three different conditions:

a)non cultivated bone blocks (dry);

b)non cultivated bone blocks, soaked in osteo-endothelial differentiation medium for 30 days (immersed);
c) bone blocks loaded with ADSCs in osteo-endothelial differentiation mediumfor 30 days (cultivated) (fig 2.3).
Dry (a) and immersed (b) samples were considered as controls.
Pull-out tests of the implants from the bone blocks (tensile test) were performed using a Galdabini SUN 2500 (Cardano al Campo, Italy) uni-axial testing machine equipped with a load cell of 25kN. Immediately before the test, a mounter was attached to the extension pin of each implant. After alignment and positioning of the samples in the testing machine, implants were loaded at room temperature, by setting a displacement rate equal to 1,5mm/min (Fig. 2.2). The force was measured by a multi-axial load cell (169, 170) and signals were acquired by Cronos-PL 16 data acquisition system (IMC Dataworks, Madison, WI, USA) adopting UNI-8 channels with sampling time 20 ms and sampling rate 100 kHz. Before the mechanical tests the load cell was calibrated. Before each measurement the load cell was balanced.

Scanning Electron Microscopy (SEM)

SEM analyses were performedon dental implants pulled-out respectively from dry bone blocks and from seeded blocks. Samples were fixed with 2.5% glutaraldehyde (glutaraldehyde solution Grade I, 25% in H2O; G5882, Sigma Aldrich) in 0.1 M cacodylate (sodium cacodylate trihydrate; C0250, Sigma Aldrich) buffer for 1 h before critical-point drying followed by gold-palladium coating. All micrographs were obtained using a JEOL 6360LV SEM microscope (JEOL, Tokyo, Japan). The SEM analysis was carried out at the Interdepartmental Service Center C.U.G.A.S. (University of Padova).

Statistical analysis

One-way analysis of variance (ANOVA) was used for gene expression data analyses. A repeated-measures ANOVA with a post-hoc analysis using Bonferroni's correction for multiple comparisons was performed, and t-tests were used to determine significant differences ($p<0.05$). Repeatability was calculated as the standard deviation of the difference between measurements. All testing was performed using SPSS 16.0 software (SPSS Inc., Chicago, Illinois, USA) (licensed by the University of Padova).

For mechanical pull out tests, resultant force was computed as the maximum value of force during the tensile test. Means ± SD were calculated for each condition. One-way ANOVA was used to assess for significant differences for the conditions, with statistical significance at $P < 0.05$.

3.2 IN VIVO STUDIES

3.2.1 PRECLINICAL STUDIES

3.2.1.1 FROM: Sivolella et al., 2012 Osteogenesis at implants without primary bone contact – An experimental study in dogs.

Cinical procedures

The protocol was approved by the institutional Ethic Committee for animal research. Six Labrador dogs (average weight 27.6 kg, average age 2.9 years) were used. During all surgical procedures, the animals were pre-anesthetized with xylazine (1 mg/kg intramuscular [i.m.] Ronpums,Bayer, Sao Paulo, Brazil) and ketamine (15 mg/kg i.m. Dopalens, Vetbrands, São Paulo, Brazil) and anesthetized with thionembutal (20 mg/kg intravenous [i.v.] Tiopentals, Cristália, Itapira, Brazil) During the entire surgery, the animals inhaled O2 and were kept with an intravenous infusion of saline.

The third and fourth premolars as well as the first molars were extracted bilaterally in the mandible. After 3 months of healing, muco-periosteal full-thickness flaps were elevated and, for the present experiment, the premolar area of the alveolar bony crest was selected bilaterally.

Customized cylindrical implants, 7 mm in length and 2.8 mm in diameter (ZirTi®, Zirconium Sandblasted Acid Etched Titanium; Sweden & Martina, Due Carrare, Padova, Italy), were installed. The external macromorphology of the implant was characterized by the absence of threads and the presence of a modified apical region which presented with two opposing flat surfaces (Fig. 3.1a). The aim of these flat surfaces was to stabilize the implants into the positioning devices used in the experiment. The internal side of the implant contained a thread for the placement of customized cover screw.

Two recipient sites were prepared with wider and longer cylindrical drills compared with the implant dimensions (defect sites – test). In the left side of the mandible,

the defect site was prepared using a cylindrical drill, 4.2 mm in diameter, to a depth of 7.7 mm (small defect) and a second defect site was prepared in the right side of the mandible using a drill of 5.2 mm in diameter to a depth of 8.2 mm (Large defect; Fig. 3.3a).

Aiming at avoiding any contact of the implant surface with the bony walls of the implant bed after installation (Fig. 3.1b), two customized baskets made of PEEK (Polyetheretherketone; Sweden & Martina, Due Carrare, Padova, Italy) were fabricated (Fig. 3.2a and b). The baskets had the same external morphology and dimensions of the two recipient defect sites and the same internal morphology of the implant, but a slightly larger

diameter. Only the flat surfaces at the apex of the implant were in contact with the basket

to obtain stabilization. Moreover, a notch on the most coronal border, parallel to the apical flat surfaces of the implant, served as reference for implant positioning. Firstly, at each of the two defects, the corresponding baskets were placed within the prepared recipient sites, flush with the mesio-distal bony crest. The notches were placed parallel to the mesio-distal direction for histological purposes (Fig. 3.3b). Subsequently, the implant was positioned within the basket. Straight or L-shaped plates for bone fixation (Modul System 1.2 – Titanium; Cizeta Surgical, Bologna, Italy) with at least four holes were adapted around the bony crest with one of the central holes positioned on the implant (Fig. 3.3c). The plate was subsequently attached loosely to the implant with a customized cover screw. The passive adaptation of the plate on the alveolar crest and on the implant was checked and corrected if necessary. Three locations of fixation screws were prepared with the dedicated twist drill. The implant/plate unit as well as the plastic basket were removed from the recipient defect sites. A customized sterile titanium device (Fig. 3.2a–c; Sweden & Martina, Due Carrare, Padova, Italy) with an internal chamber with the same morphology and dimensions of baskets, was used to stabilize the implant/plate assembly. A calibrated torque screwdriver

was used to tighten the customized cover screws to 25 Ncm. Care was applied to avoid rotation of the plate in respect to the implants and to maintain the predetermined orientation of the two flat surfaces at the apical portion of the implant. The implant/plate assembly was repositioned in the recipient defects sites, and the plates fixed to the alveolar bone using three fixation screws (Fig. 3.3d) of suitable length (4–12 mm). After implant positioning, a three-dimensional

gap between the implant surface and the bony walls of the implant bed was obtained that measured 0.7 and 1.2 mm in width at the small and large defects, respectively. Possible contacts between the implant and the bone were verified using a titanium periodontal probe (PCPGT11,5, STOMA®; Storz am Mark GmbH, Emmingen-Liptingen, Germany) at the large defects. At the small defects, a customized probe made of a pure titanium wire – grade 1 for laser welding, round shaped, 0.4 mm diameter (Dentaurum, Ispringen, Germany) – was used. No contacts were verified.

In the right side of the mandible, an additional recipient canal was prepared in a standard way (control site), and the plate for fixation was first adapted at the alveolar crest. Meanwhile, the implant was maintained in a basket to simulate a similar contact with the PEEK material that was obtained for the defect sites. Subsequently, the control implant was installed maintaining the flat surfaces at the apex of the implant parallel to the mesio-distal plane. The fixation plate was loosely attached to the implant using the customized cover screw, and the passivity of the system was checked and corrected if necessary. Three sites for fixation screws were prepared with the dedicated twist drill. The implant/plate assembly was removed from recipient sites and placed into the titanium device (Fig. 3.2c) to tighten the customized cover screw with the calibrated torque screwdriver to 25 Ncm. Again, the unit was placed in the experimental site, and the plate was finally fixed to the alveolar crest with three fixation screws (Fig. 3.3c).

No membranes were used to cover the experimental sites, and the flaps were sutured to allow a fully submerged healing.

Postoperative period

After the surgeries, the animals were given a vitamin compound, anti-inflammatory/analgesic drugs, and antibiotics. The animals were kept in kennels at the university's field facilities with free access to water and feed of moistened balanced dog's chow. Postoperatively, the wounds were inspected daily for clinical signs of complications and cleaning.

Sacrifice

After 3 months of healing, the animals were first anesthetized and then euthanized with an overdose of pentobarbital sodium and subsequently were perfused with a

fixative (4% formaldehyde solution) through the carotid arteries. The mandibles were retrieved en bloc and the surrounding soft tissues detached. The specimens were trimmed and immersed in the fixative solution.

Histological preparation

Individual blocks containing the implants and the surrounding soft and hard tissues were fixed in 4% formaldehyde solution followed by dehydration in a series of graded alcohols and finally embedded in resin (LR White® hard grade; London Resin Company Ltd, Berkshire, UK). The blocks were cut in a mesio-distal plane using a diamond band saw fitted into a precision slicing machine (Exakt®; Apparatebau, Norderstedt, Germany) and then, reduced to a thickness of about 50 lm using a cutting–grinding device (Exakt®; Apparatebau).

The histological slides were stained with Stevenel's blue and alizarin red and examined under a standard light microscope for histometric analysis.

Histological evaluation

In a Nikon Eclipse 50i microscope (Nikon Corporation, Tokyo, Japan) at a magnification of x100, the following landmarks were identified (Fig. 3.4): the shoulder of the implant (IS), the most coronal bone-to-implant contact (B), the implant surface (S), and the bony walls of the implant bed (W).

The following measurements were performed: (i) the vertical distance, parallel to the longitudinal axis of the implant, between IS and B (IS-B); (ii) the distance between S and W (S-W), and (iii) the width of the dense connective tissue attached to the implant (wDCT; Fig. 3.5), measured at levels obtained by dividing the length of the surface of the lateral walls of the implants into three parts and of the apical region into two parts and measuring the distance S-W and DCT in the center of each of these zones. When bone attached to the implant was present, these measurements were omitted. The mean value for the eight measurements was calculated. (iv) The distance between IS and the most coronal level of DCT (IS-DCT) was also measured.

Moreover, (v) the percentage of mineralized bone-to-implant contact (BIC%) as well as (vi) the percentage of DCT (DCT%) in relation to the length of the implant surface were assessed.

Data analysis

Mean value, standard deviation as well as range were calculated for each outcome variable. The primary variables were BIC%, S-W, wDCT, and DCT%. The differences for BIC % between the defects and the control sites as well as the differences between the defects for S-W, wDCT, and DCT% were analyzed using Wilcoxon rank sum test using PASW Statistics 18 (SPSS Inc., Chicago IL, USA). The level of significance was set at $\alpha = 0.05$.

3.2.1.2 FROM: Sivolella et al., 2013 Deproteinized bovine bone mineral particles and osseointegration of implants without primary bone contact: an experimental study in dogs.

Clinical procedures

The protocol was approved by the Institutional Ethic Committee for animal research of the University of São Paulo. Six Labrador dogs (average weight 27.6 kg, average age 2.9 years) were used. During all surgical procedures, the animals were pre-anesthetized with Xylazine® (1 mg/kg intramuscularly [i.m.] Ronpum®; Bayer, São Paulo, Brazil) and Ketamine® (15 mg/kg i.m. Dopalens; Vetbrands, São Paulo, Brazil) and anesthetized with Thionembutal® (20 mg/kg intravenously [i.v.] Tiopentals®; Cristália, Itapira, Brazil). During the entire surgery, the animals inhaled O2 and were kept with an intravenous infusion of saline. Local standard anesthesia was provided before all surgical sessions.

The third and fourth premolars as well as the first molars were extracted bilaterally in the mandible. After 3 months of healing, muco-periosteal full-thickness flaps were elevated and, for the present study, the molar area of the alveolar bony crest was selected bilaterally as experimental sites.

A detailed experimental surgical protocol was presented previously. Customized cylindrical implants, 7 mm in length and 2.8 mm in diameter (Zir-Ti®; Zirconium Sandblasted Acid Etched Titanium, Sweden & Martina, Due Carrare, Padova, Italy), were used. The external macro-morphology of the implant was characterized by the absence of threads and the presence of a modified apical region which presented with two opposing flat surfaces (Fig. 3.1a). The aim of these flat surfaces was to stabilize the implants into the positioning devices used

in the experiment. The internal side of the implants contained threads for the placement of a customized cover screw.

Two recipient sites were prepared, one at each side of the mandible, using a drill of 5.2 mm in diameter to a depth of 8.2 mm to obtain recipient sites wider and longer compared with the implant dimensions, aiming at avoiding any contact of the implant surface with the pristine bony walls of the implant bed after installation (Figs 3.1b and 4.1a). A customized basket made of PEEK (Polyetheretherketone; Sweden & Martina) was fabricated. The basket had the same external morphology and dimensions of the recipient defect sites and the same internal morphology of the implants, but a slightly larger diameter. Only the flat surfaces at the apex of the implants were in contact with the basket to obtain stabilization. Moreover, a notch on the most coronal border, parallel to the apical flat surfaces of the implants, served as reference for implant positioning.

Firstly (Fig. 4.1b), at each of the two defects, the basket was placed within the prepared recipient sites, flush with the mesio-distal bony crest. The notches were placed parallel to the mesio-distal direction for histological purposes. Subsequently (Fig. 4.1c), the implant was positioned within the basket. Straight or L-shaped plates for bone fixation (Module System 1.2 – Titanium, Cizeta Surgical, Bologna, Italy) with at least four holes were adapted around the bony crest with one of the central holes positioned on the implant. The plate was subsequently attached to the implant with a customized cover screw. The passive adaptation of the plate on the alveolar crest and on the implant was checked and corrected if necessary. Three locations of fixation screws were prepared with the dedicated twist drill. The implant/plate unit and the plastic basket were removed from the recipient defect sites. A customized sterile titanium device (Sweden & Martina) with an internal chamber with the same morphology and dimensions of the baskets was used to stabilize the implant/plate assembly. A calibrated torque screwdriver was used to tighten the customized cover screws to 25 Ncm. Care was taken to avoid rotation of the plate in respect of the implants and to maintain the predetermined orientation of the two flat surfaces at the apical portion of the implant.

In the right side of the mandible (control sites; Figs 4.1d and 4.2a), the implant/plate assembly was repositioned in the recipient defects, and the plate fixed to the alveolar bone using three fixation screws of suitable length (4–12 mm). After implant positioning, a three-dimensional gap between the implant surface and the bony walls of the implant bed was obtained that measured 1.2 mm in

width. Possible contacts between the implant and the bone were verified using a titanium periodontal probe (PCPGT 11.5, STOMA®; Storz am Mark GmbH, Emmingen-Liptingen,Germany). No contacts were disclosed.

In the left side of the mandible (test sites; Fig. 4.2b), DBBM particles (Bio-Oss®, granules particles 0.25–1 mm; Geistlich Biomaterials AG, Wolhusen, LU, Switzerland) mixed with saline were first placed within the defect to fill about 2 mm at the bottom, verified by a probe (Storz am Mark GmbH). Subsequently, the implant/plate assembly was repositioned

in the recipient defect, similarly to the control sites, and the plates were fixed to the alveolar bone using three fixation screws of suitable length. Again, the gap between the implant surface and the bony walls was checked for verifying possible contacts between the implant and the bone using the same periodontal probe. No contacts were disclosed. The remaining gap between the implant and the bony walls of the defect was filled with DBBM particles, which were gently pressed towards the apical portion of the implant with the periodontal probe.

No membranes were used to cover the experimental or control sites, and the flaps were sutured to allow a fully submerged healing.

Postoperative period

After the surgeries, the animals were given a vitamin compound (1 mL/10Kg, Potenay®; Fort Dodge Animal Health, Campinas, Brazil;), anti-inflammatory/analgesic drugs (1 mL/10Kg, Banamine®; Schering-Plough, Rio de Janeiro, Brazil), and antibiotics (0.1 mL/Kg, Pentabiotico®; Fort Dodge Animal Health). The animals were kept in kennels and on concrete runs at the university's field laboratory with free access to water and feed of moistened balanced dog's chow.

A daily inspection of the wounds for clinical signs of complications was performed.

Sacrifice

After 3 months of healing, the animals were first anesthetized and then euthanized with an overdose of Thiopental® (Cristalia Ltd., Campinas, Brazil) and subsequently perfused with a fixative (4% formaldehyde solution) through the carotid arteries. The mandibles were retrieved en bloc, and the surrounding soft tissues detached. The specimens were trimmed and immersed in the fixative solution.

Histological preparation

Individual blocks containing the implants and the surrounding soft and hard tissues were fixed in 4% formaldehyde solution followed by dehydration in a series of graded alcohols and finally embedded in resin (LR White® hard grade; London Resin Company Ltd, Berkshire, UK). The blocks were cut in a mesio-distal plane using a diamond band saw fitted into a precision slicing machine (Exakt®; Apparatebau, Norderstedt, Germany) and then reduced to a thickness of about 50 lm using a cutting–grinding device (Exakt®, Apparatebau).

The histological slides were stained with Stevenel's blue and alizarin red and examined under a standard light microscope for histometric analysis.

Histological evaluation

In a Nikon Eclipse 50i microscope (Nikon Corporation, Tokyo, Japan) at a magnification of x100, the following landmarks were identified (Fig. 4.3): the shoulder of the implant (IS), the most coronal mineralized bone-toimplant contact (B), the implant surface (S), and the pristine bony walls of the implant bed (W). The coronal end of the dense connective tissue (D) attached to the implant surface was also indentified.

The following measurements were taken: the vertical distance at the mesial and distal aspects, parallel to the longitudinal axis of the implant, between IS and B (IS-B) and IS and D (IS-D); the mean between the mesial and the distal values was used for both IS-B and IS-D. The distance between S and W (SW) and the width of the dense connective tissue attached to the implant (wDCT; Fig. 4.4) both measured at levels obtained by dividing the length of the surface of the lateral walls of the implants into three parts and of the apical region into two parts and measuring the distance S-W and wDCT in the center of each of these zones. When bone attached to the implant was present, these measurements were omitted. The mean value for the eight measurements was calculated. The percentage of bone filling of the defect was calculated based on the original dimensions of the defect (1.2 mm).

Moreover, the percentage of mineralized bone-to-implant contact (MBIC%) and the percentage of dense connective tissue (DCT%) in relation to the length of the implant surface were assessed.

A point counting procedure was used to determine the composition of the tissue in the "defect" region of all test and control sites at x200 magnification. A lattice was superposed over the tissues, and the percentage area occupied by mineralized bone, bone marrow, connective tissue, and DBBM particles partly integrated into the bone and DBBM particles surrounded only by connective tissue was determined.

Data analysis

Mean values, standard deviations, and ranges were calculated for each outcome variable.

The primary variables were MBIC%, S-W, and filling of the defect. Differences between test (with DBBM) and control sites were analyzed using Wilcoxon test for paired observations using IBM SPSS Statistics 19 (IBM Inc., Chicago, IL, USA). The level of significance was set at $\alpha = 0.05$.

3.2.1.3 From Bressan et al., 2013. Healing of buccal dehiscence defects at implants installed immediately into extraction sockets – an experimental study in dogs

The protocol was submitted to and approved by the local Ethical Committee for Animal Research.

Clinical procedures

Six Labrador dogs (mean weight approximately 27–28 kg and mean age of about 2 years) were used. During the surgical procedures, the animals were pre-anesthetized with Xylazine® [1 mg/kg intramuscular (i.m.) Ronpum®; Bayer, São Paulo, Brazil] and Ketamine® (15 mg/kg i.m. Dopalens; Vetbrands, São Paulo, Brazil) and anesthetized with Thionembutal® [20 mg/kg intravenous (i.v.) Tiopentals®; Cristália, Itapira, Brazil]. During the entire surgery, the animals inhaled O2 and were kept with an intravenous infusion of saline.

The pulp tissue of the mesial roots of 4P4 was removed, the root canals filled with gutta-percha and root canal cement (Mtwo®, Endopocket®, Epfill®; Sweden & Martina, Due Carrare, Padova, Italy). The crowns were subsequently restored with composite (Adonis®; Sweden & Martina). Full thickness flaps were elevated in the right side of the mandible, and the buccal and lingual alveolar bony plates were exposed. The fourth premolar was hemi-sectioned and the distal root removed including the corresponding portion of the crown. The bucco-lingual and mesio-distal dimensions at the coronal margin as well as the depth of the extraction socket were measured using calipers (Castroviejo; KLS Martin Group, Umkirch, Germany) and an UNC 15TM probe (Hu-Friedy, Chigaco, IL, USA), respectively. The width of the buccal and lingual bony walls was measured at a 1 and 3 mm distance apical to the alveolar bony crest using Iwanson calipers (KLS Martin Group). Cylindrical titanium implants, 3.5 mm in diameter and 11 mm in length (Osseospeed®; Astra Tech, Göteborg, Sweden) with a moderately rough surface were used. The recipient sites were prepared in such a way that the implants resulted centered in relation to the mesiodistal axes, but in contact with the inner part of the buccal bony wall (test sites; buccal positioning). The shoulder (IS) was placed at the same level of the alveolar buccal bony crest.

In the left side of the mandible, similar surgical procedures and measurements were performed. The recipient implant sites, however, were prepared in such a way that the implants resulted in contact with the inner side of the lingual bony wall (control sites; lingual positioning). After implant installation, the residual horizontal gap between the implant surface and the inner contour of the bony crest was about 1–1.5 mm at the lingual (test sites) or buccal (control sites) aspects. A standardized triangular-shaped buccal dehiscence defect, about 12 micro-threads deep (corresponding to about 2.7 mm) and

3.5mm wide (like the diameter of the implant) in the coronal region (Fig. 5.1a,b), was prepared bilaterally using a blade (BD Beaver 376400; BD Ophthalmic System, Waltham, MA, USA). An abutment was affixed to the implant and the flaps were mobilized and sutured to allow a non-submerged healing using interrupted VicrylTM 4-0 sutures (Johnson & Johnson, São José dos Campos, SP, Brazil).

After the surgeries, the animals were givena vitamin compound (Potenay®, 1 ml/10 kg; Fort Dodge Animal Health, Campinas, SP, Brazil), anti-inflammatory/analgesic drugs (Banamine®; Schering-Plough Animal Health,

Campinas, SP, Brazil; 1 ml/10 kg) and antibiotics (Pentabiotico®, 0.1 ml/kg; Fort Dodge Animal Health). The animals were kept in kennels and on concrete runs at the university's field laboratory with free access to water and feed of moistened balanced dog's chow.

A daily inspection of the wounds for clinical signs of complications and healing abutment cleaning was performed. The animals were euthanized 4 months after the surgery applying an overdose of Thiopental® (Cristalia Ltd., Campinas, Brazil) and were perfused with a fixative (4% formaldehyde solution) through the carotid arteries.

Histological preparation

Individual bone blocks containing the implant and the surrounding soft and hard tissues were fixed in 4% formaldehyde solution followed by dehydration in a series of graded ethanol solutions, and finally embedded in resin (LR White® hard grade, London Resin Company Ltd, Berkshire, UK). The blocks were cut in a bucco-lingual plane using a diamond band saw fitted in a precision slicing machine (Exakt®; Apparatebau, Norderstedt, Germany) and then reduced to a thickness of about 50 lm using a cutting–grinding device (Exakt®; Apparatebau).

The histological slides were stained with Stevenel's blue and alizarin red and examined in a standard light microscope for histometric analysis.

Histological evaluation

In a Nikon Eclipse 50i microscope (Nikon Corporation, Tokio, Japan) at a magnification of x100, the following landmarks were identified (Fig. 5.2a,b): (IS) the implant shoulder; (B) the most coronal bone-to-implant contact; (BM) the most coronal position of bone-marrow-like structure located above B; (C) the top of the adjacent bony crest; (OC) the outer contour of the alveolar ridge at the buccal aspect; (S) the implant surface at the buccal aspect at the top of the threads; (PM) the top of the peri-implant mucosa; (aJE) the apical portion of the barrier (junctional) epithelium.

The following measurements of the hard and soft tissues were performed parallel to the long axis of the implant: the vertical distance between IS and C (IS-C), IS and B (IS-B), BM and B (BM-B), and PM and B (PM-B). The vertical distances parallel to the long axis between C-B, PM-C, and PM-IS were subsequently calculated.

Moreover, the following measurements of the hard tissue dimensions were performed perpendicular to the long axis of the implant: the horizontal distance between IS and C (GAP); the horizontal distance between S and OC (S-OC) at the buccal aspect, evaluated at IS (level 0 mm) and then, apically, at each subsequent millimeter, up to 5 mm (S-OC0–5 Fig. 5.2a).

Data analysis

Mean values and standard deviations as well as 25th, 50th (median), and 75th percentiles were calculated for each outcome variable. The primary variables were IS-B and IS-C for hard tissue and PM-B for soft tissue outcomes. Differences between test (buccal positioning) and control (lingual positioning) sites were analyzed using Wilcoxon test for paired observations. The level of significance was set at $\alpha = 0.05$.

3.2.1.4 From Bressan et al., 2012. Short implants (6 mm) installed immediately into extraction sockets: An experimental study in dogs

Clinical procedures

The protocol was approved by the institutional Ethic Committee for animal research. Six Labrador dogs (mean weight approximately 27–28 kg and mean age of about 2 years) were. During all surgical procedures, the animals were pre-anaesthetized with Xylazine® (1mg/kg intramuscular [i.m.] Ronpum®, Bayer, São Paulo, Brazil) and Ketamine® (15mg/kg i.m., Dopalens, Vetbrands, São Paulo, Brazil) and anaesthetized with Thionembutal® (20mg/kg intravenous [i.v.] Tiopentals®, Cristália,Itapira, Brazil). During the entire surgery, the animals inhaled O2 and were kept with an intravenous infusion of saline.

As described previously (113), the pulp tissue of the mesial roots of 3P3 was removed, the root canals filled with gutta-percha and root canal cement (Mtwo®, Endopocket®, Epfill®; Sweden & Martina, Due Carrare, Padova, Italy). The crowns were subsequently restored with composite (Adonis®; Sweden & Martina). Full thickness flaps were elevated in the right side of the mandible, and the buccal

and lingual alveolar bony plates were exposed. The third premolar was hemi-sectioned and the distal root removed

including the corresponding portion of the crown. The bucco-lingual and mesio-distal dimensions at the coronal margin as well as the depth of the extraction socket were measured using calipers (Castroviejo; KLS Martin Group, Umkirch, Germany) and a UNC 15TM probe (Hu-Friedy, Chigaco, IL), respectively. The width of the buccal and lingual bony

walls was measured at a 1and 3-mm distance from the alveolar bony crest using Iwanson calipers (KLS Martin Group). A recipient site was prepared and a titanium implant, 4 mm in diameter and 11 mm in length (Astra Tech, Osseospeed®, Göteborg, Sweden) with a moderately rough surface was installed (control site). The implant was placed in the center of the alveolus, with the implant shoulder placed at the same level of the alveolar buccal bony crest (Fig. 6.1a). After implant installation, the vertical distance between the implant shoulder (IS) and the top of the alveolar bony crest (IS-C clinical) as well as the residual horizontal gap (GAP clinical) between the implant surface and the internal contour of the bony crest were measured with a UNC 15TM probe (Hu-Friedy, Chigaco, IL). A healing abutment was affixed to the implant (Fig. 6.1b), and the flaps were mobilized and sutured to allow a non-submerged healing using interrupted VicrylTM 4-0 sutures (Johnson & Johnson, São José dos Campos, Brazil). The same surgical procedures and measurements were performed in the left side of the mandible. However, a shorter implant (6 mm long; Astra Tech, Osseospeed®, Göteborg, Sweden) with the same diameter (4 mm) was placed (test site).

After the surgeries, the animals were given a vitamin compound (Potenay®; Fort Dodge Animal Health, Campinas, Brazil), antiinflammatory/analgesic drugs (Banamine®; Schering-Plough Animal Health) and antibiotics (Pentabiotico®; Fort Dodge Animal Health). The animals were kept in kennels and on concrete runs at the university's field laboratory with free access to water and feed of moistened balanced dog's chow.

A daily inspection of the wounds for clinical signs of complications and healing abutment cleaning was performed. The animals were killed 4 months after the surgery applying an overdose of Thiopental® (Cristalia Ltd, Campinas, Brazil) and were perfused with a fixative (4% formaldehyde solution) through the carotid arteries.

Histological preparation

Individual bone blocks containing the implant and the surrounding soft and hard tissues were fixed in 4% formaldehyde solution followed by dehydration in a series of graded ethanol solutions, and finally embedded in resin (LR White® hard grade; London resin Company Ltd, Berkshire, UK). The blocks were cut in a bucco-lingual plane using a diamond band saw fitted in a precision slicing machine (Exakt®; Apparatebau, Norderstedt, Germany) and then reduced to a thickness of about 50 µm using a cutting–grinding device (Exakt®; Apparatebau).

The histological slides were stained with Stevenel's blue and alizarin red and examined under a standard light microscope for histometric analysis.

Histological evaluation

In a Nikon Eclipse 50i microscope (Nikon Corporation, Tokyo, Japan) at a magnification of x100, the following landmarks were identified (Fig. 6.2): the implant shoulder (IS), the most coronal bone-to-implant contact (B), the top of the adjacent bony crest (C), the top of the peri-implant mucosa (PM), the apical portion of the barrier (junctional) epithelium (aJE).

The following measurements of the hard and soft tissues were performed parallel to the long axis of the implant: the vertical distance between IS and B (IS-B), IS and C (IS-C), PM and B (PM-B), and PM and aJE (PM-aJE). The horizontal distance between IS and C (GAP) was measured as well. The vertical distances between PM-C, aJE-B and PM-IS were subsequently calculated. The linear distance between PM and aJE (PM-aJE surface) and between aJE and B (aJE-B surface) were also measured following the surface of the abutment/implant unit (Fig. 6.2). The amount of bone-to-implant contact (BIC% total) was evaluated around the all implant surface between the most coronal bone-to-implant contact (B) at the buccal and lingual aspects. BIC% was also evaluated at the apical portion of the implant (BIC% apical).

Data analysis

Mean values and standard deviations as well as 25th, 50th (median) and 75th percentiles were calculated for each outcome variable. The primary variable was BIC% total and BIC% apical. Differences between test (short implants) and control (long implants) sites were analyzed using Wilcoxon signed rank test using PASW

Statistics 19 (SPSS Inc., Chicago, IL). The level of significance was set at $\alpha = 0.05$.

3.2.2 HUMAN STUDY

3.2.1.1 From Sivolella et al. 2012. Splinted and Unsplinted Short Implants in Mandibles: A Retrospective Evaluation With 5 to 16 Years of Follow-up

Patient Selection

The patients involved in the present study were treated at the Dental Clinic of the Department of Medicine, Surgery and Dentistry at the University of Padova, Italy. Over a period of 16 years (May 1992 – October 2008), a total of 109 patients (27 men and 82 women) were fitted with 280 implants supporting 135 prostheses, and formed the object of this retrospective analysis. The patients ranged between 32 to 70 years of age (mean 53 years).

The inclusion criteria were: an adequate bone volume at the implant site (at least 7 mm for long implants) as assessed by intraoral radiography and clinical examination; patients treated with at least 1 short implant (7 or 8.5 mm in length); Applegate-Kennedy Classes I and II; good general health at the time of the surgical procedure; no local inflammation or mucosal disease; implants with opposing natural teeth or fixed prostheses (implants opposing partial or total mobile prostheses were ruled out); a minimum follow-up of 5 years. The concurrent use of longer implants supporting the restorations was allowable.

The exclusion criteria were: tobacco habit (more than 10 cigarettes/day); a history of radiotherapy to the head and neck region; leukocyte disorders at the time of the surgical procedure; uncontrolled diabetes; severe jaw clenching or bruxism; inadequate patient compliance; bone grafts or local guided bone regeneration (GBR) before implant placement.

Routinely obtained documentation included: panoramic radiographs taken before the treatment and periapical radiographs taken prior to the treatment, at the time of implant placement, at the time of prosthetic rehabilitation, and yearly thereafter.

The clinical protocol observed for each implant positioned was as follows: in all patients a full-thickness mucosal flap was released and the implant was positioned after donor site drilling. The flap was closed for a submerged healing. No augmentation procedures were performed. The two-stage approach was completed after 4 to 6 months of healing, with surgical re-entry, when an appropriate transmucosal healing abutment was screwed to the implant. Removable prostheses or interim fixed bridges (Maryland bridge) were adjusted if necessary. After 2 to 4 weeks of healing, the implants were loaded with temporary screw-retained prostheses. The definitive cemented prostheses were positioned after one month of provisional functional loading. Zinc oxy-phosphate cement was used to fix the prostheses.

Study Sample

Two hundred and eighty implants were placed in the mandible for the treatment of the 109 selected patients; 44 of them were treated with 145 machined (M) implants (with a machined surface*) supporting 47 FFD (full arch fixed dentures), 6 FPD (fixed partial dentures) and 12 ST (single tooth prostheses); another 44 patients were fitted with 82 rough (R) implants (with a dual-acid-etched surface – Osseotite 3i – Palm Beach Florida USA) supporting 36 FFD, 1 FPD and 18 STs (Table 7.1). Both M (25) and R (21) implants were placed in 15 patients, supporting 15 FFD.

In the above-described prosthetic solutions, short implants were splinted to longer ones, as reflected in Table 7.1: 57% of FPD prostheses and 60% of implants for FPDs were splinted to longer implants and 100% of prostheses and 75% of implants for FFDs were splinted to longer implants. In all, 76% of the prostheses and 66% of the implants considered in the study were splinted to longer implants.

The length of the implants was 7 mm in 139 cases and 8.5 mm in 141. The fixture diameter was 3.75 mm for 185 implants (88 of them were 8.5 mm long, and 97 were 7 mm long), and 95 fixtures were 4 mm in diameter (52 of them were 8.5 mm long, and 43 were 7 mm long). The features of the implants (surface treatment, length and diameter) and their distribution (site) are given in Table 7.2. Seven implants placed in 5 patients were not loaded (6 M and 1 R). If a patient could not be followed up with consecutive annual examinations, the corresponding implants were classified as “dropout implants”.

Clinical and Radiographic Assessments

At follow-up examinations, peri-implant tissues and implant health were assessed using the following parameters: (i) suppuration (presence/absence) (171); (ii) plaque index (score 0-3) according to Mombelli & Lang (172); (iii) probing pocket depth and probing attachment level (173); (iv) bleeding on probing (score 0-3) (171); (v) percussion with evidence of metal (functional ankylosis) or dull sound (fibrous integration in the area of implant placement) (174); (vi) persistent pain or paresthesia.

All cases showing peri-implant inflammation were treated according to the Mombelli and Lang guidelines (172). Intraoral radiographs were taken using the parallel technique to control projection geometry using as exposure parameters 65-90 kV, 7.5-10 mA and 0.22-0.25 s.

The method used to obtain the intraoral periapical radiographs and upload them in the computer was consistent with other reports in the literature (175-177). No customized X-ray holder was provided for any of the patients. A standardized measurement protocol was used (175-177) and the reference measurement was the implant neck diameter, i.e. 3.75 or 4 mm; the measurement system considered the perpendicular distance from the implant shoulder (IS) to the first visible bone-to-implant contact (C) along an ideal line running parallel to the fixture's longitudinal axis; measurements were taken on the mesial and distal sides of each implant (figure 7.1). To correct for any dimensional distortion in the X-ray, the apparent size of each implant (measured directly on the radiograph) was compared with the known implant neck diameter (at the most coronal level of the prosthetic interface), and the following equation:

Implant neck diameter on X-ray ÷ True implant neck diameter = MBL on X – ray ÷ True MBL

was used to establish reasonably accurately the extent of any vertical bone loss on the mesial and distal sides of the implant. MBL measurements were obtained by two operators (A.D.F. and E.B.) blinded to each other's findings.

Radiographs were taken at the time of loading, 12 months later, and annually thereafter; the X-ray images were stored on a PC and analyzed with suitable software to measure peri-implant bone resorption (marginal bone loss, MBL) by comparing intraoral periapical radiographs obtained at the baseline (at the time of

loading) and at latest follow-up evaluation. This analysis was done for each implant-supported prosthesis. Measurements started not after implant placement, but after loading, because the aim was to measure the trend of marginal bone loss (MBL) of the functioning implants (161, 171-177). In fact, the MBL measurement before loading could be related to other “external” factors, e.g. bone remodeling, peri-implant soft tissue healing or surgical procedure (Figure 7.2).

Implants and Prostheses: Success, Survival and Failure

The following parameters were used to define implant success, as suggested by Albrektsson et al. (178), Buser et al. (179) and Roos et al. (180): (i) bone resorption in measurement areas no more than 1 mm during the first year after implant placement, and 0.2 mm a year thereafter; (ii) probing depth no more than 3 mm for each implant site (mesial, distal, buccal, lingual-palatal); (iii) no abutment or implant mobility.

The implant survival rate was calculated considering the following as survivors: (i) implants showing clinical and radiographic signs of peri-implantitis (amenable to treatment); (ii) implants supporting functional, symptom-free prostheses but showing a mean bone loss rate exceeding the limits established for the study (i.e. no more than 1 mm during the first year after implant placement, and 0.2 mm a year thereafter).

Clinical mobility was mandatory for implant removal and the corresponding implants were regarded as “failures”.

Prosthetic failure was defined as one of the following conditions: (i) permanent prosthetic framework warpage or breakage; (ii) abutment or implant-to-abutment connecting screw breakage; (iii) framework-to-abutment fixing screw damage. Prosthetic complications were attributed to the following events: (i) prosthesis detachment; (ii) abutment-to-framework screw loosening; (iii) permanent porcelain veneer warpage or breakage. A prosthesis presenting none of the previous conditions (failures or complications) was defined as a “success”; otherwise it was defined as a “survivor”.

Statistical Analysis

The Wilcoxon signed rank test was used to compare the prognosis of the implants with different lengths (7 mm vs 8.5 mm), diameters (3.75 mm vs 4 mm) and surface treatments (M vs R). For descriptive data, mean values, standard

deviations and frequencies were calculated at patient, prosthesis and implant level. The primary outcome variable was MBL. Life-table analyses were performed, considering implant loss and implant failure as dichotomous events, as explained previously. All tests was performed using a software package.

Finally, a multilevel model with marginal bone loss as the dependent variable was used to determine the relationship between the predictors: implant length (7 vs 8.5 mm), diameter (3.75 vs 4 mm) and surface treatment (M vs R). A regression model was also constructed to analyze factors influencing MBL considering three levels: patient, type of implant, and implant site, with changes in bone level relative to the implant margin at follow-up as the dependent variable. The normality of the residuals at the different levels was also tested. The factors tested were: implant length (7 vs 8.5 mm), diameter (3.75 vs 4 mm) and surface treatment (M vs R).

Regression coefficients were estimated using IGLS (iterative generalized least squares). Nested models were tested for significant improvements in model fit by comparing the reduction in -2LL (-2 log likelihood) with a chi-squared distribution. A statistical package specifically designed for multilevel modeling was used.

4. RESULTS

4.1 IN VITRO STUDIES

4.1.1 From Brun et al. 2013. Mechanisms underlying the attachment and spreading of human osteoblasts: From transient interactions to focal adhesions on vitronectin-grafted bioactive surfaces

Surface characterization and peptide density

Successful silanization of the glass surface upon reaction with APTES was demonstrated using XPS analysis by the presence of N1s signals. On the sample surfaces the amine groups were partially protonated (N2/N1 = 0.4 where N2 = protonated, N1 = unprotonated nitrogens). Peptide immobilization was demonstrated for all functionalized surfaces by: (a) an increase in the C/Si ratio as compared to the silanized surface, (b) increase in the C3/C1 ratio, where C3 was related to peptide carbons and C1 to aliphatic carbons, (c) increase in the N/Si ratio, and (d) decrease in the N2/N1 ratio. The C/Si and N/Si ratios were higher for the nonspecifically compared to the specifically immobilized peptides, indicating that the quantity of immobilized peptides was higher for the former (HVPunsp 3.5%, HVPsp 1%, RGDunsp 2%, RGDsp 0.8%, RAD 1.7%), most probably because of different steric hindrance between fully protected and partially deprotected peptides. As determined by the radiolabeling procedure the peptide densities were: HVPunsp = 36.50 pmol cm-2, HVPsp = 6.95 pmol cm-2, RGDunsp = 20.85 pmol cm-2, RGDsp = 5.56 pmol cm-2, RAD = 17.7 pmol cm-2. As reported elsewhere [19] the peptide density for the titanium disks were HVPsp = 63 pmol cm-2, RGDsp = 16 pmol cm-2. As determined by AFM the APTES coating formed a relatively flat, continuous, thin film with roughness parameters (Table 1.2) consistent with the presence of small aggregates (0.6 nm high) in the z-profile analysis (Fig. 1.1A). The covalently grafted RGDsp formed small and dispersed surface aggregates with an increased surface roughness (Fig. 1.1B) whereas the covalent attachment of HVPsp formed more and larger peptide aggregates (3.5 nm high, 29 nm wide, Fig. 1.1C). In grafted surfaces, roughness parameters were increased as compared to APTES coated surfaces (Table 1.2). RAD glass surfaces were characterized by a relatively rough surface (Table 1.2) with

aggregates of 3.9 nm in high shown by the z-profile analysis (Fig. 1.1D). Following unspecific immobilization RGD showed a quite similar roughness and a presence of large aggregates (3.9 nm high, Fig. 1.1E) similarly to the RAD surface, while HVP formed a relatively flat, continuous, and thin film with sparse aggregates (3.4 nm high, 25 nm wide, Fig. 1.1F).

Surface topography affects osteoblasts adhesion

The extracellular matrix composition and structure act as guidance cues during cellular migration and wound healing and strictly affect cellular behaviour (12). To investigate the effects of RGD and HVP peptides on adhesion and morphology, human osteoblast cells were seeded on functionalized glass surfaces for 2 h, a time previously reported to ensure optimal adhesion to functionalized surfaces (14). Cells were then subjected to immunocytochemistry to investigate expression and distribution of β-actin positive fibres.

As reported in Fig. 1.2A, unspecifically immobilized RGD peptide caused widespread and homogeneous distribution of β-actin-related signal in the intracellular compartment. However, specifically functionalized RGD fostered the organization of β-actin positive fibres leading to an oriented pattern. Following 2 h in culture the expression and distribution of β-actin were comparable in osteoblast cells seeded onto glasses unspecifically and specifically functionalized with HVP peptide. Nevertheless the specific immobilization of HVP increased expression and organization of stress fibres after 6 h in culture.

Cellular attachment was investigated by TIRF microscopy on osteoblasts seeded for 2 h on coverslips silanized or functionalized with unspecifically and specifically immobilized RGD and HVP peptides. In TIRF the incident light leads to the exclusive excitement of the fluorophores lying at 80–200 nm around the aqueous medium–glass interface. Osteoblasts stained with FM 1-43 and seeded on silanized glass coverslips reported weak fluorescent signal with no area of increased dye concentration. Similarly, RGD or HVP unspecifically functionalized surfaces showed a homogeneous adhesion pattern with few cellular protrusions (Fig. 1.2B). Osteoblasts cultured on coverslips functionalized with specifically immobilized RGD or HVP peptides, however, showed a unique distribution of fluorescent signals. Indeed, cells seeded on RGDsp proved an increased fluorescent intensity and signalling pattern localized to discrete areas of the cell membrane consistent with focal adhesion formation (20). Osteoblasts cultured

onto HVPsp functionalized glass surfaces were characterized by a dense formation of membrane structures protruding from one pole of the cells resembling filopodia, i.e. membrane formations at the leading edge of migrating cells involved in sensing guidance cues (21). Indeed, HVPsp functionalized glass surfaces statistically increased the calculated averaging number of filopodia. Thus, evaluating five randomly selected fields from at least four different samples we revealed 9.5 ± 0.28 filopodia per cell in HVPsp glass surfaces as compared to 0.95 ± 0.75 filopodia per cell in HVPunsp coverslips ($P < 0.001$). Silanized glass surfaces, RGDsp and RGDunsp grafted coverslips did not statistically increase the number of filopodia (average number per cell: 1 ± 0.57, 3.5 ± 1.19, 1.5 ± 0.5, respectively). We next evaluated the role of CDC42 a Rho-subfamily GTPase protein involved in formation, extension and maintenance of filopodia (22). As determined by quantitative RT-PCR, CDC42 mRNA transcript levels significantly increased in human osteoblast cells cultured in HVPsp grafted surfaces ($P < 0.02$, Fig. 1.3A). Moreover pre-treatment of osteoblasts with ML141, a pharmacological inhibitor of Cdc42, shortened the filopodia developed by osteoblasts cultured in HVPsp grafted surfaces (Fig. 1.3B).

HVPsp grafted surfaces induce osteoblasts adhesion through different membrane cellular pathways

In accordance with data obtained by immunocytochemical and TIRF analysis, subsequent experiments were performed only on surfaces functionalized with specifically immobilized peptides. To evaluate selective cellular adhesion skills, human osteoblast and fibroblast cells were seeded onto coverslips specifically functionalized with RGD, HVP and mutant (mut) peptide RAD. After 2 h fibroblasts adhered to silanized and peptides grafted glass surfaces, showing a higher adhesion efficiency on RGDsp functionalized surfaces ($P < 0.05$ vs. fibroblasts seeded on silanized and mut glass, Fig. 1.4A). Osteoblasts adhered more efficiently to RGDsp and HVPsp functionalized glasses as compared to silanized and mutant supports. HVPsp grafted surfaces, moreover, bound osteoblasts with the highest avidity ($P < 0.05$ vs. RGDsp) and selected osteoblasts adhesion as compare to fibroblasts ($P < 0.01$).

In an attempt to examine the cellular pathways involved in recognition, attachment and cell adhesion to RGDsp or HVPsp functionalized surfaces osteoblasts were pre-treated with anti-αvβ3 integrin antibody (αvβ3 Ab) or with a mixture of

glycosidases (GAGase), enzymes able to remove the most widespread distributed proteoglycans. Following 2 h of culture the adhesion to different functionalized glass surfaces was evaluated by the MTT test. As reported above (Fig. 1.4A), untreated osteoblast cells adhered more efficiently to RGDsp and HVPsp functionalized glass surfaces than to coverslips functionalized with mutant peptide ($P < 0.05$ and $P < 0.01$, respectively). Pre-treatment with αvβ3 Ab or GAGase did not affect cellular attachment to mutant peptide (Fig. 1.4B) while differentially influenced osteoblasts adhesion to the RGDsp or HVPsp grafted surfaces, meaning that different membrane molecular patterns were involved. Indeed, the adhesion of osteoblasts to HVPsp but not to RGDsp grafted coverslips was dramatically reduced by GAGase treatment (difference vs. untreated cells: 32201 ± 3026 and 7294 ± 1513, respectively), indicating that proteoglycan-mediated interactions are mandatory in cells attachment to HVPsp functionalized surfaces. Osteoblasts incubated with anti-αvβ3 Ab escaped not only attachment to RGDsp functionalized surfaces but also to HVPsp grafted ones (difference vs. untreated cells: 26542 ± 66 and 17615 ± 2831, respectively), suggesting that integrin and proteoglycans are both involved in osteoblast attachment to HVPsp peptide.

HVPsp grafted surfaces induce osteogenic phenotype

As demonstrated by quantitative real-time PCR, RGDsp and HVPsp functionalized surfaces induced gene expression associated with the osteoblastic lineage in primary human osteoblasts but not in fibroblasts (Fig. 1.5). Human alkaline phosphatase (ALPL) mRNA transcript level, a non-bone-specific marker of growing cells, was significantly increased in osteoblasts seeded on RGDsp grafted glass surface whereas vitronectin (VTN) cDNA increased in osteoblast cells cultured on RGDsp and HVPsp surfaces as compare to cells seeded on glasses functionalized with mutant peptide ($P < 0.05$; Fig. 1.5A and B). HVPsp functionalized supports exclusively induced osteopontin (SPP1) and runt-related transcription factor 2 (RUNX2) gene expressions in human osteoblasts (Fig. 1.5C and D).

RGDsp and HVPsp peptides differentially elicit FAK activation in osteoblasts

To scrutinize the downstream signalling elicited in osteoblasts by integrin αvβ3 or proteoglycan-mediated adhesion, cells were cultured on RGDsp and HVPsp functionalized glass surfaces for 30 min–6 h. By immunocytochemistry

phosphorylated FAK-related signals were barely detectable in osteoblasts seeded for 180 min on coverslips functionalized with mutant peptide (Fig. 1.6A). 30 min after seeding p-FAK immunoreactivity was, however, evident in cells seeded on surfaces functionalized with RGDsp and lasted during the culture period. On HVPsp functionalized glasses p-FAK-related signals increased only at 180 min. However, as demonstrated by Western blotting analysis (Fig. 1.6B and C) at longer culture times (6 h) FAK phosphorylation was more pronounced in osteoblasts seeded on coverslips functionalized with HVPsp peptide than in cells cultured on RGDsp grafted surfaces.

In order to evaluate the role of FAK-induced signals in cellular phenotype, osteoblasts were incubated with a chemical inhibitor of FAK phosphorylation and the osteogenic phenotype was monitored by quantitative RT-PCR. Inhibition of FAK significantly reduced the osteogenic-related gene expression in a peptide dependent fashion (Table 1.3).

HVPsp peptide retains adhesion and differentiation skills on titanium surfaces

Since bone implants are commonly made of titanium, the following question was raised: is the osteoblast behaviour observed on RGDsp and HVPsp functionalized glass surfaces also maintained on titanium ones? Adhesion studies were performed on titanium supports having the same surface area of glass coverslips and functionalized with RGDsp and HVPsp peptides. It was found that following 2 h of culture, fibroblasts and osteoblasts adhered to Ti supports (Fig. 1.7A) but contrary to data reported for glass surfaces (Fig. 1.4A), functionalization of Ti surfaces had no effect on fibroblast adhesion. Osteoblast adhesion, however, increased on RGDsp and HVPsp grafted Ti surfaces with a significant raise only in the osteoblasts seeded on HVPsp grafted Ti surfaces ($P < 0.02$ vs. non-functionalized Ti). As assessed by the cellular adhesion test, pretreatment of osteoblasts with anti-αvβ3 Ab affected cell adhesion to RGDsp functionalized Ti surfaces but not to the HVPsp ones

while pre-treatment of cells with GAGase reduced adhesion to HVPsp grafted Ti (Fig. 1.7B). Finally, RUNX2 and SPP1 mRNA transcript levels increased in osteoblasts cultured on peptide grafted Ti surfaces as compared to cells cultured on non-functionalized supports or fibroblasts seeded on grafted Ti supports (Table 1.4). Pre-treatment with anti-αvβ3 Ab or GAGase drastically diminished the SPP1

mRNA transcript levels in osteoblasts seeded, respectively, on RGDsp and HVPsp functionalized Ti surfaces (Fig. 1.7C).

4.1.2 From A novel in vitro technique to evaluate dental implant osseointegration.

The use of dental implants has become wide spread as prosthetic therapy for patients with missing teeth. The success of an implant relies on the presence of adequate bone quantity and quality at the placement site because the implant needs to undergo ‘‘osseointegration’’. In this context, an increased interest in the improvement of osseointegration through topographic and chemical dental implant surface modifications was observed over the last years (4, 181, 182). Bidimensional in vitro studies are usually applied in order to test the biocompatibility of the new material before to start with in vivo test direct to evaluate the osteointegration of the novel implant surfaces in comparison with control ones on cell cultures. These tests attempt to track cell morphology, adhesion, migration, synthesis and deposition of extracellular matrix compounds, cell death related to potentially toxic effects of some agents derived from the biomaterial, histology of the implant osteointegrated, measurement of BIC (bone implant contact) (183, 184).

Current ethical issues restrict the use of animals for experimental purposes in many countries, and encourage to perform preclinical in vitro assays (185), also in the field of dental implant osseointegration (182. 183).

To this view, in this work a novel method to predict dental implant osseointegrationin vitro is proposed. Starting from the experience on stem cell biology and tissue engineering strategy for the in vitro reconstruction of a bone like tissue, available in laboratory (76) we have developed a method to evaluate in vitro the osteointegrative properties of implants. This method require 3 phases as reported in figure 2.3.

In vitro generation of a scaffold combined with an implant.

Customized cylindrical implants were inserted in the bone blocks by means of two customized drilling guides (Figure 2.1b) with a twist drill and dedicated drill stops.

In vitro reconstruction of a 3D bone like tissue.

ADSc are seeded into a scaffold combined with the implant prepared in the previous phase and their commitment into osteogenic line is evaluated by means gene expression (Figure 2.4). The expression of the selected genes (ALPL, CD31, COL1A1, KDR, RUNX2, and PPARG, and PPAR) was evaluated in relation to the expression of a reference gene (GAPDH). Cells seeded on tissue culture polystyrene in cDMEM for 30 days were used as control for data normalization. The expression of osteoblast markers in ADSCs seeded around the dental implants inserted into bone blocks is higher compared to the control condition. Similar results were obtained when comparing the expression level of the same markers in ADSCs seeded on tissue culture plates in presence of osteo-endothelial differentiation medium to the control (Figure 2.1).

Mechanical test: pull-out test

The pull-out test is performed in order to measure the force needed to extract an embedded insert from a concrete mass. The test is performed in quadruplicate and in three different conditions:a)non cultivated bone blocks (dry); b) non cultivated bone blocks, soaked in osteo-endothelial differentiation medium for 30 days (immersed); c) bone blocks loaded with ADSCs in osteo-endothelial differentiation medium for 30 days (cultivated). Dry (a) and immersed (b) samplesare considered as controls.

The results of the mechanical tests, summarized in figure 2.5, show that the highest average pull-out strength value was observed in the cultivated group (7.66 N ±1.30) wheather results for dry and immersed samples were similar (average values 1.52 N ± 0.70 and 1.96 ± 0.56, respectively). Interesting, the pull-out force increased about 4 times after cultivation. Significant differences were observed for cultivated specimens related to the others ($P<0.05$), and no statistical difference was observed between dry and immersed samples ($P>0.05$). In order to confirm that this pull out force is due to the presence of the cells, we performed SEM analyses on dental implants pulled-out respectively from dry bone blocks (Figure 2.6a) and from seeded blocks (Figure 2.6b). As can be seen in Figure 2.3b,

ADSCs adhering to the surface of the removed implants show an osteoblast morphology.

4.2 RESULTS FROM IN VIVO STUDIES

4.2.1 PRECLINICAL STUDIES

4.2.1.1 From Sivolella et al., 2012. Osteogenesis at implants without primary bone contact – An experimental study in dogs.

The healing period was uneventful. During the last month, one cover screw at the small and two at the large defects as well as three at the control sites were slightly exposed to the oral cavity. Cleaning of the cover screw was initiated. No signs of chronic inflammation/
infection were observed at any of the sites during the experimental period. No artifacts occurred, nor were there any tissue blocks destroyed. Hence, test and control sites yielded an n = 6.
At sacrifice, all cover screws were still in place. Moreover, no gaps were identifiable between the fixation plate and the implant shoulder as well as between the fixation plate and the cover screw. In almost all specimens, at least one fixation screw was included in the histological section. All visible fixation screws, but one at a control site, demonstrated optimal osseointegration and no signs of inflammation.
In five of six implants at the small defects, a limited amount of bone-to-implant contact was found (5.3%) mostly located in the apical half of the implant (Fig. 3.6a). The most coronal contact of the bone to the implant was, in fact, at 4.4 mm apically to the implant shoulder (IS-B). At the large defect sites, only one implant showed a small amount of bone in contact with the apical region (ISB = 6.4 mm; BIC% = 0.3%), whereas no bone was found in contact in the other sites (Fig. 3.6b). Conversely, all control implants were osseointegrated in mature bone presenting with an IS-B of about 1 mm and a BIC% of 46.1% (Fig. 3.6c).

Statistically significant differences were found for BIC% comparing the small and large defects, and between defects and controls (Table 3.1).

The original defects were only partly filled with newly formed bone. A residual defect surrounding the implant was found at all sites where the surface was not in contact with the bony walls (Fig. 3.6a and b). The walls of the defects (W) were composed of mature bone that yielded a cortical nature (Fig. 3.6a and b). The width of the residual defects (SW) was 0.39 ± 0.17 and 0.50 ± 0.09 mm at the small and large defects, respectively. The difference did not reach statistical significance. Considering the original size of the defects, the corresponding fill was 43.7 ± 24% and 58.7 ± 7.5% at the small and large defects, respectively (Table 3.2).

The residual defects contained two connective tissues characterized by two different densities (Figs 3.7a–d and 3.8a–d). (i) A layer of dense connective tissue (DCT) was observed adherent to the implant surface, coronally located on average at 0.34 ± 0.45 and 0.38 ± 0.69 mm from IS (IS-DCT), at the small and large defects, respectively.

DCT was in some specimens seen in continuity with a similar, but thicker tissue, above the level of the bony crest. DCT was rich in fibers and fibroblast-like cells, both orientated parallel to the surface of the implant. The average width of DCT (wDCT) was 0.08 ± 0.04 and 0.10 ± 0.06 mm, at the small and large defects, respectively (Table 3.3). The difference was not statistically significant. (ii) A low density connective tissue, rich in vessels and characterized by less fibers compared with the DCT, was observed in the space between DCT and W. Bone marrow was often observed within the residual defect, in continuity with the surrounding bone. The percentage of the implant surface covered by DCT (DCT%) was 92.8 ± 7.60% and 95.6 ± 5.7% at the small and large defects, respectively (Table 3.3). The difference did not yield statistical significance.

DCT was also observed in some areas at the control implant surfaces (Fig. 3.9a), similar to that at the defect sites (Fig. 3.9b).

4.2.1.2 From Sivolella et al., 2013. Deproteinized bovine bone mineral particles and osseointegration of implants without primary bone contact: an experimental study in dogs.

The healing was uneventful. During the last month, two cover screws at the control were slightly exposed to the oral cavity. Cleaning of the cover screw was initiated. No signs of chronic inflammation/infection were observed at any of the sites during the experimental period. No artifacts occurred, nor were there any tissue blocks destroyed. Hence, test and control sites yielded an n = 6.

At the histological evaluation, all cover screws were still in place (Fig. 4.5a-l). Moreover, no gaps were identifiable between the fixation plates and the implant shoulders as well as between the fixation plates and the cover screws. In almost all specimens, at least one fixation screw was included in the histological section. All visible fixation screws demonstrated no loosening or fracture, and histologically, optimal osseointegration and no signs of inflammation were evident.

Histological linear measurements are reported in Table 4.1. The average of IS-B was 0.96 ± 2.35 mm and 0.54 ± 1.31 mm for control and test sites, respectively ($P > 0.05$). The mean mineralized bone-to-implant contact percentage (MBIC%) was approximately 4% both at the control and at the test sites, and hence, no statistically significant differences could be detected. Mineralized bone-to implant contact was only observed in two of the twelve implants, in one control (Figs 4.5f and 4.6a) and in one test implant (Figs 4.5h and 4.6b), respectively, in which a similar MBIC% was found (~24%).

The original defects were only partly filled with newly formed bone. A residual defect surrounding the implant was found at all sites where the surface was not in contact with the pristine bony walls. The average distance S-W was 0.48 ± 0.12 mm and 0.88 ± 0.41 mm at the control and test sites, respectively, the difference being statistically significant. Considering that the original gap of 1.2 mm, the percentage of the defect fill was 60.0 ± 9.7% and 26.8 ± 34.1% for control and test sites, respectively, obviously mirroring a statistically significant higher degree of filling of the former in comparison with that of the latter sites.

A layer of dense connective tissue was observed adherent to most of the implant surfaces (Figs 4.6b,c and 4.7a-d). The average IS-D was 1.44 ± 1.84 mm and 0.36 ± 0.66 mm for control and test sites, respectively ($p > 0.05$). The percentage of dense connective tissue adherent to the surface in relation to the length of the implant was similar, 84.9 ± 17.8% and 88.5 ± 16.7% for control and test sites, respectively.

The dense connective tissue was, in some specimens, in continuity with a similar, but thicker connective tissue, above the level of the bony crest. The average wDCT was the same for both the control and the test implants (0.12 mm).

Table 4.2 reports the morphometric data. Mineralized bone, bone marrow, and connective tissue were evaluated. Moreover, in the test group, DBBM particles partly integrated into the bone and DBBM particles surrounded only by connective tissue were also assessed (Figs 4.6b, d, and 4.7a-d). No statistically significant differences were observed between control and test sites for any of the morphometric parameters, except for the percentage of bone marrow, which was greater in the control (37.2 ± 12.8%) compared with the test sites (12.9 ± 9.9%).

4.2.1.3 From Bressan et al., 2013. Healing of buccal dehiscence defects at implants installed immediately into extraction sockets – an experimental study in dogs

Clinical evaluation

The dimensions of the alveolar extraction sockets are reported in Table 5.1. No statistically significant differences were found for any of the variables evaluated between test and control sites.

During the healing period, no complications were observed, and all implants were available for histological analysis.

Histological evaluation

No artifacts occurred during the histologic preparation, and hence, test and control sites yielded an n = 6.

The data related to the hard tissues measurements are reported in Table 5.2.

A partial regeneration of the buccal bony crest was found both at the test and control sites (Fig. 5.3a,b). At the test sites, where the implants were positioned buccally, the distance IS-C was 1.71 ± 1.20 mm. However, bone-to-implant contact level was found at a similar apical limit of the 2.7 mm deep original defect as documented by the distance IS-B (2.50 ± 1.21 mm). At the control sites, a more coronal level of the bony crest (IS-C = 0.68 ± 0.63 mm) as well as of the coronal border of osseointegration (IS-B 1.69 ± 0.99 mm) were observed compared with test sites. The differences yielded statistical significance. Marginally remaining

bone defects were found buccally and lingually, both at the test and control sites. The depth of the residual buccal defects was slightly lower at the test (0.78 ± 0.85 mm) compared with the control sites (1.01 ± 1.17 mm). The difference did not reach statistical significance. At the lingual aspect, the depths of the remaining defects were higher at the test (2.09 ± 1.01 mm) compared with the control sites (1.01 ± 0.48 mm), the difference being statistically significant. In most instances, the defects were occupied in their apical portion by a bone-marrow-like tissue in direct contact with the implant surface (Fig. 5.4a–c). The mean distances between B and BM ranged between about 0.3–0.6 mm. The horizontal width of the defects ranged between 0.36–0.42 mm at the buccal and 0.39–0.81 mm at the lingual aspects. None of the differences were statistically significant.

The mean values of S-OC0–5 both at the test and control sites after 4 months of healing are reported in Fig. 5.5. A wider width of the bony ridge at the buccal aspect was found at the control than at the test sites. No statistically significant differences were found at any of the levels evaluated.

The data related to the soft tissue dimensions are reported in Table 5.3. The soft tissues were well developed around the abutment/fixture unit, and scarce inflammatory infiltrates were found within the connective peri-implant tissues. The dimensions of the peri-implant mucosa in relation to PM-C were similar in the two groups. Also, the distance PM-B was similar at the buccal aspect while, at the lingual aspect, a higher value was observed at the test (4.69 ± 1.20 mm) compared with the control sites (4.01 ± 0.68 mm), even though the difference did not yield statistical significance. The top of the mucosa (PM) was located more coronally at the control compared with the test sites with respect to IS, both at the buccal (3.41 vs. 2.56 mm, respectively) and lingual aspects (3.53 vs. 3.00 mm, respectively). None of the differences reached a statistical significance.

4.2.1.4 From Bressan et al., 2012. Short implants (6 mm) installed immediately into extraction sockets: An experimental study in dogs

Clinical evaluation

The dimensions of the alveolar extraction sockets are reported in Table 6.1. The buccolingual dimensions were 4.2 ± 0.3 and 4.8 ± 0.8 mm at the test and control

sites, respectively. The difference did not reach statistical significance. The width of the buccal bony crest 1 mm below the top of the crest was lower at the test compared with the control sites. The difference was statistically significant.

After implant installation, the implant shoulder was located deeper in relation to the top of the lingual bony crest of 0.6 ± 0.5 and 0.6 ± 0.9 mm at the test and control sites, respectively (IS-C clinical; Table 6.2).

Small horizontal gaps (GAP clinical) occurred at the control sites between the implant surface and the inner contour of the alveolar bony crest (Table 6.2). At the test site, the horizontal GAP was minimal (0.1 mm). The difference to the control sites did not reach statistical significance.

During the healing period, no complications were observed and all implants were available for histological analysis.

Histological evaluation

No artifacts occurred during the histologic preparation; hence, test and control sites yielded an n = 6.

The implants appeared to be well integrated into mature bone (Fig. 6.3a and b). BIC % total was slightly higher at the test compared with the control sites (54.4 ± 14.2% and 49.0 ± 20.2% (Table 6.3). The difference, however, was not statistically significant. The apical region of the implant presented with newly formed bone attached to the surface both at the test and control sites (Fig. 6.4a –d). The BIC%-apex was about 33% and 21% at the test and control sites, respectively. Again, the difference did not reach statistical significance.

Both at the test and control sites, the bony walls were partly resorbed at the buccal and lingual aspects (Table 6.3). The bony crest (C) as well as the most coronal bone-to-implant contact point (B) were located more apically at the test compared with the control sites. However, the differences did not reach statistical significance both at the buccal and lingual sites.

Small residual defects were detectable around the marginal portion of the implant (GAP, Table 6.3).

The soft tissues appeared to be well adapted around the neck of the implant and the healing abutment. No inflammatory infiltrates were found within the connective peri-implant tissue. The dimensions of the peri-implant mucosa were similar in both groups (Table 6.4).

When the straight vertical measurements (assessed in the long axis of the implant) of the peri-implant soft tissues were compared with the measurements assessed along the surface of the implant, statistically significant differences were revealed, with the latter assessment always being greater than the former (Table 6.4).

4.2.2 HUMAN STUDIES

4.2.2.1 From Sivolella et al. 2012. Splinted and Unsplinted Short Implants in Mandibles: A Retrospective Evaluation With 5 to 16 Years of Follow-up

As at the time of data collection (2009), 7 implants were removed before loading and were considered as “early failures”: 6 of them were 7 mm long (with diameters of 3.75 mm and 4 mm in 3 and 4 cases, respectively); and 1 was 8.5 mm long (and 3.75 mm in diameter). The mean follow-up for the 280 implants was 9 years (range 5-16 years). Complications were observed for 8 implants in 8 patients, involving clinical signs of peri-implantitis in all 8 cases. Causal mechanical treatment and local antibiotic therapy were administered, followed by guided bone regeneration in 2 cases, using bovine bone mineral and collagen membrane to treat the peri-implant defects. No further pathological progression of bone loss was observed at subsequent follow-up visits for 4 implants, while the other 4 implants had to be removed (Table 7.3).

During the follow-up, 14 patients with 39 implants (corresponding to 13.9% of the implants placed) and 14 prostheses were lost to follow-up and considered as “dropouts”.

The reasons for dropping out were death in 3 cases, while the other 11 patients could not be reached.

A multilevel model analysis was performed to explore the covariates influencing bone loss at the implant site, starting from an empty model that included no covariates (Table 7.4), which generated a mean value of 1.45 mm for bone loss and a total unexplained variance of 0.45 (42% attributed to variability between sites, 36% between implants, and 22% between patients). None of the predictors considered in the final model (years of follow-up, opposing teeth, implant diameter,

implant length, implant surface treatment) had a significant impact on bone loss between the baseline and the follow-up examinations. There were no statistically significant differences between the variables. Since MBL measurements were obtained by two operators blinded to each other's findings, the correlation between the two measurements was calculated with Pearson's correlation test (r=1). A p value of 0.05 was detected using years of follow-up as a covariate, with a mean yearly bone loss of 0.04 mm. For all the short implants considered, the mean MBL was 1.38 mm (SD 0.45 mm) on the mesial side of the fixture, and 1.36 (SD 0.5 mm) on the distal side. The MBL findings relating to M and R implants are given in Table 7.5.

Survival and success rates (SSR and SR) were calculated using life-table analysis for the M and R short implants (Table 7.6). For the M fixtures, the 16-year SSR was 95.7%, and the corresponding SR was 93.9%. For the R fixtures, the 16-year SSR and SR were 97.2 and 95.2%, respectively.

The SSR for M implants was not significantly lower (p=0.17) than for R implants after 16 years of use, while the 16-year SR was slightly lower for M than for R implants, though the difference was not statistically significant (p=0.47).

No significant difference emerged when Wilcoxon's signed rank test was used to compare the long-term prognosis (at 10 and 16 years) between different lengths (7 mm vs 8.5 mm), diameters (3.75 mm vs 8.5 mm) and surface treatments (M vs R), for which the calculated p-values were respectively: p =0.38 (lengths), p =0.34 (diameters) and p=0.47 (surface treatments).

The following prosthetic complications were recorded. There were 8 cases of decementation: the prostheses were fixed in place again with zinc phosphate cement or zinc-eugenol oxide cement. Veneer chipping occurred on 21 partial prostheses: 2 were STs, 15 were FPDs, and 4 were FFDs; only 14 of these prostheses were removed, veneered and put back in place. Two abutment screws worked loose: after decementing the 2 ST prostheses, the screws were torqued again according to the manufacturer's recommendations and the occlusal contact was checked again. There were 2 cases of abutment screw breakage concerning 2 ST prostheses: after removing the crowns, the broken screws were removed and replaced; the 2 abutments were placed in position and the single crowns were attached with zinc phosphate or zinc-eugenol oxide cement. No prosthetic failures were observed during the follow-up. On the whole, 33 prosthetic complications

were recorded in 29 patients. The prosthetic success rates were thus 75.7% and 77.3% for patients and prostheses, respectively.

5. DISCUSSION

The presented studies lead to numerous issues for discussion.

During osseointegration the interaction of cells with foreign surfaces is mainly regulated by the physicochemical properties of the material. Indeed hydrophilic, positively charged and nanostructured substrates make adhesion sites more accessible to membrane receptors (186). HVPand RGD-grafted surfaces were characterized by XPS and AFM analysis and subsequently tested for the selective attachment and spread of human osteoblast cells. The images obtained by immunocytochemistry and TIRF microscopy (Figs. 1.2 and 1.6) indicate that, unlike unspecifically immobilized sequences, specifically immobilized RGD and HVP peptides affect the membrane imprint and the stress fibre organization. However, the different peptide densities obtained on unspecifically and specifically functionalized glass surface did not completely rule out the influence of peptide concentrations on the observed cellular behavior. In our study osteoblasts attach at RGDunsp and HVPunsp grafted glass surfaces (peptide density >20 pmol cm-2) without forming focal adhesions whereas on RGDsp and HVPsp grafted surfaces (peptide density <7 pmol cm-2) cells adhere through focal contacts spreading with well-organized stress fibres (Fig. 1.2). Our data apparently disagree with other reports. For example, Shahal and colleagues have recently pinpointed that only RGD densities higher than 23 pmol cm-2 induce cellular spread and peripheral actin organization (187). Nevertheless, since the RGD peptides considered in this study presents four RGD motifs per chain the densities of active motifs on both unspecifically and specifically functionalized surfaces are, indeed, very close to the previously reported threshold concentration (187). Moreover, despite the different peptide densities the cellular adhesion capability evaluated in specifically functionalized titanium surfaces was similar or even improved as compared to specifically functionalized glass surfaces (Figs. 1.4 and 1.7), suggesting that the enhanced performance of the surfaces might result from the projections of amino acidic chains properly interacting with devoted cellular membrane structures (187). In this setting different nanoroughness of material surfaces might greatly influence cell attachment. Thus, nano-scale surfaces features of differently etching materials modulate surface free energy and wettability and finally decrease fibroblast adhesion but tether osteoblasts (189). Moreover nanostructure with features

usually below 100 nm influences the clusterization of membrane structures involved in attachment and critically controls spatial adhesion of cells (188).

Two broad categories of adhesion sites can be distinguished as ‘‘focal complexes’’ associated with lamellipodia and filopodia supporting protrusion and traction at the cell front and as ‘‘focal adhesions’’ at the termini of stress fibre bundles that serve in longer term anchorage (190). In our study, human osteoblasts cultured for 2 h on HVPsp grafted coverslips develop filopodia (Fig. 1.2B) highly dynamic cytoplasmic extensions provided of sensory and mechanical roles (187) whereas RGDsp peptide tethers cells on glass and titanium surfaces mainly through integrin receptors. It is widely recognized that surface-dependent differences in membrane structures binding regulate cellular responses and modulate osteoblastic differentiation (191). Indeed, integrin-mediated cellular adhesion induces mitogen-activated protein kinase (MAPK) and focal adhesion kinase (FAK) (192). FAK autophosphorylation (p-FAK) connects the membrane adhesion patches to the actin cytoskeleton acting as gatekeepers for extracellular signals regulating cell adhesion, differentiation, bone regeneration and mechano-transduction (193). Unlike RGDsp, HVPsp peptide blunts p-FAK expression within 3 h of cultures (Fig. 1.6A), consistent with downregulated FAK and Rho expression during filopodia extension (194). Nevertheless, HVPsp grafted surfaces finally support stable osteoblasts differentiation (Figs. 1.5–7). Our experimental observations strongly support the hypothesis that the simultaneous grafting of both bioactive peptides could exert synergistic effects, thus promoting the specific bond of human osteoblasts compelling to differentiation.

The development of in vitro techniques for the study of implant osseointegration find new applications in three-dimensional tissue engineering models.

Our results demonstrate that when we insert an implant in a scaffold enriched with ADSCs (namely “live scaffold”) committed into osteoblastic like phenotype (confirmed by gene expression analyses), the cells colonize the implant surface with osteoblast-like morphology as revealed by SEM images. The presence of osteoblasts adhering to dental implant surfaces is also described in retrieved implants in vivo animal and human studies. Subsequent Pull-out test confirmed that if the implants are inserted in a live scaffolds, we need a significant higher force to extract the implants compared to the controls represented by a scaffolds

on which cells were not present. Pull-out tests were performed to evaluate the implant stability, related to contact between dental implant surface and the cellularized mineral matrix. They are mainly applicable for non-threaded cylinder type implants, whereas most of clinically available fixtures are of threaded design, and their interfacial failures are dependent on shear stress (195). In the present study, an increased stability of moderately rough cylindrical flat implants over time was achieved, due to the spreading, the proliferation, and the differentiation of ADSCs cultured in the 3D scaffolds in the presence of osteo-endothelial differentiation medium. In fact, average pull-out strength value resulted increasing about 4 times after cultivation when compared to controls (dry and immersed). Results confirmed the achieved osseointegration in vitro in the test samples and were consistent with the presence of osteoblasts revealed by gene expression.

Pull-out tests have been widely performed in vitro using polyurethane blocks, which simulate mechanical properties of human bone (196). They have been used for mechanical tests on orthopedic implants (197) and on dental implants (198, 199, 200, 201). However, solid rigid polyurethane blocks can be used as an alternative for human jaw bone to determine the primary stability of the implants, but cannot evaluate the secondary stability related to the dynamic process of osseointegration. Thus, in vivo investigations are needed to detect the extent of bone formation along the implant surface. Ex vivo mechanical tests (torque, pull-out, push-out) usually measure the amount of force or torque to interface failure of implants in bone. In a rabbit tibial dental implant healing model, Seong and co-workers found that failure load at pull-out test was significantly correlated withsecondary implant stability (202). Their results agrees with studies done by Baker et al. (203). They investigated in short-term healing in the rabbit tibia two different implant surfaces. The dual-etched surface demonstrated a more rapid rate of pull-out strength gain than the machined surface and remained significantly stronger throughout the 8 weeks of the study, even though in both the groups the pull-out force increased over time in relation to secondary implant stability

To the best of our knowledge, no study has been published using a 3D tissue-engineered bone model to evaluate dental implant osseointegration in vitro, for this, mechanical pull-out data, acquired with the presented novel method, are not comparable with others in current both in vitro and in vivo studies.

There is not doubts that our in vitro studies have not been able to reproduce the dynamic environment that involves the in vivo bone-implant interaction, and that

our results have to be confirmed in animal models,but we can assume that osseointegration, defined as the close structural and functional contact between bone and implant (204), Is achieved in this 3D in vitro tissue-engineered bone model.

The same moderately rough implant surface used in the study on osseointegration in the in vitro three-dimensional tissue engineering model, was used for the study on peri-implant bone formation in animal experimental conditions.

The first in vivo experiment evaluated the healing at implants placed into two standardized defects of different sizes larger than the dimensions of the implant in order to avoid contact with the implant bed after installation. After three months of healing, only small areas of bone were found in contact with the implant surface, mainly located in the apical half of the implant. BIC% for the total implant circumference was, however, higher at the small compared to the large defects. The fact that no initial contact between the implant bed and the surface of the implant was assured at implant installation means that the direct bone-to-implant contact observed in the present study may be interpreted as contact osteogenesis (89). Obviously, the implant surface used in the present study provided a microstructure that was conducive to osseointegration, as demonstrated in the control sites and also in the defects sites, even though to a limited extent. Although unlikely, it cannot be excluded that the bony contact with the implant observed in the present study at the defect sites may have originated as a result of a proliferation from parent bone, i.e. distance osteogenesis (89).

The results from the present study are in agreement with another experiment in rabbits (93) in which cylindrical titanium implants with three different diameters were inserted into the center of 3.7mm standardized holes prepared in the tibia of rabbits. The implants were stabilized by the use of a plate anchored to the surrounding bone. One implant had the same diameter of the hole, while two had reduced diameters so that, after implant placement, residual three-dimensional gaps of different dimensions (0.35mm and 0.85mm) occurred between the lateral walls of the defect and the implant surface. It was shown that, after 4 and 12 weeks of healing, only the implants in contact with the bony walls yielded a proper integration. This indicated the necessity of initial bone contact for the osseointegration process. It has to be stressed, however, that the cp titanium implants installed in that model were machined with no additional surface treatment.

In the present experiment, 0.7mm and 1.2mm wide defects around implants were obtained. The defects <1mm presented the condition to allow the newly formed bone to cross the gap by one single jump (osteogenic jumping distance; 77, 205, 78) while, in the larger defects, more jumps were needed by the woven bone to bridge the gap. Nevertheless, also in the small defects a very low degree of osseointegration was observed.

Another experiment (94) on implants without initial bone contact was performed on the mandibular ramus of rats. A rigid hemispheric non-resorbable capsule was fixed onto the ramus with screws. A hole was prepared in the middle portion of the capsule, and an implant with a rough (SLA) surface was placed through the hole. In one side of the mandible (control) a contact was obtained between the apex of the implant and the bone surface of the ramus, while, on the contralateral side, the implant apex was placed not in contact with the bone (test). At the test sites, no bone was formed at any time of healing intervals from 1-9 months while, at the control sites, newly formed bone in contact with the implant was observed increasing over time, and filling a secluded space underneath the capsule. It was argued that the lack of osseointegration at the test sites was due to implant micro-mobility that facilitated the formation of a layer of loose and fibrous connective tissue interposed between newly formed bone and the implant surface.

In the present study, efforts were made to obtain a secure primary stability of all implants using positioning devices. In fact, the fixation plate was accurately adapted to the alveolar crest in order to achieve a passive, but intense stability. Three fixation screws were used in all sites to assure a three-dimensional fixation. This, in turn, means that micro-movements were unlikely to occur. In fact, 5 out of 6 at the small and 1 out of 6 implants at the large defects presented bone in contact with the implants, even though to a limited extent. To assure that contact of the implant surface with the bed was avoided circumferentially at the time of installation precise instruments were used for the installation of the implants and the circumferential gap was checked applying a titanium periodontal probe. Nevertheless, it cannot be excluded that the initial gap (S-W distance) was reduced in some regions, thus favoring bone formation in the peri-implant gap.

In the present model, membranes to cover the entrance of the circumferential defects were not applied. This means that the defects were not in themselves secluded. Moreover, the flaps were repositioned on the top of the defects to allow a fully sub-merged healing. It can be speculated that connective tissue from the

supracrestal region migrated between the bony walls and the implant surface interfering with the osseointegration process. After three months, the defects were filled with newly formed bone that did not reach the implant surface in its entire length. A space from the implant of about 0.4-0.5mm filled with connective tissue was maintained. A similar pattern of healing was previously described in an experimental study in dogs (83). Recipient sites, 10mm in length and 2.8mm in width, were prepared. The most coronal 5mm of the recipient sites were widened and implants were installed. A circumferential marginal gap, 5mm deep and 1.25mm wide, was obtained. Membranes were placed on the experimental sites. After 1 month of healing, the marginal defects were filled with newly formed bone that was, however, attached to the implant surface only in the apical portion of the defects. A 0.4mm thick connective tissue, similar to that of the present study, was found to be interposed between the front of the newly formed bone and the implant surface. A similar outcome was described in a subsequent experiment in dogs in which marginal defects of different sizes were prepared around implants and no membranes were applied (87). Again, connective tissue, comparable in dimension and characteristics to that observed in the present study, was found interposed between the newly formed bone and the implant.

In the previously described studies (83, 87), only 1-2 months of healing were allowed. It should be emphasized, however, that in a similar experiment in dogs, an almost complete resolution of the defects was found after 4 months of healing independently of whether or not membranes had been used (78).

In the present study, the residual defects at the test sites contained two connective tissues characterized by two different densities. The layer of dense connective tissue (DCT), approximately 0.08-0.10mm in width, was observed adherent to most of the implant surface (about 93-96%). This tissue was described previously in other experiments in dogs (83, 87) and it was suggested that this condensed connective tissue may represent an osteoid that, over time, may become mineralized and hence, integrated to the implant surface. In the present study, however, the presence of a DCT did not favorite osseointegration after three months of healing.

In the studies described above (83, 87), osseointegration within the defect initiated where the implant was primarily embedded into the parent bone, that is in the region of the implant adjacent to the base of the defect, and then proliferated coronally on the implant surface. This may have a clinical relevance in relation to

implants installed into fresh extraction sockets or in chronic bone defects or in conjunction with sinus floor elevation.

The second in vivo experiment evaluated osseointegration at implants placed at a distance of at least 1.2mm from the pristine implant bed. The resulting circumferential defect was left to fill with either a blood coagulum alone or was additionally filled with demineralized bovine bone mineral (DBBM), at the control and test sites, respectively. A minimal percentage of mineralized bone-to-implant contact (MBIC%= 4%) was found, irrespective of the use of DBBM particles. The minimal MBIC% found in the present study for the control sites confirmed the results of the previous study with the same design. It is evident from the present and the previous study that the size of the circumferential defect, and the initial contact with the recipient bony walls, had a determining role for the formation of a direct bone to implant contact. This is also in agreement with a similar experimental study in rabbits (93).

In the present study, great care was applied to obtain a primary implant stability. The importance of this prerequisite for the osseointegration process of implants has also been documented in a rat model (94).

The application of DBBM at the bottom and into the circumferential large defect at the test sites in the present study did not influence the minimal osseointegration. In fact, none of the linear variables evaluated showed statistically significant differences with the exception of those related to filling of the defect. In essence, the distance between the front of the newly formed bone and the implant surface reflected a better filling of the defect at the control (S-W 0.5mm) compared to the test (S-W 0.9mm) sites. Also, the percentage of defect filling with newly formed bone was about 60% and 27% at the control and test sites, respectively. It may be speculated that the filling of the large circumferential defects with DBBM may have impinged on the healing process by jeopardizing the development of the vascular structures necessary for bone formation (206) and hence, connective tissue proliferated into the gap from the coronal regions of the mucosae.

While at the control sites, the periphery of the remaining bony defect reflected the shape of the implants, in the apical regions of the test sites it represented a “pear-shape” where the DBBM particles were mainly surrounded by connective tissue. However, this often appeared to be denser when in contact with the graft indicating that the mineralization process may have been initiated, but certainly not finished. It may be speculated that the observation period of 3 months may not

have been enough for new bone formation on the surface of DBBM particles, since those were only partly embedded into mature bone. Moreover, some particles were found beyond the dimensions of the original defect. This is indicative for the fact that the graft particles may have been pushed into the bone marrow spaces at the time of surgery. When packing of DBBM particles is too dense, this would result in limitations in capillary growth and neo-angiogenesis (207, 208, 209). Furthermore, the risk of crushing DBBM particles and loosing the trabecular architecture when using force, hereby altering the DBBM resorption pattern, is also possible (210). Dense packing may also result in a higher percentage of DBBM particles occupying the defect (211)

In the present study, the percentage of DBBM particles in the defects after 3 months was about 35%. This, in turn, denotes a denser packing of the graft material compared to results of other studies in which 13-31% of residual DBBM percentage was found (95, 211, 97, 112). Despite the possibility of having densely packed the biomaterial in the present study, 13% of the evaluated area was occupied by graft particles integrated in bone, hereby confirming the osteoconductive properties of DBBM (96). Although not evaluated in detail, in some of the areas where DBBM appeared to be present in a high percentages (Figs. 4.5H and L), a good integration of the biomaterial was achieved, while in other specimens that showed lower percentages of DBBM (Fig. 4.5 I and K), a low integration of the biomaterial was found.

Rarely, DBBM particles were found in contact with the implant surface, a fact that was already shown in other experimental studies in animals (97, 95, 96).

Both at the control and test sites, a dense layer of connective (DCT) tissue was found, surrounding completely the implant, with the exception of the areas that yielded osseointegration. The presence of this DCT has been reported previously (83, 212, 87, 84) The function of this tissue is still unclear. It has been shown that such tissue formed new bone during healing, and consequently, it was proposed that the tissue may represent an osteoid tissue that, over time, may become mineralized (83). In agreement with the previous study the presence of a DCT was not associated with any osseointegration after 3 months of healing in the present study, however.

It has been demonstrated that, at marginal defects around implants, bone formed from the lateral pristine bony walls and the base of the defect during the first months of healing reaching a distance from the implant surface of about 0.4mm

(83, 87). Osseointegration, however, started from the parent bone at the base of the defects, and migrating coronally during the subsequent months of healing (83, 84, 87). The fact that osseointegration started from the parent bone primarily in contact with the implant surface was also shown in several other studies (9, 85, 86, 213).

In the present study, DBBM particles did not improve bridging of the defect and did not favor osseointegration. This fact is in agreement with results from other experimental studies (97, 98, 214, 215). Nevertheless, DBBM particles were partly integrated in newly formed bone. This has been explained to the higher affinity of the forming bone to the graft surface compared to that of the implant surface (216).

In the present study, no membranes were used to create a secluded space of the defects. Consequently, the osseointegration process of an implant with a large circumferential defect under the principle of guided tissue regeneration cannot be discussed.

It may very well be speculated that if an occlusive membrane protected a circumferential defect of a remarkable size, it may be completely filled and the implant osseointegrated. Moreover, the influence of DBBM in such a situation would have to be explored.

Another dental implant surface (Osseospeed®; Astra Tech) was used in our animal studies on peri-implant bone healing and osseontegration in animal experimental models where selective bone defects were created in critical conditions such as post extraction alveolar bone.

The Osseospeed surface is obtained as well as with the sandblasting procedure also with a procedure of chemical type: fluoridation. The titanium surface once sandblasted, is treated with fluoride ions. In vivo tests have demonstrated that the presence of dioxide titanium with a negative charge, favours the deposition of calcium ions onto the implant, which in turn show a great affinity with the phosphate groups contained in many organical molecules (proteins, glycans, etc.). the presence of fluoride ions on the implant surface facilitate and strengthen such biological mechanisms; fluoride as a matter of fact (being highly electronegative), increases the speed of sedimentation of the calcium ions and causes an increase in the density of the bone trabecular structure, by stimulating the activity of the osteoprogenitor cells and the alkaline phopshatase, too. It is demonstrated, in vitro, the presence of weak secondary bonds between calcium ions and groups of

phosphate on a TiOblast surface; whilst such bonds become of a strong covalent type if the surface itself is coated with fluoride ions which are released in the surrounding space following the establishment of such bond (217).

The third animal experiment evaluated the influence of the positioning of the implant within the extraction socket in the presence of a standardized artificially created buccal bony defect.

The implants at the test sites were placed in a buccal positioning within the extraction sockets, while, at the control sites, the position was lingual. The bony crest, after 4 months of healing, was located at about 1.7 and 0.7 mm apically to the implant margin at the test and control sites, respectively. This, in turn, means that a bone gain of the buccal bony crest of about 1 and 2 mm compared with the original depth of the defect (2.7 mm) was observed at the test and control sites, respectively. Despite the presence of the buccal dehiscence, and the absence of any regenerative procedures, the level of the buccal bony crest after the healing at the test sites was similar to that reported in other experimental studies in which implants of the same diameter were installed in the center of a fresh extraction socket (e.g. 117, 118). Also at the control sites, the position of the bony crest was at a similar level corresponding to those of another experimental study (117) in which the implants were placed in a lingual position.

At the buccal aspect of the control sites, a higher volume of regenerated bone within the bony crest as well as a more coronal level of osseointegration within the defect was observed compared with the test sites. The importance of the positioning of the implant within the extraction socket was already specified both in clinical (132) and in animal experiments (117, 118, 133). In the present study, a buccal defect was prepared at the experimental sites. Other animal experiments produced similar buccal dehiscence defects at implants installed in sockets immediately after tooth extraction (112, 124-130). Most of these studies, however, used augmentation procedures with or without membranes. The results reported were generally superior at sites where regenerative procedures were applied. However, at control sites, where no treatment was rendered, some bone formation was also observed, although to a limited extent (124, 126, 127, 130). In an experiment in dogs (129), implants were installed immediately into extraction sockets. In one side of the mandible, 3 9 3 mm large dehiscence defects were made, while, in the contra lateral side, no defects were created. After 4 months of healing, a bone gain at the defect sites ranged from 0.3 to 0.8 mm. It should be

emphasized, however, that the implants used in that experiment were wider than the extraction sockets, so that the buccal surface of the implants was very close to or exceeding the profile of the extraction socket. In contrast, the implant profile of the present experiment was maintained within the contour of the buccal alveolar bony ridge at the test sites as well. Consequently, a regeneration of the bony crest of 1.3 and 2.3 mm was observed at the test and control sites, respectively. This difference may be explained by the different distances between the implant surface and the outer contour of the buccal bony ridge. In experiments in dogs (112, 118), implants with a diameter similar to that of the sockets were installed immediately after tooth extraction, and the healing was compared with that of implants of smaller diameter, placed in the center of the alveolus. After implant installation, the distance between the implant surface and the outer contour of the bony ridge was larger at the small compared with the large diameter implants. After 4 months of healing, the levels of the bony crest and of the coronal end of osseointegration were closer to the implant margin at the smaller diameter implant sites. It was concluded that the distance between the implant surface and the outer contour of the buccal alveolar bony crest influenced the degree of resorption of the buccal bony plate (112).

Buccal dehiscence-type defects have also been studied at implants installed in healed alveolar ridges (218-226). In experiments in dogs, the healing of buccal acute defects of 3–4 mm of height was studied at implants with a moderately rough modified surface (223, 226) without the use of regenerative procedures. It was shown that implants with a moderately rough modified surface may promote bone regeneration and osseointegration within the defect after 8–12 weeks of healing.

In the present study, residual marginal defects occurred after 4 months of healing. While at the buccal aspect, defects of similar amplitude were observed at the test and control sites, at the lingual aspects deeper defects were found at the test (2.1 mm; buccal positioning) compared with the control sites (1.0 mm; lingual positioning). The difference was statistically significant. This is in agreement with the data from an animal experiment (111) in which the healing of artificially circumferential marginal defects (artificial defect) around implants was compared with that of implants installed into sockets immediately after tooth extraction (natural defect). Despite the fact that bony crest resorption was higher at the

natural compared with the artificial defects, remaining marginal defects were still present after 4 months of healing that were deeper at the natural compared with the artificial defects. At the lingual sites, the depth of the remaining defects was about 0.9 and 2.2 mm at the artificial and natural defects, respectively.

However, it must be anticipated that the application of a barrier covering the initial defects, with or without the use of a filler material (114, 102), may have resulted in a better filling of the defects and hence, an influence of implant positioning could not have been visualized.

A soft tissue, similar to bone marrow, was often found occupying the apical portion of the defects and in close contact with the implant surface. This bone-marrow-like tissue was delimited in the coronal region by the peri-implant soft tissue. In some specimens, in the coronal region of the defects, a layer of dense connective tissue, similar to that described in previous animal studies in dogs (83), was found interposed between the bone-marrow-like tissue and the implant surface. This bonemarrow-like tissue may develop in the following period of healing into a mineralized bone that may become attached to the implant surface, and consequently improving the coronal level of osseointegration. This may also explain the gain of bone level attachment observed on radiographs during the first year of healing in a clinical study (107) in which implants were installed into alveoli immediately after tooth extraction.

The fourth animal experiment evaluated the influence on the healing of hard and soft tissues at short and long implants (6 mm vs. 11 mm) installed into sockets immediately after tooth extraction.

A slightly higher, though not statistically significant, osseointegration was found at the test (short implants) compared with the control sites (54.4% vs. 49.0%). This tendency of higher bone-to-implant contact for shorter implants may be due to the fact that the control implants were installed deeper into the alveolar bone reaching an area with higher trabecular alveolar bone density than the test implants that with their apical extension generally reached the center of the alveolar process. This region is usually of a looser trabecular morphology resulting in very little pressure being applied during implant installation. Consequently, bone formation may be initiated immediately without any prior resorption occasionally observed in dense alveolar bone (227).

As the residual bony housing of the extracted tooth was similar in the test and the control sites (approximately 11 mm), the control implant filled the alveolus in its entire length, while the short test implant left a space of approximately 5 mm filled with coagulum after installation. Obviously, no pressure was applied to the apical outline of the test implant, while at the control sites, the apical outline of the implants was prepared into alveolar bone. Again, this difference in location of the tip of the implant may have influenced the osseointegration process. The fact that the proportion of bone to implant contact at the apical termination of the test implant was 33% vs. 21% at the apical termination of the control implants would support a concept of improved osseointegration in areas with looser trabecular bony.

Bone resorption was observed both at the marginal buccal and lingual aspects. This buccal resorption was about 2.0 and 1.2 mm at the test and control sites, respectively. Considering the initial positioning of the implant shoulder in relation to the lingual bony crest, the corresponding lingual resorption was about 1.0 and 0.8 mm at the test and control sites, respectively.

The resorption of the alveolar bony crest after installation of implants immediately into extraction sockets has been documented in several clinical (108, 109) and experimental studies (111, 113, 137, 118, 228, 229). It is important to emphasize that the positioning of the implant within the extraction socket influences both the buccal and the lingual bony crest resorption. In an experiment in dogs (117), implants were installed into the distal alveoli of the third premolars immediately after tooth extraction. In the control sites, the implants were placed in the center of the alveolus while, at the test sites, the implants were installed more lingually and apically. After 4 months of healing, less buccal bone resorption had occurred at the test compared with the control sites. However, more lingual bone resorption was observed at the test compared with the control sites. While at the control sites the buccal bone resorption was larger compared with lingual aspects, the resorption at the test sites was similar for the two aspects. This, in turn, means that the positioning of the implant affects bone resorption both buccally and lingually.

In the present experiment, more buccal bone resorption was observed at the test compared with the control sites (difference 0.8 mm), even though this difference

was not statistically significant. This outcome may be explained by the various coronal sizes of the extraction sockets. A smaller initial buccal gap was observed at the test compared with the control sites. Moreover, the width of the bony crest was smaller at the test compared with the control sites. This resulted in a lower distance between the implant surface and the outer contour of the buccal bony crest at the test compared with the control sites. This observation may have established the conditions for a higher bone resorption on the buccal aspects.

The distance of the implant surface in relation to the outer contour of the bony crest (OC; 108) has been recognized as an important factor affecting the final position of the bucco-lingual bony walls in respect to the implant margin (109, 117, 118, 131, 132). In an experiment in dogs (118), larger implants that filled completely the alveolus were compared with narrower implants installed in the center of the extraction sockets. This, in turn, means that the surface of the implant was closer to the outer contour of the bony crest (OC) at the test compared with the control sites. After 4 months of healing, a higher degree of bony crest resorption was observed at the wider compared with the narrower implant sites, both at the buccal and lingual aspects. A similar experiment subsequently performed in dogs (229) confirmed these findings.

The difference of the distances IS-B and ISC between test and control sites should be considered with caution because of the fact that the dimensions of the alveoli were slightly different. For this reason, these two distances were not considered as primary outcome variables. The use of a randomized side selection (right or left) as test or control sites might have decreased the influence of this confounding factor. The BIC% performed between the two references points B (most coronal bone-to-implant contact) at the buccal and lingual aspects was used as primary outcome variable.

The top of the peri-implant mucosa (PM) at the buccal aspect was located more apically in relation to the implant shoulder (IS) at the test compared with the control sites, but the dimensions of the mucosae were similar for test and control sites. This is related to the position of the buccal bone located more apically at the test compared with the control sites.

Assessing the height of the mucosal cuff in two ways (vertical and surface assessment) revealed significant differences irrespective of the length of the

implants installed. The surface measurements were always larger than the vertical measurements. It is noteworthy to realize that the majority of these differences are found within the connective tissue adaptation to the implant rather than in the area of the barrier (junctional) epithelium, the latter yielding a dimension of typically 2.0–2.5 mm (232). The differences between the connective tissue adaptation measurements assessed by the two different methods has to be explained on the basis of the geometry at the implant should which — in the implants installed in the present study — followed a concept of “platform switching”.

The validation of the moderately rough implant surface in vitro and in vivo models has led over time to the increasing use of implant with smaller size than the standard used in past. In particular, the use of short implants, with intraosseous longitudinal dimension less than 10mm, represents today the first choice in the clinical treatment of edentulism associated with severe alveolar atrophy.
In the past, short implants in the posterior maxilla or mandible were associated with lower prosthesis SSRs (156, 157). Several reasons were put forward to explain this situation. One reason could be that, compared with longer implants of comparable diameter, there is less boneto-implant contact when short implants are used, simply because the surface area of the implant is smaller; peri-implant inflammation associated with MBL could lead to a loss of implant stability more easily for a short implant than for a standard one. Short implants are also generally placed more posteriorly, where alveolar bone quality is relatively poor, especially in the maxilla.
In contrast, the present study reported 16-year SSRs and SRs of 95.7% and 93.9%, respectively, for M short implants and 97.2% and 95.2% for R short implants. None of the variables considered (implant surface, length, or diameter) were found to influence implant survival significantly, and none of them were statistically associated with implant failure. This result could be because some failures (seven ‘‘early’’ failures and four after loading) reduced the power of the statistical analysis and the chances of detecting potential risk factors.

This trend should be confirmed by prospective, randomized clinical trials on short implants not splinted to longer implants because a factor that might influence the relative SSRs of short and long implants is the use of splinting, and the majority of the short implants examined in this study were splinted to longer implants.

Much larger sample sizes than those involved in the current study would be required to ascertain the presence and size of any splinting effect. From a descriptive perspective, successful long-term osseointegration was observed with short implants in the present series, irrespective of whether the clinical situation dictated the use of splinting.

Another limitation of this retrospective study could be that non-standardized radiographs are taken, and the resulting measurements could make it more difficult to compare peri-implant bone levels. Even so, the calibration of the measurement system used in the present study aims to minimize any dimensional image distortion, as reported previously by Romeo (161, 177).

In a retrospective clinical study, Malò et al (230) tested the hypothesis that short implants in atrophied jaws might achieve much the same longterm implant SSRs as longer implants in larger bone volumes. They studied 237 consecutively treated patients with 408 short Bra nemark implants, of which 131 were 7 mm long and 277 were 8.5 mm long. Eight implants failed in seven patients before the 6-month follow-up point, giving a cumulative SSR of 97.1% at 5 years, suggesting that short implants are a viable option in both jaws; however, only 88 of these implants had >5-year follow-up, and the power of these conclusions needs to be increased with longer-term results on a more significant sample. Regarding this last aspect, the findings of the present report are worthy of note because they span a period of 16 years; conversely, implant mobility could not be assessed for partial and complete dentures (as in the previously mentioned study) because the prostheses were not removed to check this parameter. Only radiographs were used to identify any periimplant changes occurring during the follow-up.

Sanchez-Garce et al. (231) described the performance of 273 implants 10 mm in length, placed in patients with severe alveolar bone resorption, with a follow-up in the range of 18 months to 12 years (mean of 81 months). In all, 20 failures were recorded (7.33%), with a global implant survival of 92.67%. The SSR was 92.82% for the 10-mm implants and 92.5% for the shorter implants; the failure rates were also similar in the two groups. The authors concluded that short implants ‘‘are a good treatment alternative for patients with severe alveolar resorption of both jaws.’’

Another recent retrospective study with a mediumto long-term follow-up (8 years)

was conducted by Anitua and Orive (232) on 661 patients with 1,287 short implants (<8.5 mm). They reported overall SSRs of 99.3% and 98.8% for the implantbased and subject-based analyses, respectively. Nine of the 1,287 implants were lost during the observation period. The authors concluded that treatment with short implants is safe and predictable, providing that strict clinical protocols are adopted. It is important to bear in mind, however, that the same amount of MBL occurring around a standard implant and around a short implant could implicate a greater risk of stability loss for the latter. A recent three-dimensional finite element analysis by Ormianer et al (233) on stress and strain patterns of one-piece and two-piece implant systems in bone concluded that only small-diameter (3.0-mm) one-piece implants in low-density bone exhibited stress levels that might adversely affect MBL stability.

In contrast, the influence of implant length and diameter on SSRs was discussed in a review by Renouard and Nisand (141) on a total of 53 human studies. They concluded that an adapted surgical preparation and the use of implants with a textured surface led to SSRs for short implants comparable with those achieved with longer ones. As for implant diameter, it was reported that, with an adapted surgical preparation, new implant designs, and adequate indications, there was no relationship between implant SSR and implant diameter.

In the present clinical trial, comparable long-term prognostic rates were recorded for short implants with M and R surface treatments, as reported by Telleman et al. (234). Renouard and Nisand (141) found that results tended to be better if oxidized implants were used instead of M implants, but the 5% difference they identified was not statistically significant. Nevertheless, it should be noted that the eight cases of early failures reported here referred to both M (n = 4) and R (n = 4) implants: the small size of our sample prevents any additional comment on this aspect. With a larger sample of early failures, it would also be interesting to see whether shorter implants have more complications in the initial healing period attributable to the previously mentioned potential biomechanical disadvantage of a reduced boneto-implant contact. The review by Renouard and Nisand (141) on short implants also stated that no specific pattern was observable concerning the time of the failure of short implants.

Conversely, when Feldman et al (235) compared the SSRs of short implants with

M and R surfaces, they demonstrated a statistically significant difference in the cumulative SSRs (91.6% for the M and 97.7% for the R implants). However, systematic reviews on short implants (141, 155, 233, 235) have come to the conclusion that an adapted surgical preparation and the use of acid-etched implants achieve SSRs for short implants that are comparable with those obtained with longer ones.

An advantage of placing short implants is that it obviates the need for additional surgery; therefore, this treatment is simpler, with the patient able to undergo a single surgical procedure. The number of visits and the treatment costs are also substantially reduced, and this implant therapy could be more accessible to larger numbers of patients and dental surgeons.

Additional investigations on the influence of bone quality and implant site (maxillary versus mandibular, anterior versus posterior) (236) will probably clarify the importance of the surface treatment of the fixture on the survival of short implants.

6. CONCLUSIONS

The presented studies show the variety of approaches to the validation of the osseointegration process. Some conclusions can be drawn. The molecular treatment of the implant surface, which consequently takes on connotations of bioactive surface, seems to represent a key to get to osseointegration, wich is recognized as a complex phenomenon of cell interaction with dental implant surface.

For example, data coming from the first presented study, suggest that combining data from TIRF analysis and blocking adhesion assays (Figs. 1.2 and 1.5), RGD and HVP functionalized surfaces engage human osteoblasts through different mechanisms. Indeed, RGDsp-grafted glass surfaces quickly induce strong and stable adhesion favouring the formation of focal contacts while HVPsp functionalized surfaces initially attach osteoblasts using proteoglycan-mediated weak binding and promote filopodia formation. Indeed, proteoglycans play a major role in cell adhesion to HVPsp grafted supports whereas the integrin αvβ3 is involved in osteoblasts attachment to both RGDsp and HVPsp functionalized surfaces (Fig. 1.5). These data suggest that HVPsp oriented peptide supports osteoblasts attachment through both mechanisms, each equally mandatory for osteoblasts adhesion and differentiation. Engineering materials functionalized with HVPsp peptide result in enhanced osteoblast binding and osteogenic activities that eventually will enhance the integration of biomaterials.

Tissue engineering has show its validity in the second experiment on in vitro osseointegration, where a novel biomimetic alternative to in vivo animal models was presented. This tridimensional in vitro metodh could be useful to evaluate the dynamic of bone-implant interactions that lead to osseointegration, utilizing and comparing different dental implant surfaces.

The surface treatment that leads to a moderate roughness (about S_a = 2 μm) of the implant surface promotes the process of peri-implant bone formation, which may find its limits related to the distance between the implant and the surrounding bone wall, being the latter artificially prepared or a component of a residual post extraction cavity. In fact, osteogenesis on the implant surface was obtained also when initial contact of the implant surface with the implant bed has deliberately been avoided. This phenomenon was influenced by the dimensions of the defect.

However, the degree of osseointegration was very low both at the small and the large defects compared to the control sites.
The concept of contact osteogenesis does not seem to be confirmed for distances greater than 1.2 mm, prevailing the distance osteogenesis model.
DBBM grafting of the artificial gap did not favor osteogenesis on the implant surface as well, and did not enhance the ability to bridge the distance in a defect wider than 1mm, even if graft particles were integrated into mature bone close to the implant surface.
New bone formation and osseointegration have similar behaviour in artificial and natural peri-implant defect. The placement of implants in a lingual position into extraction sockets allowed, in the third animal study, a higher degree of bone formation at buccal alveolar dehiscence defects compared with a placement in a buccal position.
The lack of statistically significant differences between for osseointegration parameter (BIC%) of immediate implants post extractive long (11mm) versus short (6mm) is of great importance from a clinical point of view. It is further validated the fact that the bone quality, in terms of entities osseointegration (BIC%) is inversely proportional to the bone density, given the same primary obtainable stability. "Shorts" implants can find more fields of clinical application, as confirmed by the last retrospective clinical study which shows high rates of survival rate (SSR) and success rate (SR) in the long term (follow-up 16 years) for both implant surfaces smooth surface (M) and rough (R). The M implants had a 16-year SSR of 95.7% and a 93.9% of corresponding SR, whereas the 16-year SSR and SR for the R implants were 97.2% and 95.2%, respectively.

The future research on osseointegration, and the related clinical implications, will focus on the development of nanostructured and bioactive surfaces. Preclinical studies, given the reduction in the course of the testing on animals of medium and large size, will integrate three-dimensional models of tissue engineering in vitro, using cell lines dedicated to the study of implant interactions with hard tissues, but also with the oral soft tissues, that are the point of potential transition between the contaminated oral environment and the alveolar bone.
The increasing need to treat edentulous patients of advanced age with bone defects of different nature, which involves the reduction of the size of the alveolar bone, associated with a tendency to minimally invasive treatments (not only from

the biological point of view, but also economical), lead increased use of reduced length implants. They have to date success and survival rates comparable to systems of greater length, demonstrated by clinical studies with long follow-up, such as the one presented here. The osseointegration of short implants and the ability to support the biomechanical masticatory load on the prosthesis connected to them, is certainly linked to the formation of a valid bone-implant interface. The maintenance of osseointegration along the implant surface, and in particular in the most coronal area, next to the prosthetic components projecting in the oral cavity, is nowadays one of the most important research field. The focus will be on the stability of the peri-implant soft tissues, which in turn is probably also related to host factors that are still not well defined.

REFERENCES

1. Brånemark, P.I. Osseointegration and its experimental background. The Journal of Prosthetic Dentistry 1983:50: 399–410.
2. Brånemark, P.I., Zarb, G.A. & Albrektsson, T. Tissue-integrated prostheses: osseointegration in clinical dentistry. Chicago: Quintessence 1985 p 27.
3. Le Guéhennec, L., Soueidan, A., Layrolle, P. & Amouriq, Y. Surface treatments of titanium dental implants for rapid osseointegration. Dental Materials 2007;23: 844–54.
4. Wennerberg, A. & Albrektsson, T. Effects of titanium surface topography on bone integration: a systematic review. Clinical Oral Implants Research 2009;20(Suppl. 4): 172–184.
5. Terheyden, H., Lang, N.P., Bierbaum, S. & Stadlinger, B. Osseointegration--communication of cells. Clinical Oral Implants Research 2012;23: 1127–35.
6. Nguyen, D.T., Orgill, D.P. & Murphy, G.F. Biomaterials For Treating Skin Loss. Chapter 4: The Pathophysiologic Basis for Wound Healing and Cutaneous Regeneration, 25–27. Boca Raton/ Cambridge: CRC Press (US) & Woodhead Publishing (UK/Europe), 2009.
7. Stadelmann, W.K., Digenis, A.G. & Tobin, G.R. Physiology and healing dynamics of chronic cutaneous wounds. American Journal of Surgery 1998;176: 26S–38S.
8. Berglundh, T., Abrahamsson, I., Lang, N.P. & Lindhe, J. De novo alveolar bone formation adjacent to endosseous implants. Clinical Oral Implants Research 2003;14:251–62.
9. Abrahamsson, I., Berglundh, T., Linder, E., Lang, N.P. & Lindhe, J. Early bone formation adjacent to rough and turned endosseous implant surfaces. An experimental study in the dog. Clinical Oral Implants Research 2004;15: 381–392.
10. Bosshardt, D.D , Salvi, G.E., Huynh-Ba, G., Ivanovski, S., Donos, N. & Lang, N.P. The role of bone debris in early healing adjacent to hydrophilic and hydrophobic implant surfaces in man. Clinical Oral Implants Research 2011;22: 357–364.
11. Lang, N.P., Salvi, G.E., Huynh-Ba, G., Ivanovski, S., Donos, N. & Bosshardt, D.D. Early osseointegration to hydrophilic and hydrophobic implant surfaces in humans. Clinical Oral Implants Research 2011;22: 349–356.

12. Donos, N., Hamlet, S., Lang, N.P., Salvi, G.E., Huynh-Ba, G., Bosshardt, D.D. & Ivanovski, S. Gene expression profile of osseointegration of a hydrophilic compared with a hydrophobic microrough implant surface. Clinical Oral Implants Research 2011;22: 365–372.

13. Ivanovski, S., Hamlet, S., Salvi, G.E., Huynh-Ba, G., Bosshardt, D.D., Lang, N.P. & Donos, N. Transcriptional profiling of osseointegration in humans. Clinical Oral Implants Research 2011;22: 373–381.

14. Midwood, K.S., Williams, L.V. & Schwarzbauer, J.E. Tissue repair and the dynamics of the extracellular matrix. The International Journal of Biochemistry and Celullar Biology 2004;36: 1031–1037.

15. Schultz, G.S. & Wysocki, A. Interactions between extracellular matrix and growth factors in wound healing. Wound Repair and Regeneration 2009; 17: 153–162.

16. Taipale, J. & Keski-Oja, J. Growth factors in the extracellular matrix. FASEB Journal 1997; 11: 51– 59.

17. Lansdown, A.B.G. Calcium: a potential central regulator in wound healing in the skin. Wound Repair and Regeneration 2002;10: 271–285.

18. Wilson, C.J., Clegg, R.E., Leavesley, D.I. & Pearcy, M.J. Mediation of biomaterial-cell interactions by adsorbed proteins: a review. Tissue Engineering 2005;11: 1–18.

19. Vroman, L. Effect of adsorbed proteins on the wettability of hydrophilic and hydrophobic solids. Nature 1962;196: 476–477.

20. Nakanishi, K., Sakiyama, T. & Imamura, K. On the adsorption of proteins on solid surfaces, a common but very complicated phenomenon. Journal of Bioscience and Bioengineering 2001;91: 233 –244.

21. Lee, M.H., Oh, N., Lee, S.W., Leesungbok, R., Kim, S.E., Yun, Y.P. & Kang, J.H. Factors influencing osteoblast maturation on microgrooved titanium substrata. Biomaterials 2010;31: 3804–3815.

22. Ferencyk, M., Rovensky, J., Matha, V. & Herold, M. Kompendium der Immunologie. Wien: Springer. (2006)

23. Smith, H.W. & Marshall, C.J. Regulation of cell signalling by uPAR. Nature Reviews Molecular Cell Biology 2010;11: 23–36.

24. Perkins, D.J. & Kniss, D.A. Blockade of nitric oxide formation down-regulates cyclooxygenase-2 and decreases PGE2 biosynthesis in macrophages. Journal of Leukocyte Biology 1999;65: 792–799.

25. Witte, M.B. & Barbul, A. Role of nitric oxide in wound repair. American Journal of Surgery 2002;183: 406–412.

26. Ruoslahti, E. & Yamaguchi, Y. Proteoglycans as modulators of growth factor activities. Cell 1991;64: 867–869.

27. Friedl, P. & Bröcker, E.B. The biology of cell locomotion within three-dimensional extracellular matrix. Cellular and Molecular Life Sciences 2000;57: 41–64.

28. Murdoch, C., Giannoudis, A. & Lewis, C.E. Mechanisms regulating the recruitment of macrophages into hypoxic areas of tumors and other ischemic tissues. Blood 2004;104: 2224–2234.

29. Bosco, M.C., Puppo, M., Blengio, F., Fraone, T., Cappello, P., Giovarelli, M. & Varesio, L. Monocytes and dendritic cells in a hypoxic environment: spotlights on chemotaxis and migration. Immunobiology 2008;213: 733–749.

30. West, X.Z., Malinin, N.L., Merkulova, A.A., Tischenko, M., Kerr, B.A., Borden, E.C., Podrez, E.A., Salomon, R.G. & Byzova, T.V. Oxidative stress induces angiogenesis by activating TLR2 with novel endogenous ligands. Nature 2010;467: 972–976.

31. Lansdown, A.B.G., Sampson, B. & Rowe, A. Experimental observations in the rat on the influence of cadmium on skin wound repair. International Journal Experimental Pathology 2001;82: 35–41.

32. Hitchon, C., Wong, K., Ma, G., Reed, J., Lyttle, D. & El-Gabalawy, H. Hypoxia-induced production of stromal cell-derived factor 1 (CXCL12) and vascular endothelial growth factor by synovial fibroblasts. Arthritis & Rheumatism 2002; 46: 2587–2597.

33. Wierzbicka-Patynowski, I. & Schwarzbauer, J.E. The ins and outs of fibronectin matrix assembly. Journal of Cell Science 2003;116(Pt 16): 3269–3276.

34. Corselli, M., Chen, C.W., Crisan, M., Lazzari, L. & Péault, B. Perivascular ancestors of adult multipotent stem cells. Arteriosclerosis, Thrombosis and Vascular Biology 2010; 30: 1104–1109.

35. Lamagna, C. & Berger, G. The bone marrow constitutes a reservoir of pericyte progenitors. Journal of Leukocyte Biology 2006;80: 677–681.

36. Chen, D., Zhao, M. & Mundy, G.R. Bone morphogenetic proteins. Growth Factors 2004;22: 233– 241.

37. Sieber, C., Kopf, J., Hiepen, C. & Knaus, P. Recent advances in BMP receptor signaling. Cytokine & Growth Factor Reviews 2009;20: 343–355.

38. Garimella, R., Tague, S.E., Zhang, J., Belibi, F., Nahar, N., Sun, B.H., Insogna, K., Wang, J. & Anderson, H.C. Expression and synthesis of bone morphogenetic proteins by osteoclasts: a possible path to anabolic bone remodeling. Journal of Histochemistry and Cytochemistry 2008;56: 569–577.

39. Sims, N.A. & Gooi, J.H. Bone remodeling: multiple cellular interactions required for coupling of bone formation and resorption. Seminars in Cell & Developmental Biology 2008;19: 444–451.

40. Colfen, H. Biomineralization: a crystal-clear view. Nature Material 2010;9: 960–961.

41. Golub, E.E. Role of matrix vesicles in biomineralization. Biochimica et Biophysica Acta 2009;1790: 1592–1598.

42. Olszta, M.J., Cheng, X., Jee, S.S., Kumar, R., Kim, Y.Y., Kaufman, M.J., Douglas, E.P. & Gower, L.B. Bone structure and formation: a new perspective. Materials Science and Engineering Reports 2007;58: 77–116.

43. Degidi, M., Scarano, A., Petrone, G. & Piattelli, A. Histologic analysis of clinically retrieved immediately loaded titanium implants: a report of 11 cases. Clinical Implant Dentistry and Related Research 2003;5: 89–93.

44. Boyce, B.F. & Xing, L. Osteoclasts, no longer osteoblast slaves. Nature Medicine 2006;12: 1356– 1358.

45. Martin, T., Gooi, J.H. & Sims, N.A. Molecular mechanisms in coupling of bone formation to resorption. Critical Reviews in Eukaryotic Gene Expression 2009;19: 73–88.

46. Boyce, B.F. & Xing, L. Functions of RANKL/ RANK/OPG in bone modeling and remodeling. Archives of Biochemistry and Biophysics 2008;473: 139–146.

47. Poole, K. & Reeve, J. Parathyroid hormone – a bone anabolic and catabolic agent. Current Opinion in Pharmacology 2005; 5: 612–617.

48. Takahashi, N., Maeda, K., Ishihara, A., Uehara, S. & Kobayashi, Y. Regulatory mechanism of osteoclastogenesis by RANKL and Wnt signals. Frontiers in Bioscience 2011;16: 21–30.

49. Graves, D.T., Li, J. & Cochran, D.L. Inflammation and uncoupling as mechanisms of periodontal bone loss. Journal of Dental Research 2011;90: 143–153.

50. Yu, X., Huang, Y., Collin-Osdoby, P. & Osdoby, P. Stromal cell-derived factor-1 (SDF-1) recruits osteoclast precursors by inducing chemotaxis, matrix

metalloproteinase-9 (MMP-9) activity, and collagen transmigration. Journal of Bone and Mineral Research 2003;18: 1404–1418.

51. Väänänen, H., Zhao, H., Mulari, M. & Halleen, J. The cell biology of osteoclast function. Journal of Cell Science 2000;113: 377–381.

52. Karmakar, S., Kay, J. & Gravallese, E.M. Bone damage in rheumatoid arthritis: mechanistic insights and approaches to prevention. Rheumatic Disease Clinics of North America 2010;36: 385– 404.

53. Koga, T., Inui, M., Inoue, K., Kim, S., Suematsu, A., Kobayashi, E., Iwata, T., Ohnishi, H., Matozaki, T., Kodama, T., Taniguchi, T., Takayanagi, H. & Takai, T. Costimulatory signals mediated by the ITAM motif cooperate with RANKL for bone homeostasis. Nature 2004;428: 758–763.

54. Weinstein, R.S., Chen, J.R., Powers, C.C., Stewart, S. A., Landes, R.D., Bellido, T., Jilka, R.L., Parfitt, A. M. & Manolagas, S.C. Promotion of osteoclast survival and antagonism of bisphosphonate induced osteoclast apoptosis by glucocorticoids. Journal of Clinical Investigation 2002;109: 1041–1048.

55. Dossa, T., Arabian, A., Windle, J.J., Dedhar, .S., Teitelbaum, S.L., Ross, F.P., Roodman, G.D. & St-Arnaud, R. Osteoclast-specific inactivation of the integrin-linked kinase (ILK) inhibits bone resorption. Journal of Cellular Biochemistry 2010;110: 960–967.

56. Pederson, L., Ruan, M., Westendorf, J.J., Khosla, S. & Oursler, M.J. Regulation of bone formation by osteoclasts involves Wnt/BMP signalling and the chemokine sphingosine-1-phosphate. Proceedings of the National Academy of Sciences USA 2008;105: 20764–20769.

57. Vukicevic, S. & Grgurevic, L. BMP-6 and mesenchymal stem cell differentiation. Cytokine & Growth Factor Reviews 2009;20: 441–448.

58. Matsuo, K. & Irie, N. Osteoclast-osteoblast communication. Archives of Biochemistry and Biophysics 2008;473: 201–209.

59. Mundy, G.R. & Elefteriou, F. Boning up on ephrin signaling. Cell 2006;126: 441–443.

60. Gray, C., Boyde, A. & Jones, S.J. Topographically induced bone formation in vitro: implications for bone implants and bone grafts. Bone 1996;18: 115–123.

61. Knothe Tate, M.L. Whither flows the fluid in bone? An osteocyte's perspective. Journal of Biomechanics 2003;36: 1409–1424.

62. Temiyasathit, S. & Jacobs, C.R. Osteocyte primary cilium and its role in bone mechanotransduction. Annals of the New York Academy of Sciences 2010;1192: 422–428.

63. Colopy, S.A., Benz-Dean, J., Barrett, J.G., Sample, S. J., Lu, Y., Danova, N.A., Kalscheur, V.L., Vanderby, R. Jr, Markel, M.D. & Muir, P. Response of the osteocyte syncytium adjacent to and distant from linear microcracks during adaptation to cyclic fatigue loading. Bone 2004;35: 881 –891.

64. Santos, A., Bakker, A.D. & Klein-Nulend, J. The role of osteocytes in bone mechanotransduction. Osteoporosis International 2009;20: 1027–1031.

65. Turner, C.H., Warden, S.J., Bellido, T., Plotkin, L.I., Kumar, N., Jasiuk, I., Danzig, J. & Robling, A.G. Mechanobiology of the skeleton. Science Signaling 2009;2: Pt3.

66. Cejka, D., Herberth, J., Branscum, A.J., Fardo, D.W., Monier-Faugere, M.C., Diarra, D., Haas, M. & Malluche, H.H. Sclerostin and Dickkopf-1 in Renal Osteodystrophy. Clinical Journal of the American Society of Nephrology 2010;6: 877–882.

67. Dalton, B.A., McFarland, C.D., Underwood, P.A. & Steele, J.G. Role of the heparin binding domain of fibronectin in attachment and spreading of human bone-derived cells. Journal of Cell Science 1995;108: 2083–92.

68. Dee, K.C., Andersen, T.T. & Bizios, R. Design and function of novel osteoblast- adhesive peptides for chemical modification of biomaterials. Journal of Biomedical Materials Research 1998;40: 371–377.

69. Dettin, M., Bagno, A., Gambaretto, R., Iucci, G., Conconi, M.T., Tuccitto, N., Menti, A.M., Grandi, C., Di Bello, C., Licciardello, A. & Polzonetti, G. Covalent surface modification of titanium oxide with different adhesive peptides: surface characterization and osteoblast-like cell adhesion. Design and function of novel osteoblast- adhesive peptides for chemical modification of biomaterials. Journal of Biomedical Materials Research Part A 2009;90: 35–45.

70. Kim, S.H., Turnbull, J. & Guimond, S. Extracellular matrix and cell signalling: the dynamic cooperation of integrin, proteoglycan and growth factor receptor. Journal of Endocrinology 2011;209: 139–151.

71. Cohen, M., Joester, D., Geiger, B. & Addadi, L. Spatial and temporal sequence of events in cell adhesion: from molecular recognition to focal adhesion assembly. ChemBioChem 2004;5:1393–1399.

72. Puleo, D.A. & Nanci, A. Understanding and controlling the bone–implant

interface. Biomaterials 1999;20: 2311–2321.

73. Bauer, A.L., Jackson, T.L. & Jiang, Y. Topography of extracellular matrix mediates vascular morphogenesis and migration speeds in angiogenesis. PLOS Computational Biology 2009;5: e1000445.

74. Zanetti, A.S., Sabliov, C., Gimble, J.M. & Hayes, D.J. Human adipose-derived stem cells and three-dimensional scaffold constructs: a review of the biomaterials and models currently used for bone regeneration. Journal of Biomedical Materials Research Part B, Applied Biomaterials 2013;101: 187–199.

75. Shen, F.H., Werner, B.C., Liang, H., Shang, H., Yang, N., Li, X., Shimer, A.L., Balian, G. & Katz, A.J. Implications of adipose-derived stromal cells in a 3D culture system for osteogenic differentiation: an in vitro and in vivo investigation. The Spine Journal: Official Journal of the North American Spine Society 2013; 13: 32–43. See comment in PubMed Commons below

76. Gardin, C., Bressan, E., Ferroni, L., Nalesso, E., Vindigni, V., Stellini, E., Pinton, P., Sivolella, S. & Zavan, B. In vitro concurrent endothelial and osteogenic commitment of adipose-derived stem cells and their genomical analyses through comparative genomic hybridization array: novel strategies to increase the successful engraftment of tissue-engineered bone grafts. Stem Cells and Development 2012;21: 767-777..

77. Schenk, R.K. & Willenegger, H.R. Zur Histologie der primären Knochenheilung. Modifikationen une Grenzen der spaltheilung in Abhängigkeit von der Defktgrösse. Unfallheilkunde 1977;80: 155–160.

78. Botticelli, D., Berglundh, T., Buser, D. & Lindhe, J. The jumping distance revisited. An experimental study in the dog. Clinical Oral Implants Research 2003;14: 35–42.

79. Botticelli, D. Healing of marginal defects around implants. Thesis, Department of Periodontology, Institute of Odontology, The Sahlgrenska Academy at Göteborg University, Goteborg, Sweden, 2006.

80. Knox, R., Caudill, R. & Meffert, R. Histologic evaluation of dental endosseous implants placed in surgically created extraction defects. The International Journal of Periodontics & Restorative Dentistry 1991;11: 365–375.

81. Akimoto, K., Becker, W., Persson, R., Baker, D.A., Rohrer, M.D. & O'Neal, R.B. Evaluation of titanium implants placed into simulated extraction sockets: a study in dogs. The International Journal of Oral & Maxillofacial Implants 1999;14: 351–360.

82. Botticelli, D., Berglundh, T. & Lindhe, J. Resolution of bone defects of varying dimension and configuration in the marginal portion of the periimplant bone. An experimental study in the dog. Journal of Clinical Periodontology 2004;31: 309–317.

83. Botticelli, D., Berglundh, T., Buser, D. & Lindhe, J. Appositional bone formation in marginal defects at implants. An experimental study in the dog. Clinical Oral Implants Research 2003;14: 1–9.

84. Yoon, H.C., Choi, J.Y., Jung, U.W., Bae, E.K., Choi, S.H., Cho, K.S., Lee, H.Y., Kim, C.K. & Shim, J.S. Effects of different depths of gap on healing of surgically created coronal defects around implants in dogs: a pilot study. Journal of Periodontology 2008;79: 355–361.

85. Scala, A., Botticelli, D., Oliveira, J.A., Okamoto, R., Garcia Rangel, I. Jr & Lang, N.P. Early healing after elevation of the maxillary sinus floor applying a lateral access –A histological study in monkeys. Clinical Oral Implants Research 2010;21: 1320–1326.

86. Scala, A., Botticelli, D., Silveira Faeda, R., Garcia Rangel, I. Jr, Oliveira, J.A. & Lang, N.P. Lack of influence of the Schneiderian membrane in forming new bone apical to implants simultaneously installed with sinus floor elevation. An experimental study in monkeys. Clinical Oral Implants Research 2012;23: 175–181.

87. Rossi, F., Botticelli, D., Pantani, F., Pereira, F.P., Salata, L.A. & Lang, N.P. Bone healing pattern in surgically created circumferential defects around submerged implants: an experimental study in dog. Clinical Oral Implants Research 2012;23: 41–48.

88. Qu, J., Chehroudi, B. & Brunette, D.M. The use of micromachined surfaces to investigate the cell behavioural factors essential to osseointegration. Oral Diseases 1996;2: 102–115.

89. Davies, J.E. Mechanisms of endosseous integration. The International Journal of Prosthodontics 1998;11: 391–401.

90. Botticelli, D., Berglundh, T. & Lindhe, J. Bone regeneration at implants with turned or rough surface in combination with submerged and non-submerged protocols. An experimental study in the dog. Journal of Clinical Periodontology 2005;32: 448–455.

91. Davies, J.E. Understanding peri-implant endosseous healing. Journal of Dental Education 2003;67: 932–49.

92. Sivolella S, Bressan E, Salata LA, Urrutia ZA, Lang NP, Botticelli D. Osteogenesis at implants without primary bone contact an experimental study in dogs. Clin Oral Implants Res. 2012;23:542-9.

93. Carlsson, L., Röstlund, T., Albrektsson, B. & Albrektsson, T. Implant fixation improved by close fit. Cylindrical implant-bone interface studied in rabbits. Acta Orthopedica Scandinavica 1988;59: 272–275.

94. Lioubavina-Hack, N., Lang, N.P. & Karring, T. Significance of primary stability for osseointegration of dental implants. Clinical Oral Implants Research 2006;17: 244–250.

95. Berglundh, T. & Lindhe, J. Healing around implants placed in bone defects treated with Bio- Oss. An experimental study in the dog. Clinical Oral Implants Research 1997;8: 117–124.

96. Hämmerle, C.H., Chiantella, G.C., Karring, T. & Lang, N.P. The effect of a deproteinized bovine bone mineral on bone regeneration around titanium dental implants. Clinical Oral Implants Research 1998;9: 151–162.

97. Botticelli, D., Berglundh, T. & Lindhe, J. The influence of a biomaterial on the closure of a marginal hard tissue defect adjacent to implants. An experimental study in the dog. Clinical Oral Implants Research 2004;15: 285–292.

98. Antunes AA1, Oliveira Neto P, de Santis E, Caneva M, Botticelli D, Salata LA. Comparisons between Bio-Oss(®) and Straumann(®) Bone Ceramic in immediate and staged implant placement in dogs mandible bone defects. Clin Oral Implants Res. 2013 Feb;24(2):135-42.

99. Cornelini, R., Cangini, F., Martuscelli, G. & Wennstrom, J. Deproteinized bovine bone and biodegradable barrier membrane to support healing following immediate placement of transmucosal implants: a short-term controller clinical trial. The International Journal of Periodontics and Restorative Dentistry 2004;24: 555–563.

100. Chen, S.T., Darby, I.B. & Reynolds, E.C. A prospective clinical study of non-submerged immediate implants. Clinical outcomes and esthetic results. Clinical Oral Implants Research 2007;18: 552–562.

101. Araùjo, M.G., Linder, E. & Lindhe, J. Bio- Oss_ Collagen in the buccal gap at immediate implants: a 6-months study in the dog. Clinical Oral Implants Research 2011;22: 1–8.

102. Caneva, M., Botticelli, D., Pantani, F., Baffone, G.M., Garcia Rangel, I.J. & Lang, N.P. Deproteinized bovine bone mineral in marginal defects at implants

installed immediately into extraction sockets. An experimental study in dogs. Clinical Oral Implants Research 2011;23: 106–112.

103. Caneva, M., Botticelli, D., Morelli, F., Cesaretti, G., Beolchini, M. & Lang, N.P. Alveolar process preservation at implants installed immediately into extraction sockets using deproteinized bovine bone mineral – An experimental study in dogs. Clinical Oral Implants Research 2012;23: 789–796.

104. Favero, G., Botticelli, D., Favero, G., Garcıa, B., Mainetti, T. & Lang, N.P. Alveolar bony crest preservation at implants installed immediately after tooth extraction: an experimental study in the dog. Clinical Oral Implants Research 2013;24: 7–12.

105. Favero, G., Lang, N.P., De Santis, E., Gonzalez, B.G., Schweikert, M.T. & Botticelli, D. Ridge preservation at implants installed immediately after molar extraction. An experimental study in the dog. Clinical Oral Implants Research 2013;24: 255–261.

106. Lang, N.P., Pun, B.L., Lau, K.Y., Li, K.Y. & Wong, M.C.M. A systematic review of survival and success rates of implants placed immediately into fresh extraction sockets after at least one year. Clinical Oral Implants Research 2012;23: 42–69.

107. Botticelli, D., Renzi, A., Lindhe, J. & Berglundh,T. Implants in fresh extraction sockets: a prospective 5-years follow-up clinical study. Clinical Oral Implant Research 2008;19: 1226–1232.

108. Botticelli, D., Berglundh, T. & Lindhe, J. Hard tissue alterations following immediate implant placement in extraction sites. Journal of Clinical Periodontology 2004;31: 820–828.

109. Sanz, M., Cecchinato, D., Ferrus, J., Pjetursson, B., Lang, N.P. & Lindhe, J. A prospective, randomized- controlled clinical trial to evaluate bone preservation using implants with different geometry placed into extraction sockets in the maxilla. Clinical Oral Implants Research 2010;21: 13–21.

110. Araujo, M.G. & Lindhe, J. Dimensional ridge alterations following tooth extraction. An experimental study in the dog. Journal of Clinical Periodontology 2005;32: 212–218.

111. Botticelli, D., Persson, L.G., Lindhe, J. & Berglundh, T. Bone tissue formation adjacent to implants placed in fresh extraction sockets. An experimental study in dogs. Clinical Oral Implant Research 2006;17: 351–358.

112. De Santis, E., Botticelli, D., Pantani, F., Pereira, F.P., Beolchini, M. & Lang, N.P.Bone regeneration at implants placed into extraction sockets of maxillary incisors in dogs. Clinical Oral Implants Research 2011;22: 430–437.

113. Caneva, M., Botticelli, D., Salata, L.A., Souza, S.L.S., Bressan, E. & Lang, N.P. Flap versus “flap-less” surgical approach at immediate implants – a histomorphometric study in dogs. Clinical Oral Implants Research 2010;21: 1314–1319.

114. Caneva, M., Botticelli, D., Salata, L.A., Souza, S.L.S., Carvalho Cardoso, L. & Lang, N.P. Collagen membranes at immediate implants. A histomorphometric study in dogs. Clinical Oral Implants Research 2010;21: 891–897.

115. Caneva, M., Botticelli, D., Stellini, E., Salata, L.A., Souza, S.L.S. & Lang, N.P. Magnesium-enriched hydroxyapatite at immediate implants. A histomorphometric study in dogs. Clinical Oral Implants Research 2011;22: 512–517.

116. Caneva, M., Botticelli, D., Viganò , P., Morelli, F.,Rea, M. & Lang, N.P. Connective tissue grafts in conjunction with implants installed immediately into extraction sockets. An experimental study in dogs. Clinical Oral Implants Research 2013;24: 50–56.

117. Caneva, M., Salata, L.A., de Souza, S.S., Baffone, G., Lang, N.P. & Botticelli, D. Influence of implant positioning in extraction sockets on osseointegration. Clinical Oral Implants Research 2010;21: 43–49.

118. Caneva, M., Salata, L.A., Souza, S.L.S., Bressan, E., Botticelli, D. & Lang, N.P. Hard tissue formation adjacent to implants of various size and configuration immediately placed into extraction sockets. An experimental study in dogs. Clinical Oral Implants Research 2010;21: 885– 890.

119. Schropp, L., Wenzel, A., Kostopoulos, L. & Karring, T. Bone healing and soft tissue contour changes following single-tooth extraction: a clinical and radiographic 12-month prospective study. The International Journal of Periodontics & Restorative Dentistry 2003;4: 313–323.

120. Nemcovsky, C.E., Moses, O., Artzi, Z. & Gelernter, I. Clinical coverage of dehiscence defects in immediate implant procedures: three surgical modalities to achieve primary soft tissue closure. The International Journal of Oral Maxillofacial Implants 2000;15: 843–852.

121. Nemcovsky, C.E. & Artzi, Z. Comparative study of buccal dehiscence defects in immediate, delayed, and late maxillary implant placement with collagen

membranes: clinical healing between placement and second-stage surgery. Journal of Periodontolology 2002;73: 754–761.
122. Hassan, K.S. Autogenous bone graft combined with polylactic polyglycolic acid polymer for treatment of dehiscence around immediate dental implants. Oral Surgery, Oral Medicine, Oral Pathology, Oral Radiology, and Endodontics 2009;108: 19–25.
123. Siciliano, V.I., Salvi, G.E., Matarasso, S., Cafiero, C., Blasi, A. & Lang, N.P. Soft tissues healing at immediate transmucosal implants placet into molar extraction sites with buccal self-contained dehiscences. A 12-month controlled clinical trial. Clinical Oral Implants Research 2009;20: 482–488.
124. Becker, W., Schenk, R., Higuchi, K., Lekholm, U. & Becker, B.E. Variations in bone regeneration adjacent to implants augmented with barrier membranes alone or with demineralized freeze dried bone or autologous grafts: a study in dogs. The International Journal of Oral & Maxillofacial Implants 1995;10: 143–154.
125. Henry, P.J., Tan, A.E., Leavy, J., Johansson, C.B. & Albrektsson, T. Tissue regeneration in bony defects adjacent to immediately loaded titanium implants placed into extraction sockets: a study in dogs. The International Journal of Oral & Maxillofacial Implants 1997;12: 758–766.
126. Mao, C., Sato, J., Matsuura, M. & Seto, K. Guided tissue regeneration around dental implants in immediate extraction sockets: comparison of resorbable and nonresorbable membranes. Chinese Medical Sciences Journal 1997;12: 170–174.
127. Cho, K.S., Choi, S.H., Han, K.H., Chai, J.K., Wikesjo, U.M. & Kim, C.K. Alveolar bone formation at dental implant dehiscence defects following guided bone regeneration and xenogeneic freeze-dried demineralized bone matrix. Clinical Oral Implants Research 1998;9: 419– 428.
128. Kohal, R.J., Trejo, P.M., Wirsching, C., Hurzeler, M. B. & Caffesse, R.G. Comparison of bioabsorbable and bioinert membranes for guided bone regeneration around non-submerged implants. An experimental study in the mongrel dog. Clinical Oral Implants Research 1999;10: 226–237.
129. Rasmusson, L., Kahnberg, K.E. & Tan, A. Effects of implant design and surface on bone regeneration and implant stability: an experimental study in the dog mandible. Clinical Implant Dentistry and Related Research 2001;3: 2–8.
130. Hanisch, O., Sorensen, R.G., Kinoshita, A., Spiekermann, H., Wozney, J.M. & Wikesjö, U.M. Effect of recombinant human bone morphogenetic protein-2 in

dehiscence defects with nonsubmerged immediate implants: an experimental study in Cynomolgus monkeys. Journal of Periodontology 2003;74: 648–657.

131. Ferrus, J., Cecchinato, D., Pjetursson, E.B., Lang, N. P., Sanz, M. & Lindhe, J. Factors influencing ridge alterations following immediate implant placement into extraction sockets. Clinical Oral Implants Research 2010;21: 22–29.

132. Tomasi, C., Sanz, M., Cecchinato, D., Pjetursson, B., Ferrus, J., Lang, N.P. & Lindhe, J. Bone dimensional variations at implants placed in fresh extraction sockets: a multilevel multivariate analysis. Clinical Oral Implants Research 2010;21: 30–36.

133. Favero, G., Lang, N.P., Favero, G., Grau Leo´ n, I., Salata, L.A. & Botticelli, D. Role of teeth adjacent to implants installed immediately into extraction sockets. An experimental study in the dog. Clinical Oral Implants Research 2012;23: 402–408.

134. Quirynen, M., van Assche, N., Botticelli, D. & Berglundh, T. How does the timing of implant placement to extraction affect outcome? The International Journal of Oral & Maxillofacial Implants 2007;22: 203–223.

135. Botticelli, D., Renzi, A., Lindhe, J. & Berglundh, T. Implants in fresh extraction sockets: A prospective 5-years follow-up clinical study. Clinical Oral Implant Research 2008;19: 1226–1232.

136. Hämmerle, C.H., Chen, S.T. & Wilson, T.G. Jr Consensus statements and recommended clinical procedures regarding the placement of implants in extraction sockets. The International Journal of Oral & Maxillofacial Implants 2004;19: 26–28.

137. Araujo, M.G., Sukekava, F., Wennström, J.L. & Lindhe, J. Ridge alterations following implant placement in fresh extraction sockets: an experimental study in the dog. Journal of Clinical Periodontology 2005;32: 645–652.

138. Covani, U., Crespi, R., Cornelini, R. & Barone, A. Immediate implants supporting single crown restoration: A 4-year prospective study. Journal of Periodontology 2004;75: 982–988.

139. Becker, C.M., Wilson, T.G. Jr & Jensen, O.T. Minimum criteria for immediate provisionalization of single-tooth dental implants in extraction sites: A 1-year retrospective study of 100 consecutive cases. Journal of Oral & Maxillofacial Surgery 2011;69: 491–497.

140. Gonzàlez-Martìn, O., Lee, E.A. & Veltri, M. CBCT fractal dimension changes at the apex of immediate implants placed using undersized drilling. Clinical Oral Implants Research 2012;23: 954–957.

141. Renouard, F. & Nisand, D. Impact of implant length and diameter on survival rates. Clinical Oral Implants Research 2006;17: 35–51.

142. Rossi, F., Ricci, E., Marchetti, C., Lang, N.P. & Botticelli, D. Early loading of single crowns supported by 6-mm-long implants with a moderately rough surface: A prospective 2-year follow up cohort study. Clinical Oral Implants Research 2010;21: 937–943.

143. Sun, H.L., Huang, C., Wu, Y.R. & Shi, B. Failure rates of short (≤ 10 mm) dental implants and factors influencing their failure: A systematic review. The International Journal of Oral Maxillofacial Implants 2011;26: 816–825.

144. Esposito, M., Pellegrino, G., Pistilli, R. & Felice, P. Rehabilitation of posterior atrophic edentulous jaws: Prostheses supported by 5 mm short implants or by longer implants in augmented bone? One-year results from a pilot randomized clinical trial. European Journal of Oral Implantology 2011;4: 21–30.

145. Felice, P., Soardi, E., Pellegrino, G., Pistilli, R., Marchetti, C., Gessaroli, M. & Esposito, M. Treatment of the atrophic edentulous maxilla: Short implants versus bone augmentation for placing longer implants. Five-month post-loading results of a pilot randomised controlled trial. European Journal of Oral Implantology 2011;4: 191–202.

146. Berglundh, T., Persson, L. & Klinge, B. A systematic review of the incidence of biological and technical complications in implant dentistry reported in prospective longitudinal studies of at least 5 years. Journal of Clinical Periodontology 2002; 29:197–212, discussion 232–233.

147. Pjetursson, B.E., Brägger, U., Lang, N.P. & Zwahlen M. Comparison of survival and complication rates of tooth-supported fixed dental prostheses (FDPs) and implant-supported FDPs and single crowns (SCs). Clinical Oral Implants Research 2007;18: 97–113.

148. Jung, R.E., Pjetursson, B.E., Glauser, R., Zembic, A., Zwahlen, M. & Lang NP. A systematic review of the 5-year survival and complication rates of implant-supported single crowns. Clinical Oral Implants Research 2008;19: 119–130.

149. Lang, N.P. & Salvi, G.E. Implants in restorative dentistry. In: Lindhe, J., Lang, N.P., eds. Clinical Periodontology and Implant Dentistry, 5th ed. Oxford: Blackwell Munksgaard 2008:1138–1145.

150. Chiapasco, M., Zaniboni, M. & Boisco, M. Augmentation procedures for the rehabilitation of deficient edentulous ridges with oral implants. Clinical Oral Implants Research 2006;17: 136–159.

151. Donos, N., Mardas, N. & Chadha, V. Clinical outcomes of implants following lateral bone augmentation: Systematic assessment of available options (barrier membranes, bone grafts, split osteotomy). Journal of Clinical Periodontology 2008;35: 173–202.

152. Pjetursson, B.E., Tan, W.C, Zwahlen, M., & Lang, N.P. A systematic review of the success of sinus floor elevation and survival of implants inserted in combination with sinus floor elevation. Journal of Clinical Periodontology 2008;35: 216–240.

153. Rocchietta, I., Fontana, F., & Simion, M. Clinical outcomes of vertical bone augmentation to enable dental implant placement: A systematic review. Journal of Clinical Periodontology 2008;35: 203–215.

154. Hagi, D., Deporter, D.A., Pilliar, R.M. & Arenovich, T. A targeted review of study outcomes with short (< or = 7 mm) endosseous dental implants placed in partially edentulous patients. Journal of Periodontology 2004;75: 798–804.

155. Kotsovilis, S., Fourmousis, I., Karoussis, I.K. & Bamia, C. A systematic review and meta-analysis on the effect of implant length on the survival of rough-surface dental implants. Journal of Periodontology 2009;80: 1700–1718.

156. Romeo, E., Bivio, A., Mosca, D., Scanferla, M., Ghisolfi, M. & Storelli, S. The use of short dental implants in clinical practice: Literature review. Minerva Stomatologica 2010;59: 23–31.

157. Esposito, M., Grusovin, M.G., Felice, P., Karatzopoulos, G., Worthington, H.V. & Coulthard, P. Interventions for replacing missing teeth: Horizontal and vertical bone augmentation techniques for dental implant treatment. Cochrane Database of Systematic Reviews 2009;7:CD003607.

158. Lekholm, U., Gunne, J., Henry, P., Higuchi, K., Lindén, U., Bergström, C. & van Steenberghe, D. Survival of the Brånemark implant in partially edentulous jaws: A 10-year prospective multicenter study. The International Journal of Oral & Maxillofacial Implants 1999;14: 639–645.

159. Testori, T., Wiseman, L., Woolfe, S. & Porter, S.S. A prospective multicenter clinical study of the Osseotite implant: Four-year interim report. The International Journal of Oral & Maxillofacial Implants 2001;16: 193–200.

160. Weng, D., Jacobson, Z., Tarnow, D., Hürzeler, M.B., Faehn, O., Sanavi, F., Barkvoll, P. & Stach, R.M. A prospective multicenter clinical trial of 3i machined-surface implants: Results after 6 years of follow-up. The International Journal of Oral & Maxillofacial Implants 2003;18: 417–423.

161. Romeo, E., Ghisolfi, M., Rozza, R., Chiapasco, M. & Lops, D. Short (8-mm) dental implants in the rehabilitation of partial and complete edentulism: A 3- to 14-year longitudinal study. The International Journal of Prosthodontics 2006;19: 586–592.

162. Dettin, M., Conconi, M.T., Gambaretto, R., Bagno, A., Di Bello, C., Menti, A.M., Grandi, C. & Parnigotto, P.P. Effect of synthetic peptides on osteoblast adhesion. Biomaterials 2005;26: 4507–4515.

163. Bagno, A., Piovan, A., Dettin, M., Brun, P., Gambaretto, R., Palù, G., Di Bello, C. & Castagliuolo, I. Improvement of Anselme's adhesion model for evaluating human osteoblast response to peptide-grafted titanium surfaces. Bone 2007;41: 704–12.

164. Xiao, S.J., Wieland, M. & Brunner, S. Surface reactions of 4-aminothiophenol with heterobifunctional crosslinkers bearing both succinimidyl ester and maleimide for biomolecular immobilization. Journal of Colloid and Interface Science 2005;290: 172–183.

165. Bagno, A., Piovan, A., Dettin, M., Chiarion, A., Brun, P., Gambaretto, R., Fontana, G., Di Bello, C., Palù, G. & Castagliuolo, I.Human osteoblast-like cells adhesion on titanium substrates covalently functionalized with synthetic peptides. Bone 2007;40: 693–699.

166. Martin-Granados, C., Prescott, A.R., Van Dessel, N., Van Eynde, A., Arocena, M., Klaska, I.P., Görnemann, J., Beullens, M., Bollen, M., Forrester, J.V. & McCaig, C.D. A role for PP1/NIPP1 in steering migration of human cancer cells. PLoS One 2012;7: e40769.

167. Voltan, S, Castagliuolo, I., Elli, M., Longo, S., Brun, P., D'Incà, R., Porzionato, A., Macchi, V., Palù, G., Sturniolo, G.C., Morelli, L. & Martines, D. Aggregating phenotype in Lactobacillus crispatus determines intestinal colonization and TLR2 and TLR4 modulation in murine colonic mucosa. Clinical and Vaccine Immunology: CVI 2007;14: 1138–1148.

168. Pfaffl M.W. A new mathematical model for relative quantification in real-time RT-PCR. Nucleic Acids Research 2001;29: e45.

169. Meneghello, R., Savio, G. & Cerardi, A. Bite force and contact area evaluation in a physical-virtual environment. Research in Interactive Design Vol. 3 Springer-Verlag France, 2011.
170. Meneghello, R., Savio, G., Raffaeli, R., Cerardi, A., Turchetto, M. & Planchenstainer, L. An integrated methodology for the functional design of dental prosthesis. International Journal on Interactive Design and Manufacturing 2013;7: 103–114.
171. Mombelli, A., van Oosten, M.A., Schurch E. Jr & Lang, N.P. The microbiota associated with successful or failing osseointegrated titanium implants. Oral Microbiology and Immunology 1987;2:145–151.
172. Mombelli, A. & Lang, N.P. Clinical parameters for the evaluation of dental implants. Periodontology 2000 1994; 4: 81–86.
173. Lang, N.P., Wetzel, A.C., Stich, H. & Caffesse, R.G. Histologic probe penetration in healthy and inflamed peri-implant tissues. Clinical Oral Implants Research 1994;5: 191–201.
174. Esposito, M., Hirsch, J.M., Lekholm, U. & Thomsen, P. Biological factors contributing to failures of osseointegrated oral implants. (I). Success criteria and epidemiology. European Journal of Oral Sciences 1998;106: 527–551.
175. Weber, H.P., Buser, D., Fiorellini, J.P. & Williams, R.C. Radiographic evaluation of crestal bone levels adjacent to nonsubmerged titanium implants. Clinical Oral Implants Research 1992;3: 181–188.
176. Brägger, U. Radiographic parameters for the evaluation of peri-implant tissues. Periodontology 2000 1994; 4: 87–97.
177. Romeo, E., Lops, D., Margutti, E., Ghisolfi, M., Chiapasco M. & Vogel, G. Implant-supported fixed cantilever prostheses in partially edentulous arches. A seven-year prospective study. Clinical Oral Implants Research 2003;14: 303–311.
178. Albrektsson T., Zarb, G., Worthington, P. & Eriksson, A.R. The long-term efficacy of currently used dental implants: A review and proposed criteria of success. The International Journal of Oral & Maxillofacial Implants 1986; 1:11–25.
179. Buser, D., Brägger, U., Lang, N.P.& Nyman, S. Regeneration and enlargement of jaw bone using guided tissue regeneration. Clinical Oral Implants Research 1990;1: 22–32.
180. Roos, J., Sennerby, L., Lekholm, U., Jemt, T., Gröndahl, K. & Albrektsson, T. A qualitative and quantitative method for evaluating implant success: A 5-year

retrospective analysis of the Brånemark implant. The International Journal of Oral & Maxillofacial Implants 1997;12: 504–514.

181. Thalji, G. & Cooper, L.F. Molecular assessment of osseointegration in vivo: a review of the current literature. The International Journal of Oral & Maxillofacial Implants 2013; 28: e521–e534.

182. Novaes, A.B. Jr., de Souza, S.L., de Barros, R.R., Pereira, K.K., Iezzi, G. & Piattelli, A. Influence of implant surfaces on osseointegration. Brazilian Dental Journal 2010; 21: 471–481.

183. Coelho, P.G., Granjeiro, J.M., Romanos, G.E., Suzuki, M., Silva, N.R., Cardaropoli, G., Thompson, V.P. & Lemons, J.E. Basic research methods and current trends of dental implant surfaces. Journal of Biomedical Materials Research Part B, Applied Biomaterials 2009;88: 579–596.

184. Lemons, J.E. Biomaterials, biomechanics, tissue healing, and immediate-function dental implants. The Journal of Oral Implantology 2004;30: 318–324.

185. Oortgiesen, D.A.W., Meijer, G.J., de Vries, R.B.M., Walboomers X.F. & Jansen,J.A. Animal Models for the Evaluation of Tissue Engineering Constructs. In: Tissue Engineering [Editors: Pallua N, Suschek CV]. Springer-Verlag. Berlin, Germany: 2011. pp. 131-54.

186. Bacakova, L., Filova, E., Parizek, M., Ruml, T. & Svorcik, V. Modulation of cell adhesion, proliferation and differentiation on materials designed for body implants. Biotechnology Advances 2011;29: 739–767.

187. Shahal, T., Geiger, B., Dunlop, I.E. & Spatz, J.P. Regulation of integrin adhesions by varying the density of substrate-bound epidermal growth factor. Biointerphases 2012;7: 23–34.

188. Koo, L.Y., Irvine, D.J., Mayes, A.M., Lauffenburger, D.A. & Griffith, L.G. Co-regulation of cell adhesion by nanoscale RGD organization and mechanical stimulus. Journal of Cell Science 2002;115: 1423–1433.

189. Smith, L.L., Niziolek, P.J., Haberstroh, K.M., Nauman, E.A. & Webster, T.J. Decreased fibroblast and increased osteoblast adhesion on nanostructured NaOH-etched PLGA scaffolds. International Journal of Nanomedicine 2007;2: 383–388.

190. Mattila, P.K. & Lappalainen, P. Filopodia: molecular architecture and cellular functions. Nature Reviews. Molecular Cell Biology 2008;9: 446–454.

191. Keselowsky, B.G., Collard, D.M. & García, A.J. Integrin binding specificity regulates biomaterial surface chemistry effects on cell differentiation. Proceedings

of the National Academy of Sciences of the United States of America 2005;102: 5953–5957.

192. Wozniak, M.A., Modzelewska, K., Kwong, L. & Keely, P.J. Focal adhesion regulation of cell behavior. Biochimica and Biophysica Acta 2004;1692: 103–119.

193. Kim, J.B., Leucht, P., Luppen, C.A., Park, Y.J., Beggs, H.E., Damsky, C.H. & Helms, J.A. Reconciling the roles of FAK in osteoblast differentiation, osteoclast remodeling, and bone regeneration. Bone 2007;41: 39–51.

194. Midwood, K.S., Mao, Y., Hsia, H.C., Valenick, L.V. & Schwarzbauer, J.E. Modulation of cell–fibronectin matrix interactions during tissue repair. The Journal of Investigative Dermatology. Symposium Proceedings 2006;11: 73–78.

195. Brunski, J.B., Puleo, D.A. & Nanci, A. Biomaterials and biomechanics of oral and maxillofacial implants: current status and future developments. The International Journal of Oral & Maxillofacial Implants 2000;15: 15–46.

196. American Society for Testing Materials. Standard specification for rigid polyurethane foam for use as a standard material for testing orthopaedic devices and instruments. Report: F1839-97

197. Calvert, K.L., Trumble, K.P., Webster, T.J. & Kirkpatrick, L.A. Characterization of commercial rigid polyurethane foams used as bone analogs for implant testing. Journal of Materials Science. Materials in Medicine 2010;21: 1453–1461.

198. Bardyn, T., Gédet, P., Hallermann, W. & Büchler, P. Quantifying the influence of bone density and thickness on resonance frequency analysis: an in vitro study of biomechanical test materials. The International Journal of Oral & Maxillofacial Implants 2009;24: 1006–1014.

199. Chong, L., Khocht, A., Suzuki, J.B. & Gaughan, J. Effect of implant design on initial stability of tapered implants. The Journal of Oral Implantology 2009;35: 130–135.

200. Kim, D.R., Lim, Y.J., Kim, M.J., Kwon, H.B. & Kim, S.H. Self-cutting blades and their influence on primary stability of tapered dental implants in a simulated low-density bone model: a laboratory study. Oral Surgery, Oral Medicine, Oral Pathology, Oral Radiology, and Endodontics 2011;112: 573–580.

201. Divac, M., Stawarczyk, B., Sahrmann, P., Attin, T. & Schmidlin, P.R. Influence of residual bone thickness on primary stability of hybrid self-tapping and cylindric non-self-tapping implants in vitro. The International Journal of Oral & Maxillofacial Implants 2013;28: 84–88.

202. Seong, W.J., Grami, S., Jeong, S.C., Conrad, H.J. & Hodges, J.S. Comparison of push-in versus pull-out tests on bone-implant interfaces of rabbit tibia dental implant healing model. Clinical Implant Dentistry and Related Research 2013;15: 460–469.

203. Baker, D., London, R.M., & O'Neal, R. Rate of pull-out strength gain of dual-etched titanium implants: a comparative study in rabbits. The International Journal of Oral & Maxillofacial Implants 1999;14: 722–728.

204. Albrektsson, T. & Wennerberg, A. Oral implant surfaces: Part 1- review focusing on topographic and chemical properties of different surfaces and in vivo responses to them. The International Journal of Prosthodontics 2004;17: 536–543.

205. Schenk, R.K. Bone regeneration: biologic basis. In: Buser, D., Dahlin, C. & Schenk, R.K., eds. Guided Bone Regeneration in Implant Dentistry, 1st edition, 69, Ch. 3, 69p. Hong Kong: Quintessence Publishing Co. (1994)

206. Schenk, R.K. & Buser, D. Osseointegration: a reality. Periodontology 2000 1998;17: 22–35.

207. Coceancig, P.L.G. Alveolar bone grafts distal to the lower second molar. Journal of Maxillofacial and Oral Surgery 2009;8: 22–26.

208. Camelo, M., Nevins, M.L., Lynch, S.E., Schenk, R.K., Simion, M. & Nevins, M. Periodontal regeneration with an autogenous bone-Bio-Oss composite graft and a Bio-Gide membrane. The International Journal of Periodontics and Restorative Dentistry 2001;21: 109–119.

209. Vastardis, S., Yukna, R.A., Mayer, E.T. & Atkinson, B.L. Periodontal regeneration with peptide-enhanced anorganic bone matrix in particulate and putty form in dogs. Journal of Periodontology 2005;76: 1690–1696.

210. Fugazzotto, P.A. GBR using bovine bone matrix and resorbable and nonresorbable membranes. Part 2: Clinical results. The International Journal of Periodontics and Restorative Dentistry 2003;23: 599–605.

211. Zitzmann, N.U., Schärer, P., Marinello, C.P., Schupbach, P. & Berglundh, T. Alveolar ridge augmentation with Bio-Oss: a histologic study in humans. The International Journal of Periodontics and Restorative Dentistry 2001;21: 288–295.

212. Simion, M., Dahlin, C., Rocchietta, I., Stavropoulos, A., Sanchez, R. & Karring, T. Vertical ridge augmentation with guided bone regeneration in association with dental implants: an experimental study in dogs. Clinical Oral Implants Research 2007;18: 86–94.

213. Buser, D., Broggini, N., Wieland, M., Schenk, R.K., Denzer, A.J., Cochran, D.L., Hoffmann, B., Lussi, A. & Steinemann, S.G. Enhanced bone apposition to a chemically modified SLA titanium surface. Journal of Dental Research 2004;83: 529–533.

214. Carmagnola, D., Berglundh, T., Ara_ujo, M., Albrektsson, T. & Lindhe, J. Bone healing around implants placed in a jaw defect augmented with Bio-Oss. An experimental study in dogs. Journal of Clinical Periodontology 2000;27: 799–805.

215. Polyzois, I., Renvert, S., Bosshardt, D.D., Lang, N.P. & Claffey, N. Effect of Bio-Oss on osseointegration of dental implants surrounded by circumferential bone defects of different dimensions: an experimental study in the dog. Clinical Oral Implants Research 2007;18: 304–310.

216. Lindgren, C., Sennerby, L., Mordenfeld, A. & Hallman, M. Clinical histology of microimplants placed in two different biomaterials. The International Journal of Oral and Maxillofacial Implants 2009;24: 1093–1100.

217. Ellingsen, J.E. In: On the properties of surface-modified Titanium. Davies JE, editor. Bone engineering; em Squared Inc; Toronto, Canada: 2000. pp. 183–189.

218. Zablotsky, M., Meffert, R., Caudill, R. & Evans, G. Histological and clinical comparisons of guided tissue regeneration on dehisced hydroxylapatite-coated and titanium endosseous implant surfaces: a pilot study. The International Journal of Oral & Maxillofacial Implants 1991;6: 294–303.

219. Lundgren, A.K., Sennerby, L., Lundgren, D., Taylor, A., Gottlow, J. & Nyman, S. Bone augmentation at titanium implants using autologous bone grafts and a bioresorbable barrier. An experimental study in the rabbit tibia. Clinical Oral Implants Research 1997;8: 82–89.

220. Ito, K., Yamada, Y., Ishigaki, R., Nanba, K., Nishida, T. & Sato, S. Effects of guided bone regeneration with non-resorbable and bioabsorbable barrier membranes on osseointegration around hydroxyapatite-coated and uncoated threaded titanium dental implants placed into a surgically-created dehiscence type defect in rabbit tibia: a pilot study. Journal of Oral Science 2001;43: 61–67.

221. Casati, M.Z., Sallum, E.A., Nociti, F.H. Jr, Caffesse, R.G. & Sallum, A.W. Enamel matrix derivative and bone healing after guided bone regeneration in dehiscence-type defects around implants. A histomorphometric study in dogs. Journal of Periodontology 2002;73: 789–796.

222. Schwarz, F., Herten, M., Ferrari, D., Wieland, M., Schmitz, L., Engelhardt, E. & Becker, J. Guided bone regeneration at dehiscence-type defects using biphasic hydroxyapatite + beta tricalcium phosphate (Bone Ceramic) or a collagencoated natural bone mineral (BioOss Collagen): an immunohistochemical study in dogs. The International Journal of Oral Maxillofacial Surgery 2007;36: 1198–1206.

223. Schwarz, F., Herten, M., Sager, M., Wieland, M., Dard, M. & Becker, J. Bone regeneration in dehiscence-type defects at chemically modified (SLActive) and conventional SLA titanium implants: a pilot study in dogs. Journal of Clinical Periodontology 2007;34: 78–86.

224. Schwarz, F., Rothamel, D., Herten, M., Wüstefeld, M., Sager, M., Ferrari, D. & Becker, J. Immunohistochemical characterization of guided bone regeneration at a dehiscence-type defect using different barrier membranes: an experimental study in dogs. Clinical Oral Implants Research 2008;19: 402–415.

225. Schwarz, F., Sager, M., Ferrari, D., Herten, M., Wieland, M. & Becker, J. Bone regeneration in dehiscence-type defects at non-submerged and submerged chemically modified (SLActive) and conventional SLA titanium implants: an immunohistochemical study in dogs. Journal of Clinical Periodontology 2008;35: 64–75.

226. Schwarz, F., Sager, M., Kadelka, I., Ferrari, D. & Becker, J. Influence of titanium implant surface characteristics on bone regeneration in dehiscence- type defects: an experimental study in dogs. Journal of Clinical Periodontology 2010;37: 466–473.

227. Berglundh, T., Abrahamsson, I., Albouy, J.P. & Lindhe, J. Bone healing at implants with a fluoride-modified surface: An experimental study in dogs. Clinical Oral Implants Research 2007;18: 147–152.

228. de Sanctis, M., Vignoletti, F., Discepoli, N., Zucchelli, G. & Sanz, M. Immediate implants at fresch extraction sockets: bone healing in four different implant systems. Journal of Clinical Periodontology 2009;36: 705–711.

229. Caneva M, Botticelli D, Rossi F, Cardoso LC, Pantani F, Lang NP. Influence of implants with different sizes and configurations installed immediately into extraction sockets on peri-implant hard and soft tissues: an experimental study in dogs. Clin Oral Implants Res. 2012 Apr;23(4):396-401.

230. Malò, P., de Araujo Nobre, M. & Rangert, B. Short implants placed one-stage in maxillae and mandibles: A retrospective clinical study with 1 to 9 years of follow-up. Clinical Implant Dentistry and Related Research 2007;9: 15–21.

231. Sanchez-Garces, M.A., Costa-Berengue, X. & Gay-Escoda, C. Short implants: A descriptive study of 273 implants. Clinical Implant Dentistry and Related Research 2010;12: 26–38.

232. Anitua, E. & Orive, G. Short implants in maxillae and mandibles: A retrospective study with 1 to 8 years of follow-up. Journal of Periodontology 2010;81: 819–826.

233. Ormianer, Z., Ben Amar, A., Duda, M., Marku-Cohen, S. & Lewinstein, I. Stress and strain patterns of 1-piece and 2-piece implant systems in bone: A 3-dimensional finite element analysis. Implant Dentistry 2012;21: 39–45.

234. Telleman, G., Raghoebar, G.M., Vissink, A., den Hartog, L., Huddleston Slater, J.J. & Meijer, H.J. A systematic review of the prognosis of short (<10 mm) dental implants placed in the partially edentulous patient. Journal of Clinical Periodontology 2011;38: 667–676.

235. Feldman, S., Boitel, N., Weng, D., Kohles, S.S. & Stach, R.M. Five-year survival distributions of short-length (10mm or less) machined-surfaced and Osseotite implants. Clinical Implant Dentistry and Related Research 2004;6: 16–23.

236. Morand, M. & Irinakis, T. The challenge of implant therapy in the posterior maxilla: Providing a rationale for the use of short implants. Journal of Oral Implantology 2007;33: 257–266.

APPENDIX 1 – TABLES AND FIGURES

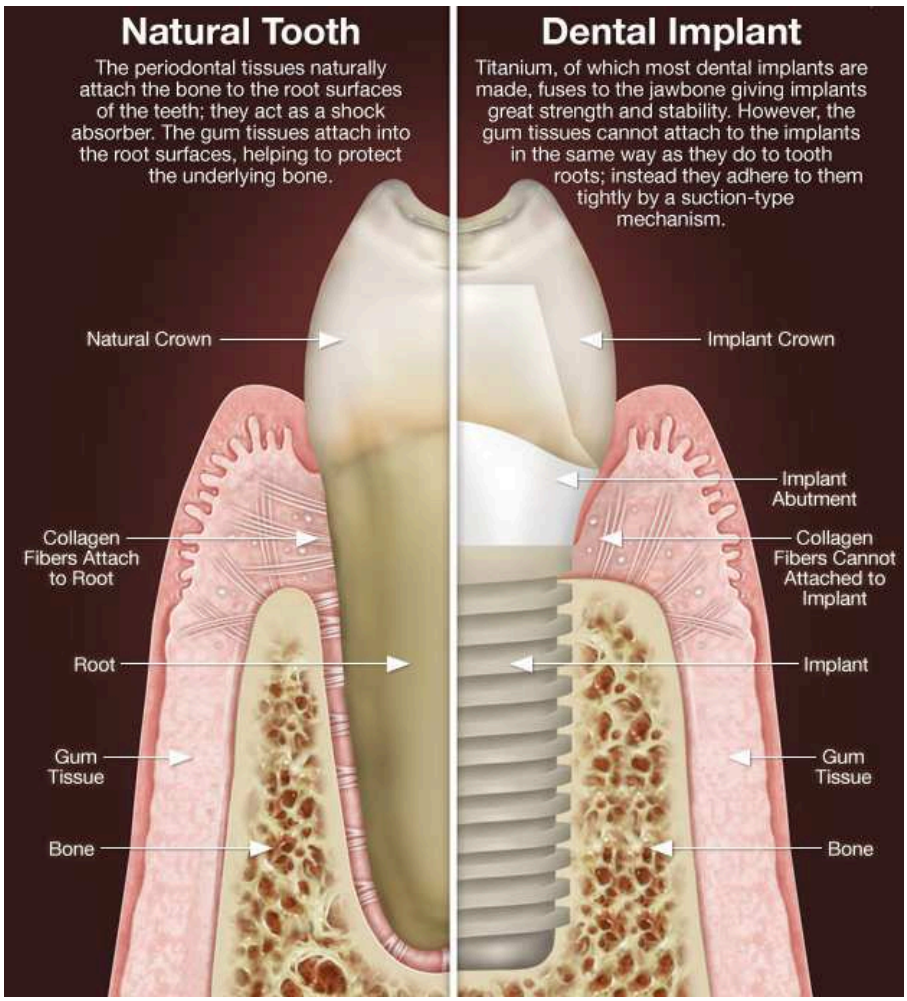

Fig.1 Natural tooth and dental implant: a schematic comparison between the two conditions and a description of their major components

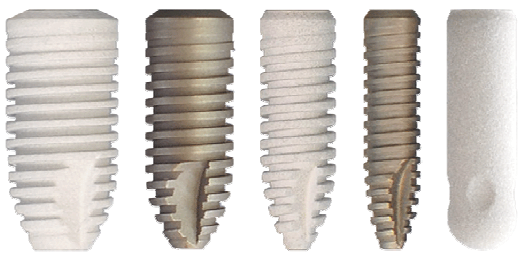

Fig. 2 Some examples of dental implant macroscopic design and surfaces.

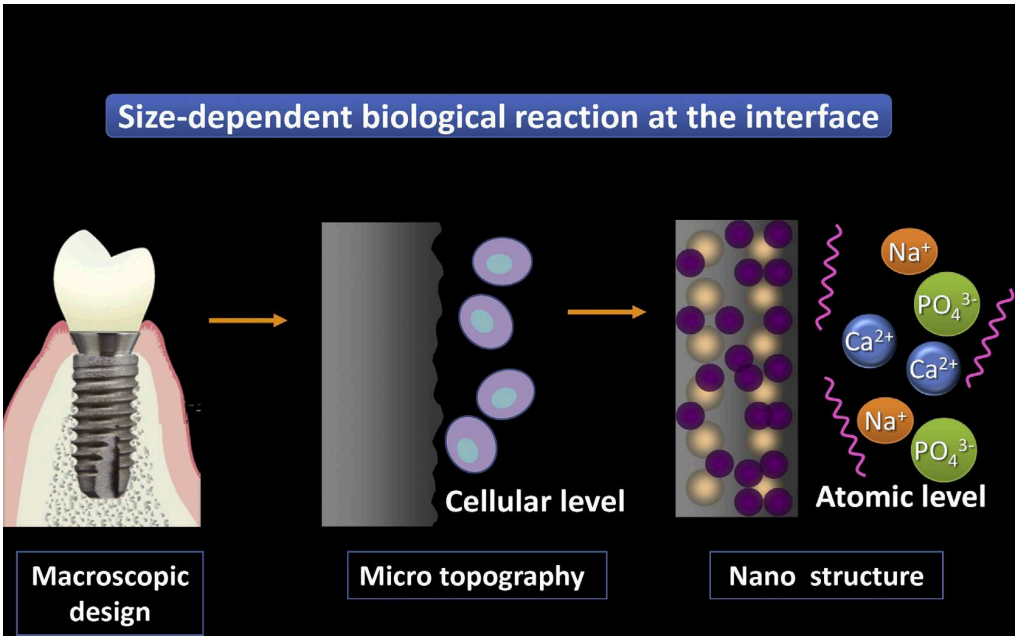

Fig. 3. General concepts of titanium implant modification.

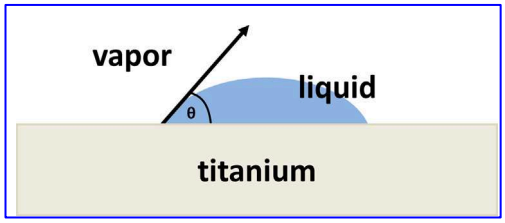

Fig. 4. A diagram for contact angle as measured by sessile drop technique.

Type of implant	Surface roughness (μm)	Contact angle (°)
cpTi	Ra = 0.22 ± 0.01[a]	55.4 ± 4.1
Ti6Al4V	Ra = 0.23 ± 0.01[a]	56.3 ± 2.7
TPS	Ra = 7.01 ± 2.09	n.d.
SLA	Sa = 1.15 ± 0.05	138.3 ± 4.2
Modified SLA	Sa = 1.16 ± 0.04	0
Plasma-sprayed HA coating	Ra = 1.06 ± 0.21	57.4 ± 3.2
Biomimetic CaP coating	Ra = 1.83 ± 0.64	13.4 ± 0.17

[a] Machined and polished surfaces.

Fig. 5. Surface properties of titanium dental implants (from Le Guehennec L. et al, 2007).

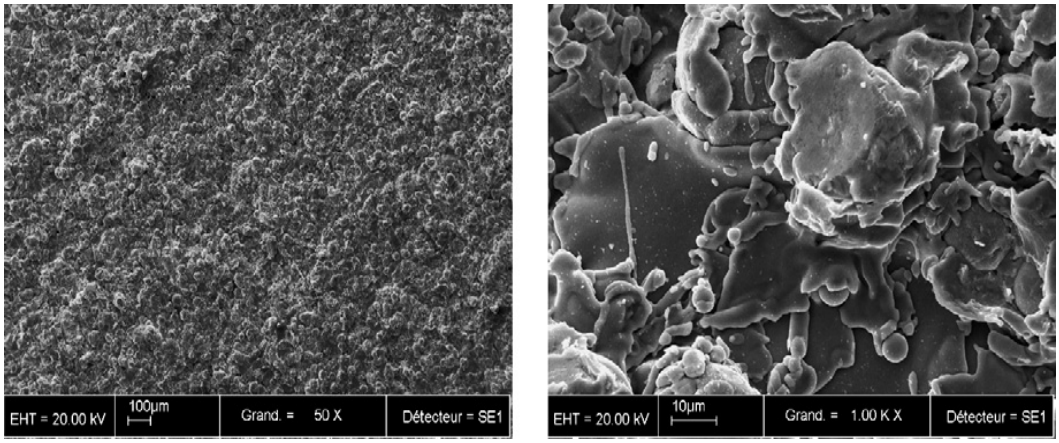

Fig. 6. SEM micrographs of a titanium plasma-sprayed (TPS) surface (from Le Guehennec L. et al, 2007)

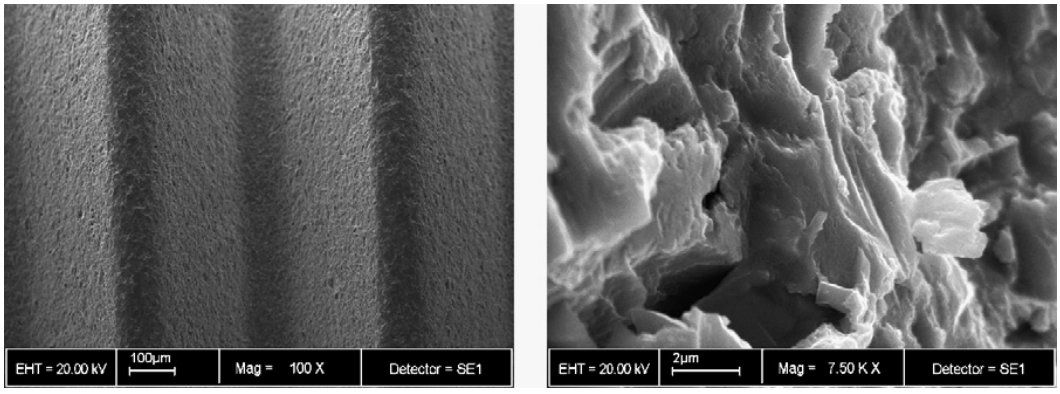

Fig. 7. SEM micrographs of a TiO blasted surface (Astratech TiOblastTM) (from Le Guehennec L. et al, 2007).

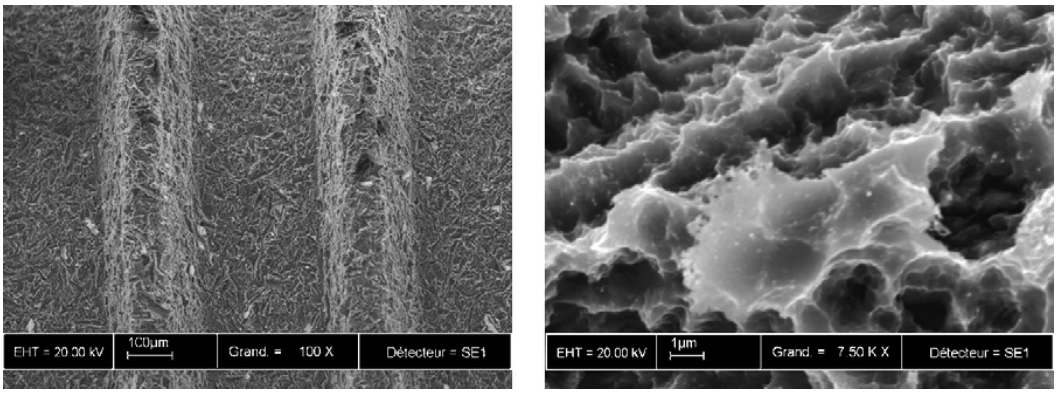

Fig. 8. SEM micrographs of an SLA surface on a titanium dental implant (SLA, Straumann AG, Switzerland) (from Le Guehennec L. et al, 2007).

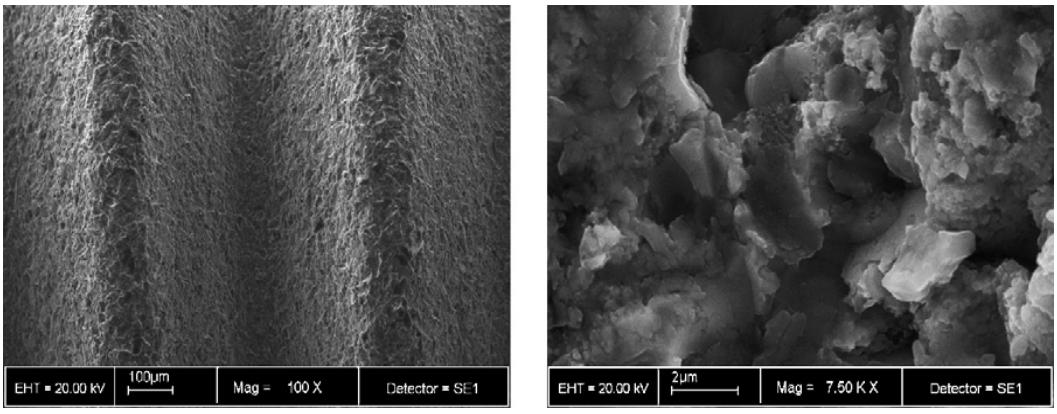

Fig. 9. SEM micrographs of treatment of titanium dental implants in a fluoride solution surface (Astratech OsseoSpeedTM) (from Le Guehennec L. et al, 2007)

.

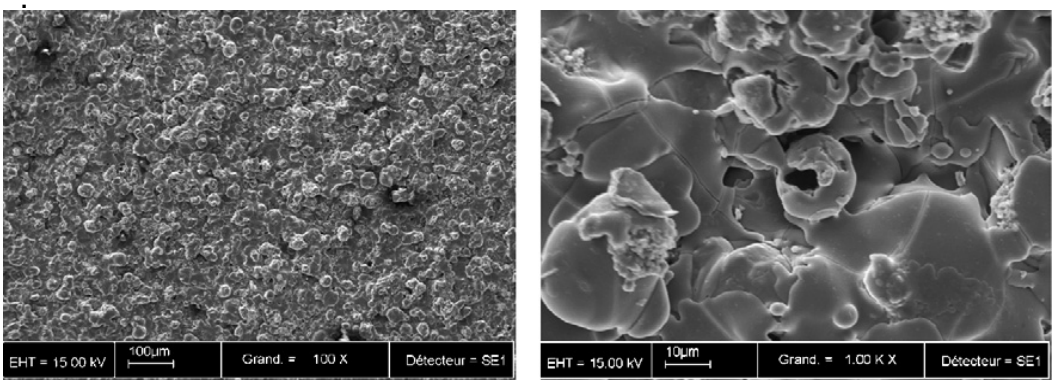

Fig. 10. SEM micrographs of a plasma-sprayed hydroxyapatite (HA) coating surface (Cam Implants BV) (from Le Guehennec L. et al, 2007)

.

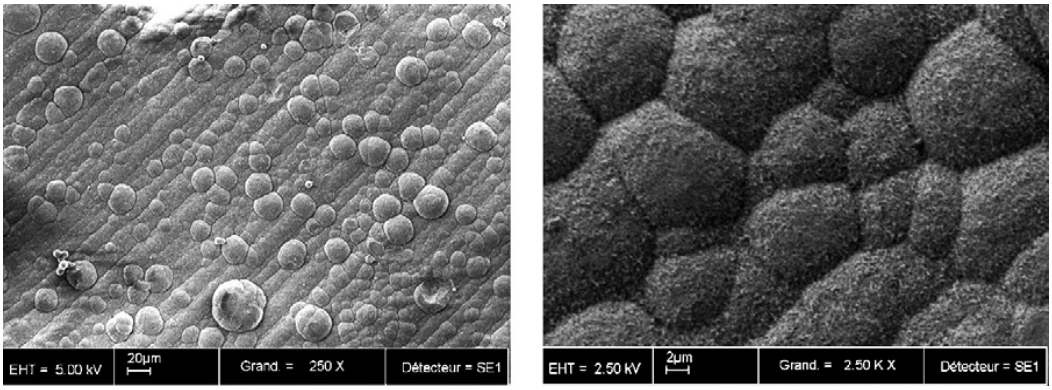

Fig. 11. SEM micrographs of a biomimetic calcium phosphate coating (from Le Guehennec L. et al, 2007)

.

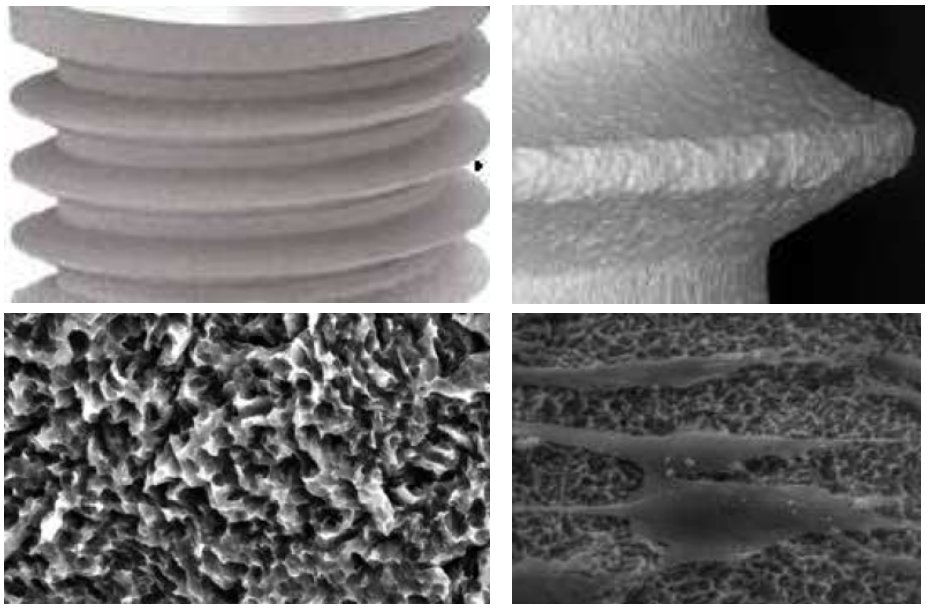

Fig. 12. One of the dental implant surface used in 3 of the reported studies: ZirTi surface (Sweden & Martina, Due Carrare, Padova IT), obtained by sand-blasting with zirconium oxide and subsequent acid etching with mineral acids.

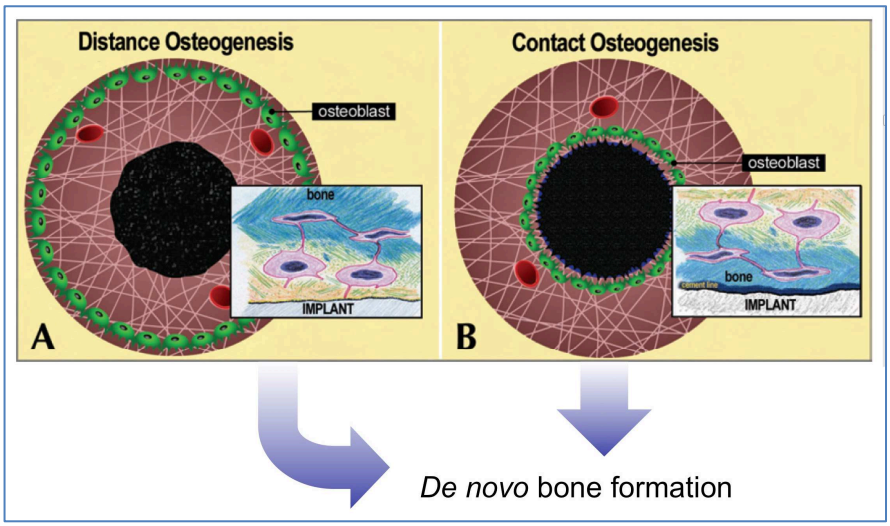

Fig. 13. Drawings from Davies JE (1998 and 2003) that show the initiation of distance osteogenesis (A) and contact osteogenesis (B) where differentiating osteogenic cells line either the old bone or implant surface respectively. The insets show the consequences of these two distinctly different patterns of bone formation. In the former the secretorily active osteoblasts, anchored into their extracellular matrix by their cell processes, become trapped between the bone they are forming and the surface of the implant. The only possible outcome is the death of these cells. On the contrary, in contact osteogenesis, *de novo* bone is formed directly on the implant surface, with the cement line in contact with the implant (insert).

Fig. 14. Cascade of events related to new bone formation on a dental implant surface (Berglundh et al, 2003).

De Novo Bone Formation

Four-stage process

1. differentiating osteogenic cells initially secrete a collagen-free organic matrix that provides nucleation sites for calcium phosphate mineralization (two non-collagenous bone proteins, osteopontin and bone sialoprotein, and two proteoglycans, but no collagen).
2. Calcium phosphate nucleation
3. Crystal growth and initiation of collagen fiber assembly
4. Calcification of the collagen compartment

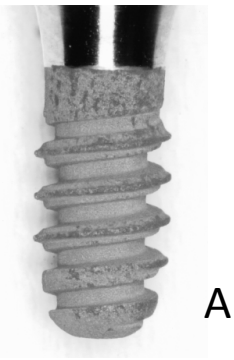

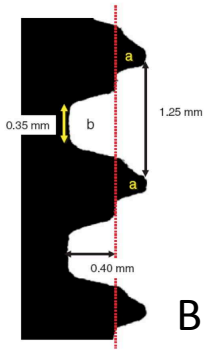

Fig 15 a-e. Figures from "De novo alveolar bone formation adjacent to endosseous implants A model study in the dog" (Berglungdh et al, 2003). (a) Experimental implant device: screw shaped titanium implant, diameter 4.1 mm, length 10 mm with circumferential trough in the endosseous part. (b) Cross-section of the wound chambers provided by the device: a, pitches engaging the bone tissue walls; b, inner U-shaped wound chamber proper. The dotted line indicates the lateral wall of the chamber, i.e. the position of the cut bone surface. (c) Wound chamber representing 2 weeks of healing. Decalcified section. Original mag. x 100. Mineralized bone coating the entire SLA chamber surface. (d) Detail of Fig. (c). Original mag. x 200. Woven bone continuous with parent bone (appositional bone formation), but newly formed bone also present on the SLA surface in areas remote of the parent bone (Contact osteogenesis). (d) Detail, Original mag. x 400. Spindle-shaped cells and collagen fibrils present around the vasculature.

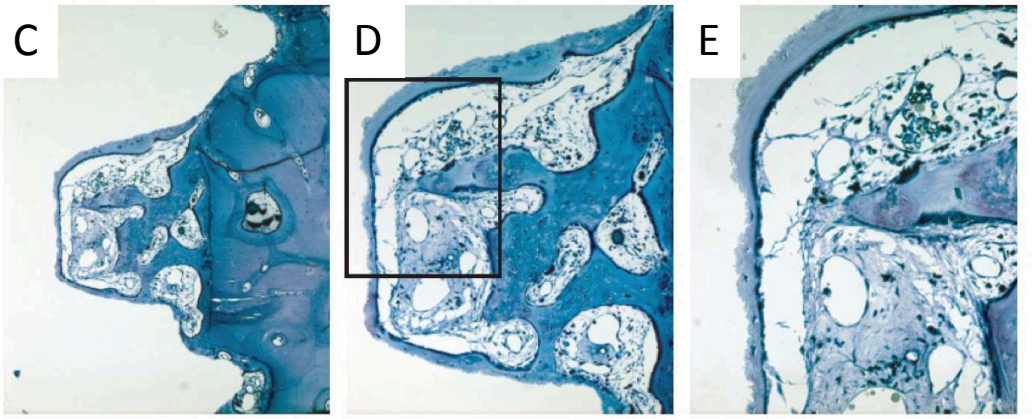

Gene (accession no.)	Oligonucleotide sequences	UPL probe	Ta (°C)
GADPH (NM_002046)	fw: 5′-cgggaagcccatcacca-3′ rv: 5′-ccggcctcaccccatt-3′	60	60
ALPL (NM_000478)	fw: 5′-ggcacctgccttactaactcc-3′ rv: 5′-cttagccacgttggtgttga-3′	1	60
VTN (NM_000638)	fw: 5′-tgagtgcaagccccaagt-3′ rv: 5′-gccatcgtcatagacccgtgt-3′	88	60
SPP1 (NM_000582)	fw: 5′-cgcagacctgacatccagta-3′ rv: 5′-ggctgtcccaatcagaagg-3′	61	60
CDC42 (NM_044472)	fw: 5′-catcggaatatgtaccgactgtt-3′ rv: 5′-tgcagtatcaaaaagtccaagagta-3′	22	60
RUNX2 (NM_001024630)	fw: 5′-cagtgacaccatgtcagcaa-3′ rv: 5′-gctcacgtcgctcattttg-3′	41	60

UPL, Universal Probe Library; fw, forward; rv, reverse; Ta, annealing temperature.

Table 1.1 The list of genes evaluated by quantitative RT-PCR.

Gene (accession no.)	Oligonucleotide sequences	UPL probe	Ta (°C)
GADPH (NM_002046)	fw: 5′-cgggaagcccatcacca-3′ rv: 5′-ccggcctcaccccatt-3′	60	60
ALPL (NM_000478)	fw: 5′-ggcacctgccttactaactcc-3′ rv: 5′-cttagccacgttggtgttga-3′	1	60
VTN (NM_000638)	fw: 5′-tgagtgcaagccccaagt-3′ rv: 5′-gccatcgtcatagacccgtgt-3′	88	60
SPP1 (NM_000582)	fw: 5′-cgcagacctgacatccagta-3′ rv: 5′-ggctgtcccaatcagaagg-3′	61	60
CDC42 (NM_044472)	fw: 5′-catcggaatatgtaccgactgtt-3′ rv: 5′-tgcagtatcaaaaagtccaagagta-3′	22	60
RUNX2 (NM_001024630)	fw: 5′-cagtgacaccatgtcagcaa-3′ rv: 5′-gctcacgtcgctcattttg-3′	41	60

UPL, Universal Probe Library; fw, forward; rv, reverse; Ta, annealing temperature.

Table 1.2 Atomic force microscopy analysis of glass surfaces.

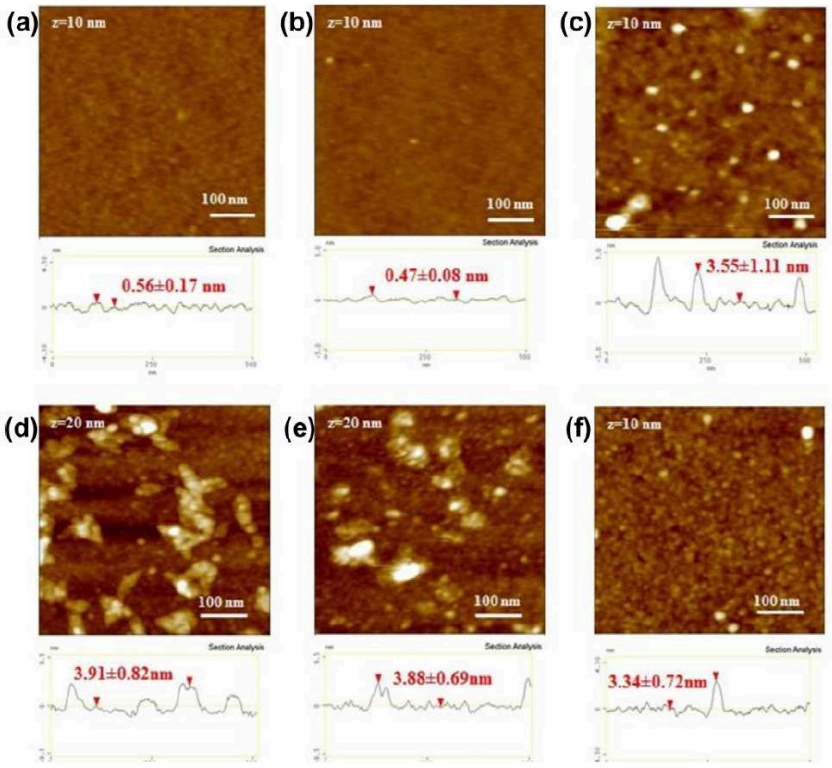

Fig. 1.1 Topographic characterization of functionalized surfaces. AFM images of (a) silanized, (b) RGDsp, (c) HVPsp, (d) RAD, (e) RGDunsp and (f) HVPunsp grafted glass surfaces. Scale bar, 100 nm.

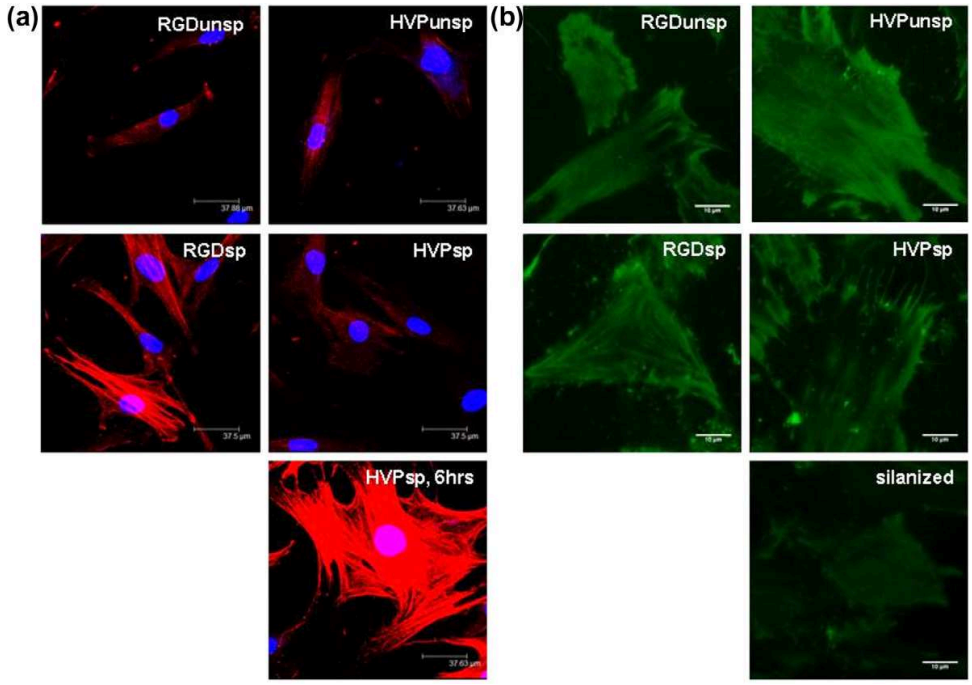

Fig. 1.2. Functionalized surfaces affect osteoblast behaviour. (a) Representative immunofluorescence analysis of osteoblast cells seeded for 2 h on differently functionalized glass surfaces and also for 6 h in HVPsp grafted supports. Osteoblasts were fixed and incubated with anti-b actin antibody (red). Nuclei were stained with TOTO-3 (blue). n = 3 per group. Scale bar, 37.5 lm. (b) Representative photomicrographs of TIRF microscopy performed on osteoblasts cultured on differently functionalized glass coverslips and probed with FM 1-43 fluorescent dye. Images were taken using a 2 megapixel CCD with CFI Plan Apochromat TIRF 60□/1.45 oil objective. n = 4 per group. Scale bar, 10 lm.

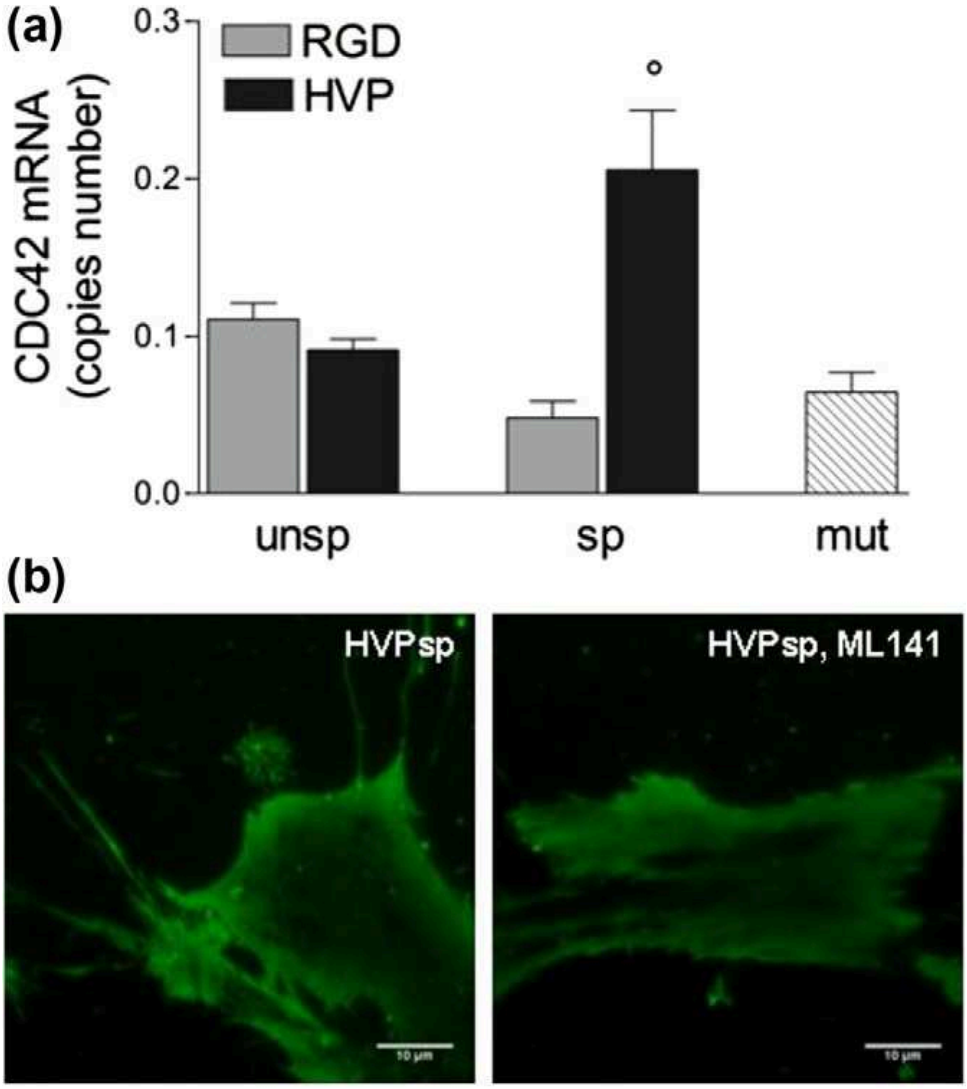

Fig. 1.3. HVPsp functionalized surfaces induce filopodia in human osteoblasts. (a) Quantitative RT-PCR analysis of CDC42 mRNA levels in human osteoblast cells seeded for 2 h onto unspecifically or specifically functionalized peptides and onto mutant peptide (mut). Data are reported as mean ± standard error of three independent experiments. °P < 0.02. (b) Representative photomicrographs of TIRF microscopy analysis performed on osteoblasts cultured for 2 h on HVPsp functionalized glass surfaces and treated for 1 h at 37 °C with 50 lM ML141, a pharma- cological inhibitor of Cdc42. n = 3 per group. Scale bar, 10 lm.

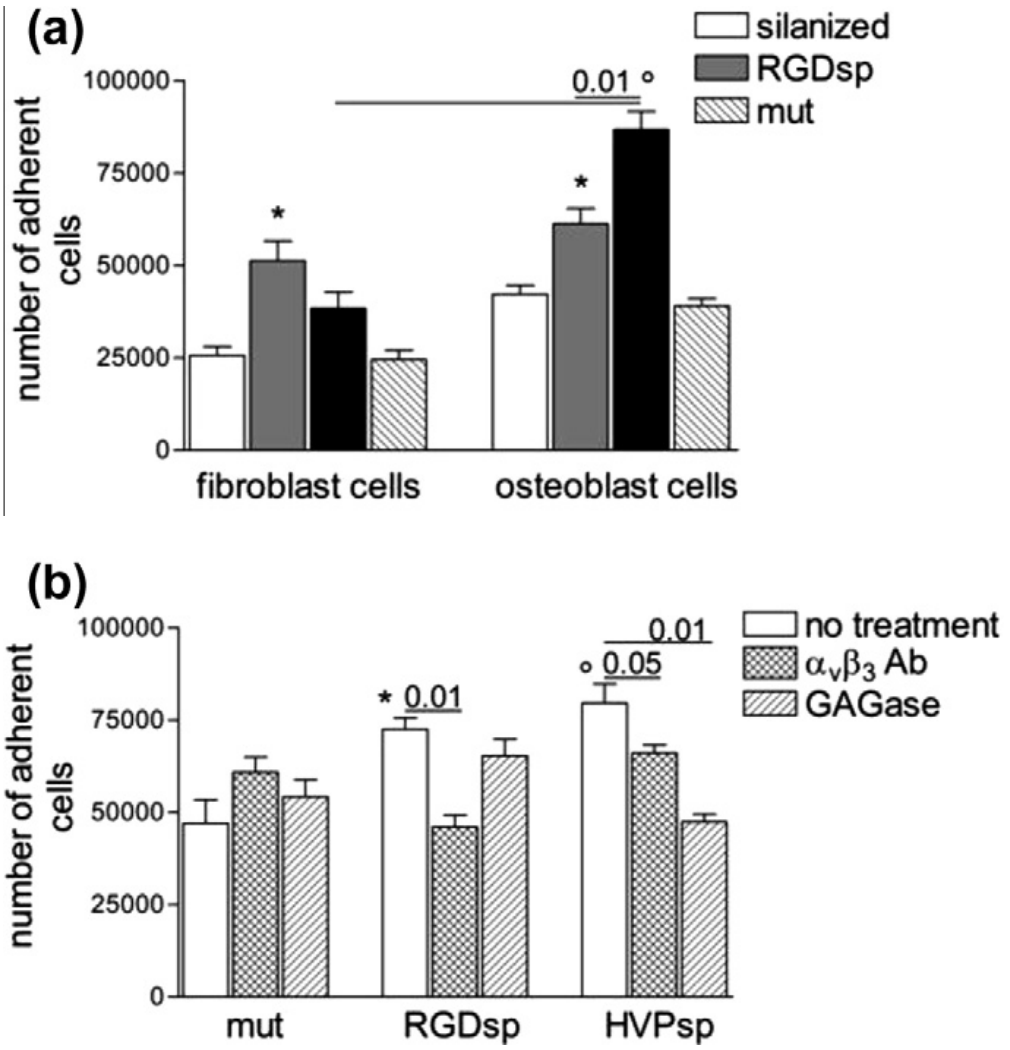

Fig. 1.4. HVPsp grafted surface preferentially induces osteoblasts adhesion through proteoglycans involvement. (a) Fibroblast and osteoblast cells were cultured for 2 h onto silanized, RGDsp, HVPsp and mutant (mut) peptides. Cellular adhesion was evaluated by MTT test and quantified by plotting data to a standard curve constructed for each experiment. Data are expressed as the mean ± standard error of four independent experiments. /P < 0.05 vs. silanized and mut surfaces. °P < 0.02 vs. silanized and mut surfaces. (b) Osteoblasts were pre-treated with anti-avb3 integrin antibody (avb3Ab) or a mixture of glycosidase (GAGase) and then cultured for 2 h onto RGDsp, HVPsp or mutant (mut) grafted surfaces. Cell adhesion was evaluated by MTT test and quantified using a standard curve constructed for each experiment. Data are reported as mean±standard error of four independent experiments. /P < 0.05 vs. non-treated osteoblasts seeded on mut surfaces; °P < 0.02 vs. non-treated osteoblasts seeded on mut surfaces.

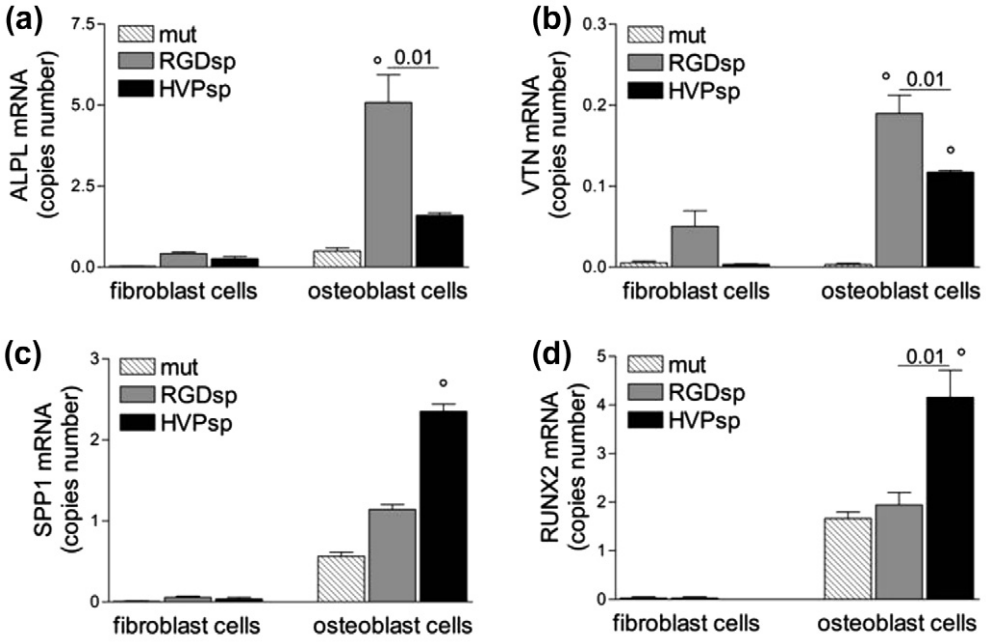

Fig. 1.5. RGDsp and HVPsp grafted surfaces induce osteogenic phenotype. Human fibroblast and osteoblast cells were cultured for 24 h onto surfaces functionalized with RGDsp, HVPsp or mutant (mut) peptides. Specific mRNA levels of human alkaline phosphatase (ALPL, a), vitronectin (VTN, b), osteopontin (SPP1, c), and runt-related transcription factor 2 (RUNX2 (d) were determined by quantitative RT-PCR analysis. Data are reported as mean ± standard error of three independent experiments. °$P < 0.02$ vs. cells cultured onto mut.

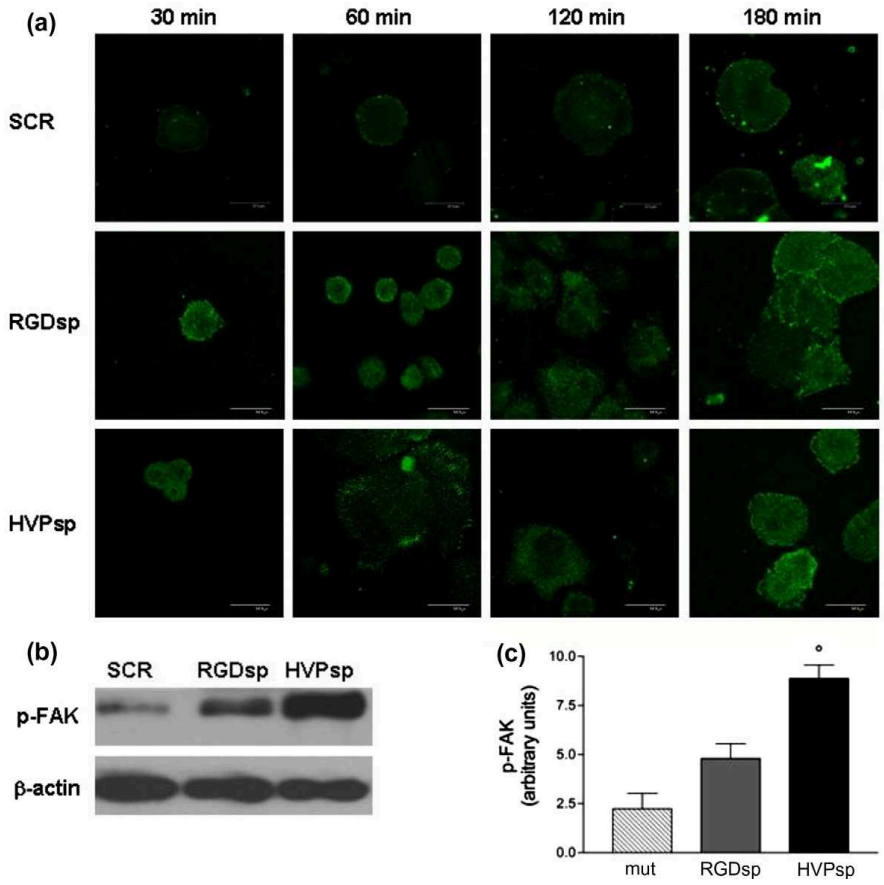

Fig.1. 6. RGDsp and HVPsp grafted surfaces differentially induce FAK activation. (a) Representative immunofluorescence analysis of osteoblast cells seeded on glass surfaces functionalized with RGDsp, HVPsp or mutant (mut) peptides. Osteoblasts were fixed and incubated with anti-pFAK antibody (green). n = 3 per group. Scale bar, 37.5 lm. (b) Representative Western blot analysis of p-FAK in protein extracts from osteoblasts cultured for 6 h on differentially functionalized surfaces. One representative blot of three is presented. b-actin was used as loading control. (c) Protein signals of p-FAK were determined by densitometric analysis of Western blotting (n = 3) using the VersaDoc Quantity One software (BioRad). Data are reported as the mean ± standard error. a.u. = arbitrary units. °P < 0.02 vs. osteoblasts cultured on mut functionalized surfaces.

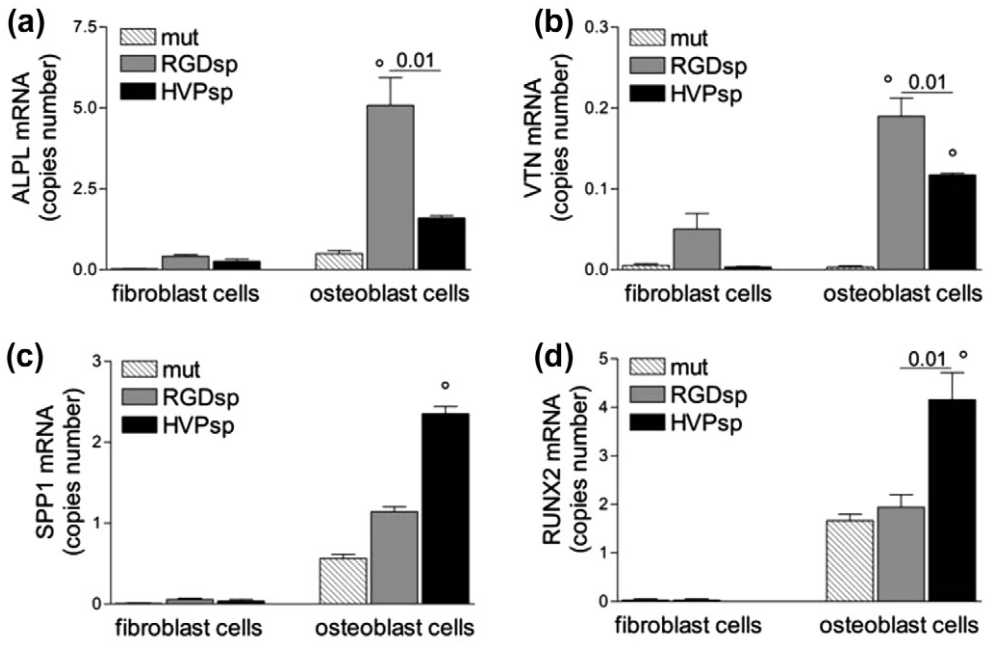

Fig. 1.5. RGDsp and HVPsp grafted surfaces induce osteogenic phenotype. Human fibroblast and osteoblast cells were cultured for 24 h onto surfaces functionalized with RGDsp, HVPsp or mutant (mut) peptides. Specific mRNA levels of human alkaline phosphatase (ALPL, a), vitronectin (VTN, b), osteopontin (SPP1, c), and runt-related transcription factor 2 (RUNX2 (d) were determined by quantitative RT-PCR analysis. Data are reported as mean ± standard error of three independent experiments. °P < 0.02 vs. cells cultured onto mut.

	RGDsp	RGDsp + FAK inhibitor	HVPsp	HVPsp + FAK inhibitor
ALPL	5.59 ± 0.42	$4.6 \times 10^{-7} \pm 0.5 \times 10^{-8}$*	1.14 ± 0.18	$1.56 \times 10^{-7} \pm 0.4 \times 10^{-8}$ *
VTN	$1.2 \times 10^{-5} \pm 7.7 \times 10^{-7}$	$9.8 \times 10^{-6} \pm 2.3 \times 10^{-8}$*	$6.3 \times 10^{-6} \pm 4.4 \times 10^{-8}$	$6.6 \times 10^{-6} \pm 4.7 \times 10^{-8}$
SPP1	1.05 ± 0.08	1.59 ± 0.03	2.57 ± 0.70	1.48 ± 0.05*
RUNX2	1.94 ± 0.25	1.78 ± 0.14	4.15 ± 0.55	2.16 ± 0.65*

Human osteoblast cells were pre-treated with FAK inhibitor and cultured for 24 h. mRNA specific levels were evaluated by quantitative RT-PCR. Data are expressed as the mean ± standard error of three independent experiments.
* $P < 0.05$ vs. no pre-treated osteoblasts cultured on corresponding functionalized surfaces.

Table 1.3. Evaluation of mRNA transcript levels in osteoblasts treated with FAK inhibitor.

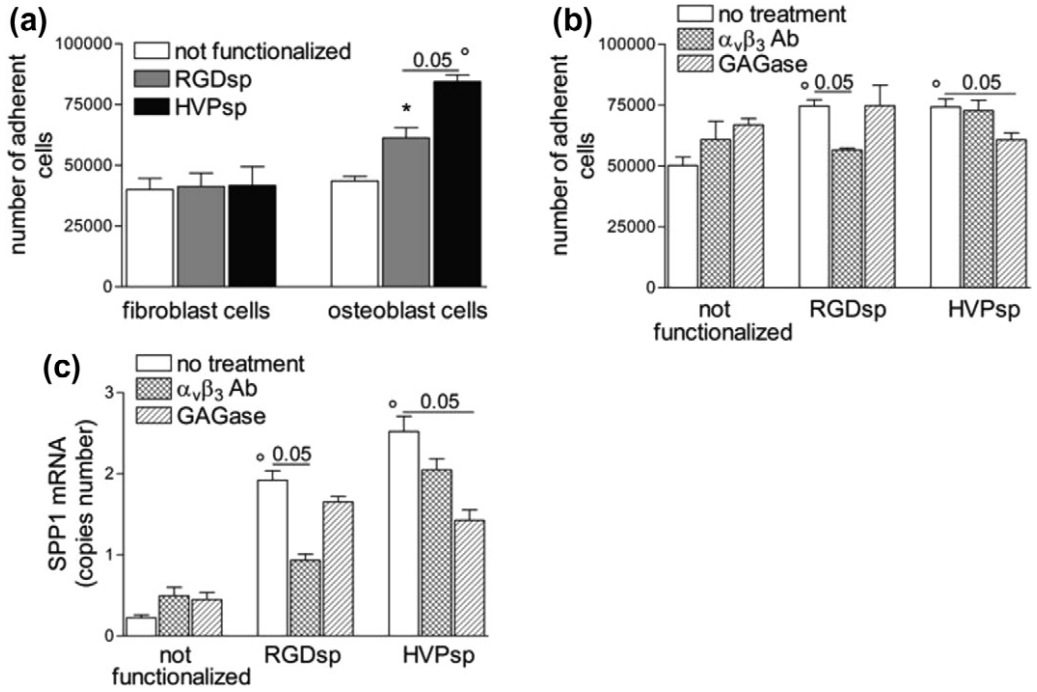

Fig. 1.7. Evaluation of osteoblast behaviour on functionalized Ti surfaces. (a) Fibroblasts and osteoblasts were cultured for 2 h on non-functionalized, RGDsp or HVPsp grafted Ti surfaces. Cellular adhesion was evaluated by MTT test and quantify by plotting data to a standard curve constructed for each experiment. Data are expressed as the mean ± standard error of three independent experiments. /P < 0.05 vs. osteoblasts seeded on non-functionalized Ti surface; °P < 0.02 vs. osteoblasts seeded on non- functionalized Ti surface. (b) Osteoblasts were pre-treated with anti-v3 integrin antibody (v3Ab) or a mixture of glycosidase (GAGase) and then cultured for 2 h on non-functionalized, RGDsp or HVPsp grafted Ti surfaces. Cell adhesion was evaluated by MTT test. Data are reported as mean ± standard error of three independent experiments. °P < 0.02 vs. non-treated osteoblasts seeded on non-functionalized surfaces. (c) Human osteoblast cells were pre-treated with v3Ab or GAGase and cultured for 24 h on non- functionalized, RGDsp or HVPsp grafted Ti surfaces. Osteopontin (SPP1) specific mRNA levels were determined by quantitative RT-PCR analysis. Data are reported as mean ± standard error of three independent experiments. °P < 0.02 vs. non-treated cells cultured on non-functionalized surfaces.

Cell type	Surfaces	RUNX2	SPP1
Fibroblasts	Non-functionalized	n.d.	$9.14 \times 10^{-3} \pm 5.4 \times 10^{-3}$
	RGDsp	n.d.	0.057 ± 0.01
	HVPsp	n.d.	0.037 ± 0.01
Osteoblasts	Non-functionalized	1.99 ± 0.43	0.197 ± 0.01*
	RGDsp	4.06 ± 0.85*	1.842 ± 0.23*
	HVPsp	5.79 ± 0.63*	2.350 ± 0.09*°

Human fibroblast and osteoblast cells were cultured on non-functionalized, RGDsp or HVPsp grafted Ti surfaces. Levels of mRNA transcripts were measured by quantitative RT-PCR. Data are reported as the mean ± standard error of three independent experiments.
* $P < 0.05$ vs. osteoblasts cultured on non-functionalized surfaces.
° $P < 0.02$ vs. fibroblasts seeded on corresponding surfaces. n.d. = not detected.

Table 1.4 mRNA transcript levels of cells cultured on functionalized Ti surfaces.

gene symbol	*forward primer (5'→ 3')*	*reverse primer (5'→ 3')*	*product length (bp)*
ALPL	GGCTTCTTCTTGCTGGTGGA	CAAATGTGAAGACGTGGGAATGG	181
CD31	TCCAGCCAACTTCACCATCC	TGGGAGAGCATTTCACATACGA	171
COL1A1	TGAGCCAGCAGATCGAGA	ACCAGTCTCCATGTTGCAGA	178
GAPDH	TCAACAGCGACACCCAC	GGGTCTCTCTCTTCCTCTTGTG	203
KDR	GGAGGAGGAGGAAGTATGTGACC	AACCATACCACTGTCCGTCTG	184
PPARG	CAGGAGATCACAGAGTATGCCAA	TCCCTTGTCATGAAGCCTTGG	173
RUNX2	AGCCTTACCAAACAACACAACAG	CCATATGTCCTCTCAGCTCAGC	175

ALPL (alkaline phosphatase, liver/bone/kidney); CD31 (PECAM-1, platelet/endothelial cell adhesion molecule 1); COL1A1 (collagen, type I, alpha 1); GAPDH (glyceraldehyde-3-phosphate dehydrogenase); KDR (kinase insert domain receptor); PPARG (peroxisome proliferator-activated receptor gamma); RUNX2 (runt-related transcription factor 2).

Table 2.1. Human primer sequences.

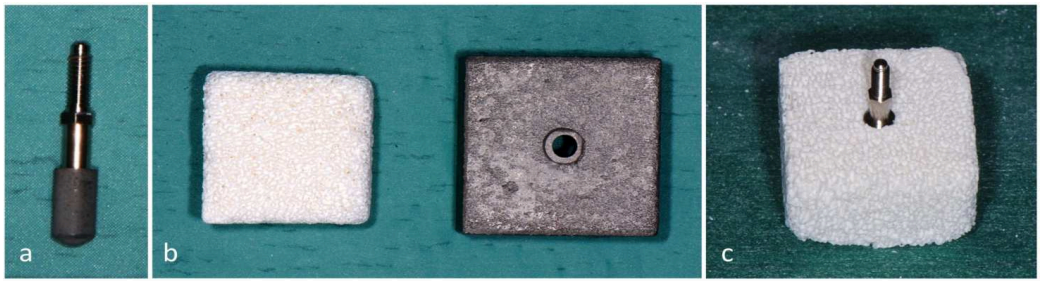

Figure 2.1. a) Customized cylindrical implant; b) bovine bone block (left) and customized drilling guide (right); c) implant positioned in the bone block.

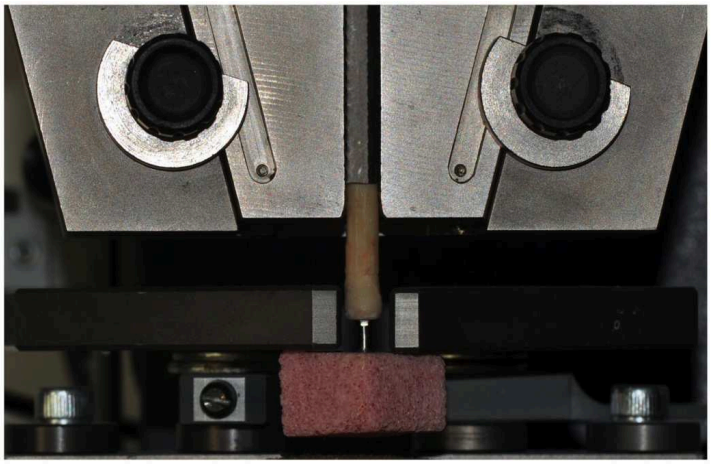

Fig. 2.2 Pull-out tests of the implants from the bone blocks (tensile test). Immediately before the test, a mounter was attached to the extension pin of each implant. After alignment and positioning of the samples in the testing machine, implants were loaded.

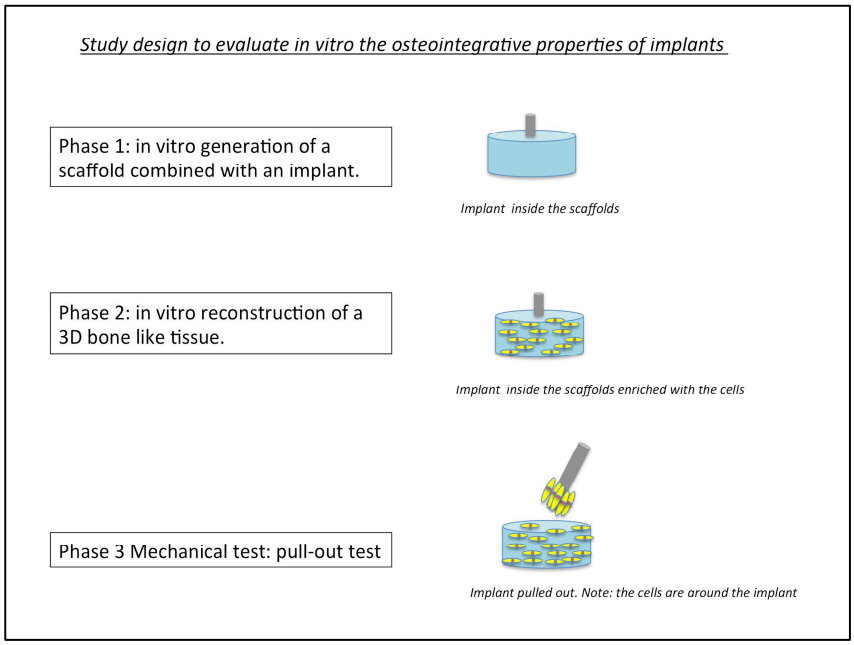

Fig. 2.3. Study design to evaluate *in vitro* the osteointegrative properties of implants.
Design of the in vitro experiment. Phase 1: in vitro generation of a scaffold combined with an implant. Customized cylindrical implants were inserted in the bone blocks. Phase 2: *in vitro* reconstruction of a 3D bone like tissue. ADSc are seeded into a scaffold combined with the implant. Phase 3 Mechanical test: pull-out test. The pull-out test is performed in order to measure the force needed to extract an embedded insert from a concrete mass.

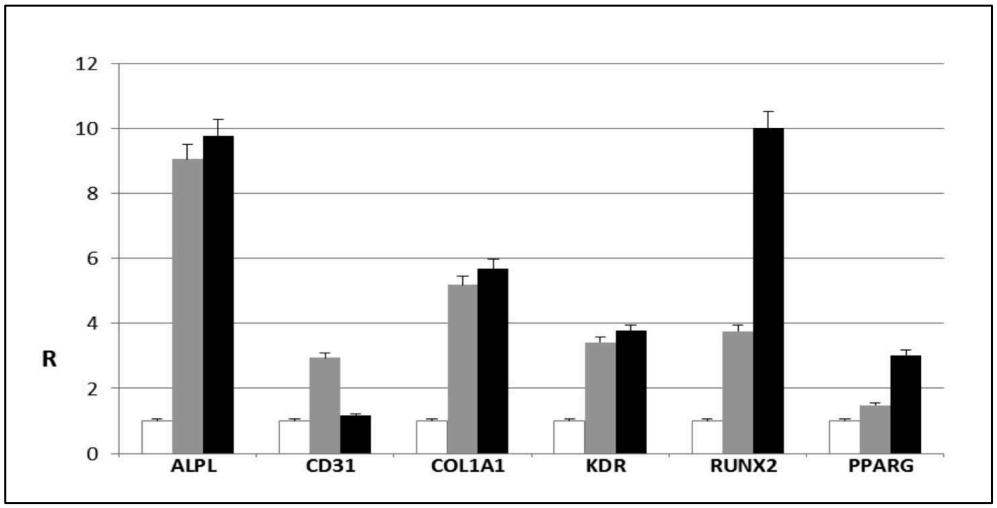

Fig. 2.4. Real-time PCR analysis of ALPL, CD31, COL1A1, KDR, RUNX2, and PPARG. Grey bars indicate the expression level of the selected genes in ADSCs seeded on the bone blocks around the dental implants in presence of osteo-endothelial differentiation medium for 30 days. Black bars represent the gene expression level of the same markers in ADSCs seeded on tissue culture polystyrene in osteo-endothelial differentiation medium for 30 days. Gene expression levels are reported as ratios (R) with respect to the mRNA expression in ADSCs seeded on tissue culture polystyrene for 30 days in cDMEM (white bars). Data are mean and SD (n=3).

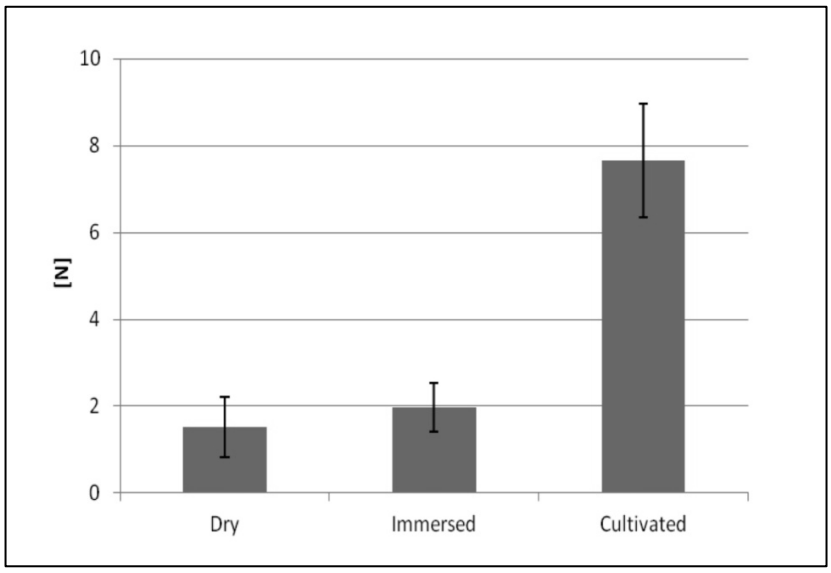

Figure 2.5. Average value and standard deviation of force (N, Newton) measured in the pull out tests, in different experimental conditions (cultivated: 7.66 N ±1.30; dry: 1.52 N ± 0.70 ; immersed: 1.96 ± 0.56). Dry vs Immersed (p=0.3664), Dry vs Cultivated (p=0.0002), Immersed vs Cultivated (p=0.0002).

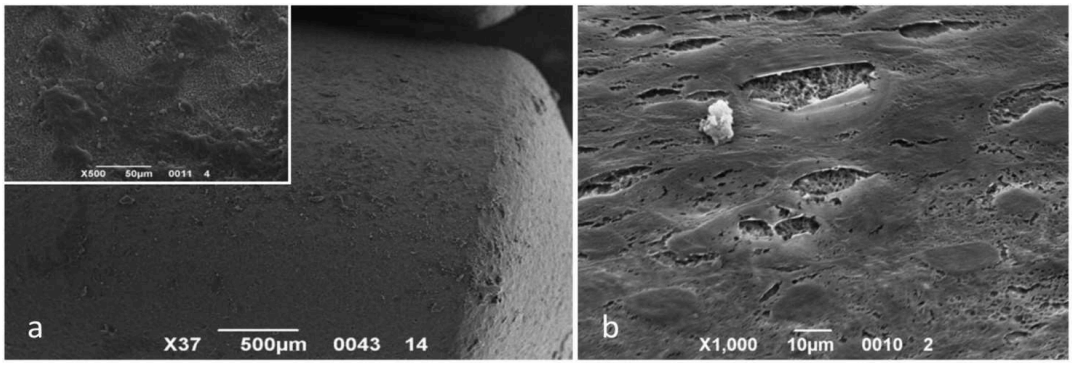

Fig. 2.6. SEM analysis of the dental implant surface a) at 37x and 500x (inset) magnification extracted from a dry bone block; b) afterpull-out in the cultivated group at 1000x magnification. A carpet of cells with an osteoblast morphology is visible on the implant surface.

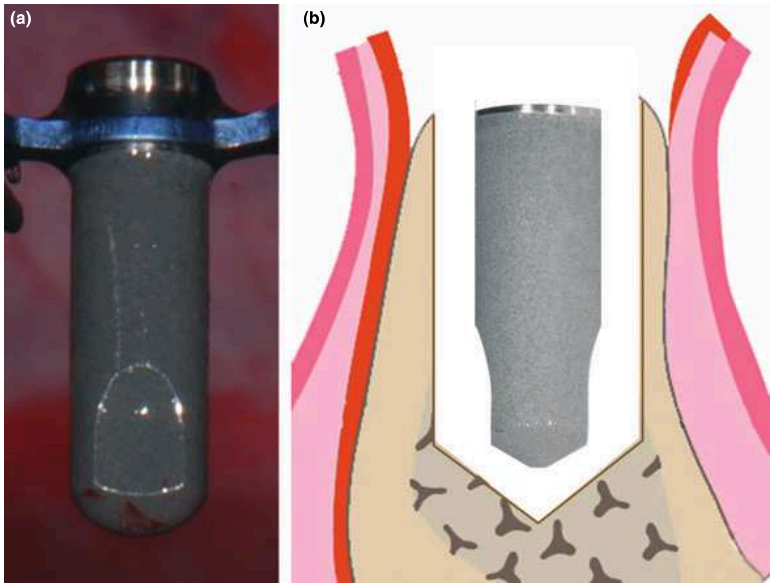

Fig. 3.1. (a) Customized cylindrical implant characterized by the absence of threads and the presence of a modified apical region which presented with two opposing flat surfaces. (b) Schematic drawing representing the implant placed within the prepared defect without any contact with the bony walls.

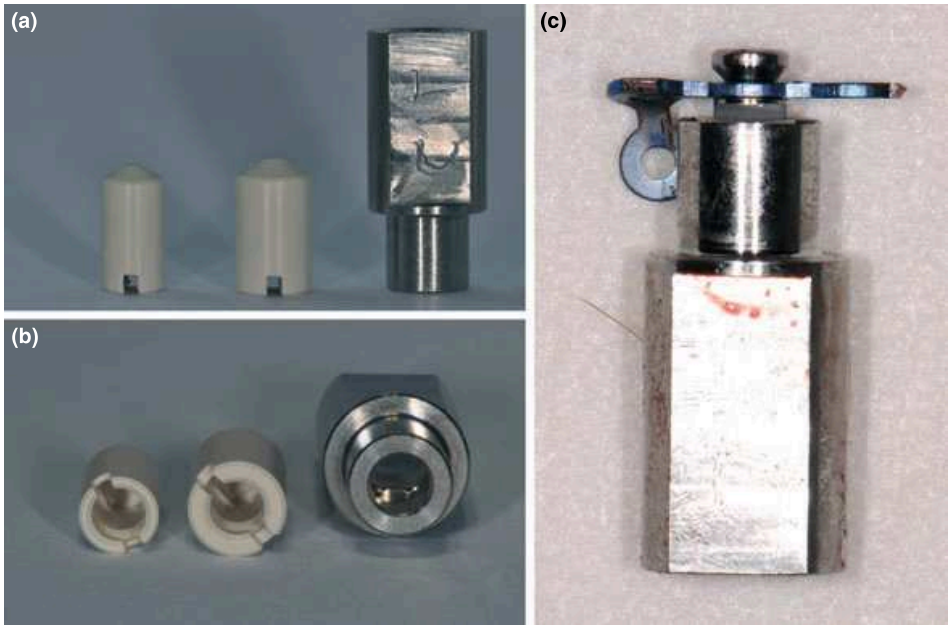

Fig.3. 2. (a, b) Customized PEEK baskets used for implant positioning within the defects. (a–c) Customized sterile titanium device used to hold the implants while tightening the cover screw to stabilize the fixation plate to the implant.

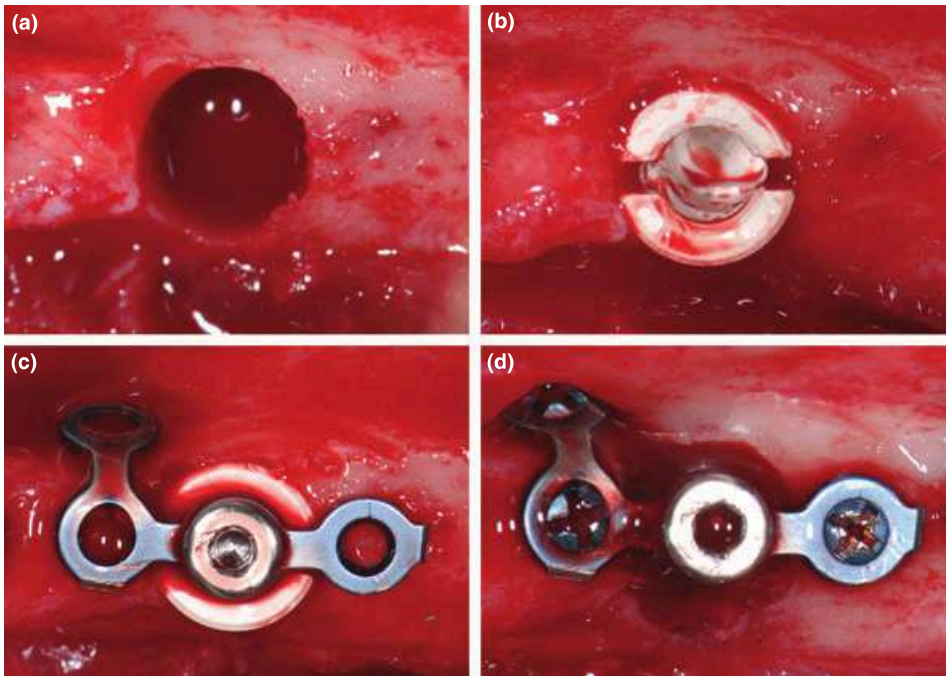

Fig. 3.3. Clinical illustration of the surgical procedures. (a) Prepared large defect. (b) PEEK basket in place. Note the alignment of the two coronal notches with the mesio-distal plane and the flat surface in the bottom. (c) After the placement of the implant within the basket, an L-shaped plate was modeled and adapted to the alveolar crest and then loosely attached to the implant with a cover screw. (d) The implant/plate assembly was repositioned in the recipient defects sites, and the plates fixed to the alveolar bone using three fixation screws.

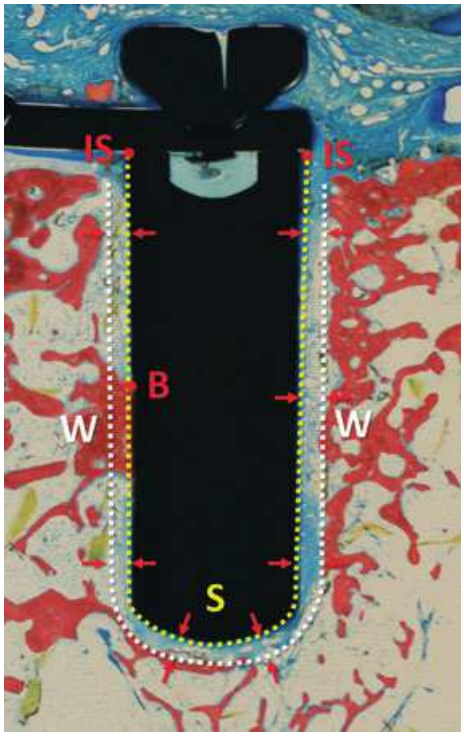

Fig. 3.4. Schematic illustration of landmarks used for histological measurements. (IS) the shoulder of the implant; (B) the most coronal bone-to-implant contact; (S) the implant surface; (W) the bony walls of the implant bed. The red arrows indicating the zones were the width of the remaining defect (S–W) and the DCT width (Fig. 5) were measured.

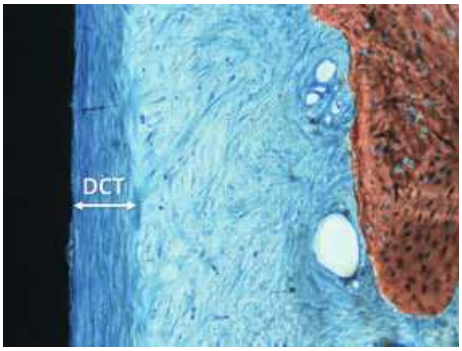

Fig. 3.5. Schematic illustration of the measurement of the width of the layer of dense connective tissue (DCT) adherent to the implant surface at small and large defects.

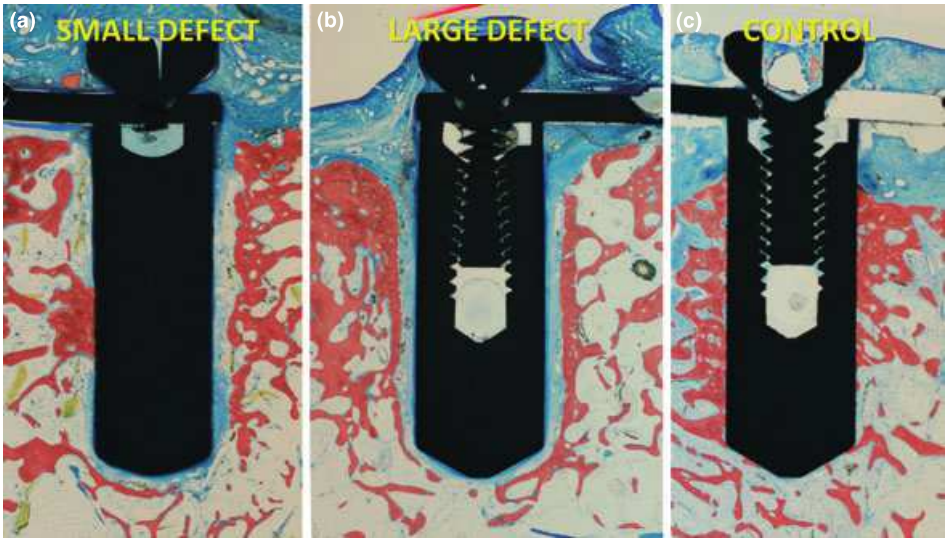

Fig. 3.6. Ground sections representing the result of healing at (a) small defect, (b) large defect, and (c) control implants. Stevenel's blue and alizarin red stain. Original magnification 912. A small amount of bone to implant contact was found at the defect sites. Cover screws were in place and no gaps were identifiable between the fixation plate and the implant shoulder as well as between the fixation plate and the cover screw.

	IS-B (mm)			BIC%		
	Small (n = 5)	Large (n = 1)	Control (n = 6)	Small (n = 6)	Large (n = 6)	Control (n = 6)
Mean and SD	4.40 (1.60)	6.42 (NA)	1.03 (0.20)	5.33 (3.71) *	0.32 (0.77) *	46.11 (14.62) *
Range	2.82–6.14	NA	0.72–1.27	0–10.6	0–1.89	23.17–63.64

Mean values, standard deviations (SD) and range (minimum – maximum).
IS, Implant shoulder; B, Most coronal bone-to-implant contact; BIC, Bone-to-implant contact. NA, Not applicable.
*$P < 0.05$ between small and large defects and between defects and control.

Table 3.1. Histological measurements after 3 months of healing

	Small defects			Large defects		
	Original defect (mm)	S–W (mm)	Defect filling %	Original defect (mm)	S–W (mm)	Defect filling %
Mean and SD	0.7 (NA)	0.39 (0.17)	43.7 (24)	1.2 (NA)	0.50 (0.09)	58.7 (7.5)
Range	NA	0.21–0.60	14.3–69.4	NA	0.40–0.64	46.7–66.7

Mean values, standard deviations (SD) and range (minimum – maximum).
S, Implant surface; W, Bony walls; NA, Not applicable.
P < 0.05.

Table 3.2. Original size of the gap at implant installation and histological measurements after 3 months of healing. N=6

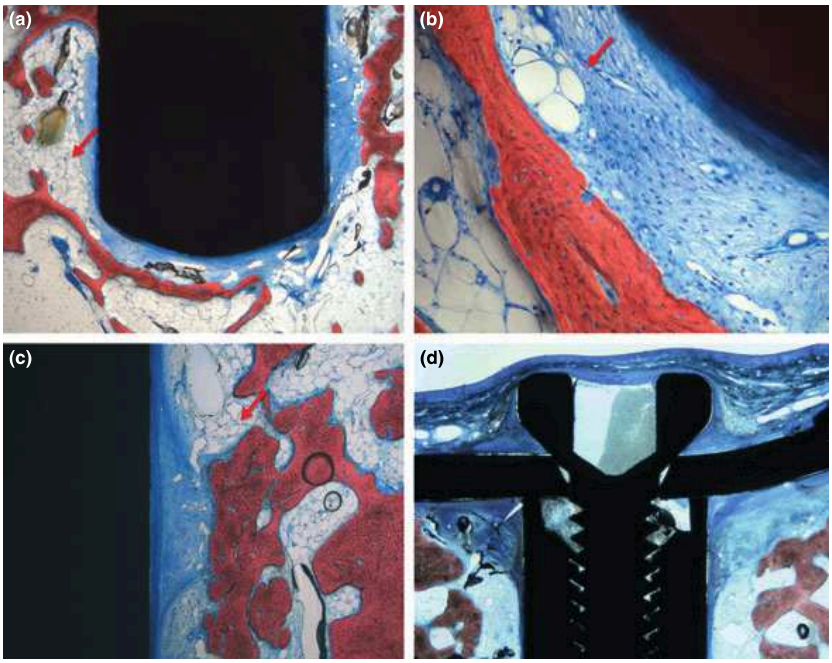

Fig. 3.7. Ground sections representing the result of healing at the large defect sites after 3 months. Stevenel's blue and alizarin red stain. The red arrows indicate bone marrow and fat cells mainly located at the periphery of the defect. (a) Apical region of the implant site illustrating the remaining defect. Original magnification 920. (b) Larger magnification (original 9200) of the left side of the apex represented in (a). Two connective tissues were included in the defect, an internal dense tissue (DCT) adherent to the implant surface and low density external tissue, inter- posed between the DCT and the bony walls. (c) DCT was sometimes seen connected with the bony walls through a denser connective tissue. Original magnification 940. (d) DCT was seen in continuity with a similar, but thicker tissue, above the level of the bony crest. Original magnification 920.

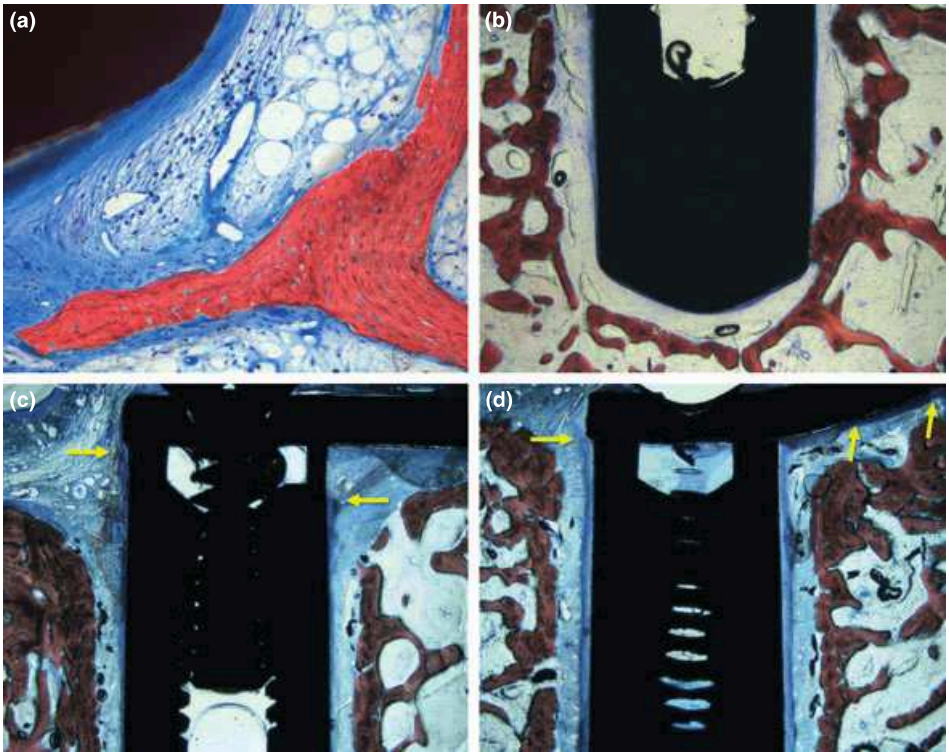

Fig. 3.8. Ground sections representing the result of healing at the large defect sites after 3 months. Stevenel's blue and alizarin red stain. (a) Apical region of the implant site illustrating the remaining defect. A layer of dense connective tissue was found adherent to the implant surface, separated from the bony walls of the defect by a low den- sity connective tissue. Original magnification 9200. (b) Small amount of bone in contact with the implant surface. Original magnification 920. (c–d) DCT was close to the implant margin and, sometimes, extending above the level of the bony crest (yellow arrows). Original magnification 920.

	IS-DCT (mm)		Width DCT (mm)		DCT%	
	Small	Large	Small	Large	Small	Large
Mean and SD	0.34 (0.45)	0.38 (0.69)	0.08 (0.04)	0.10 (0.06)	92.80 (7.60)	95.58 (5.66)
Range	0–1.13	0–1.70	0.03–0.13	0.06–0.20	79.80–100	86.86–100

Mean values, standard deviations (SD) and range (minimum – maximum).
IS, Implant shoulder; DCT, Dense connective tissue.
P < 0.05.

Table 3.3. Histological measurements after 3 months of healing .n=6

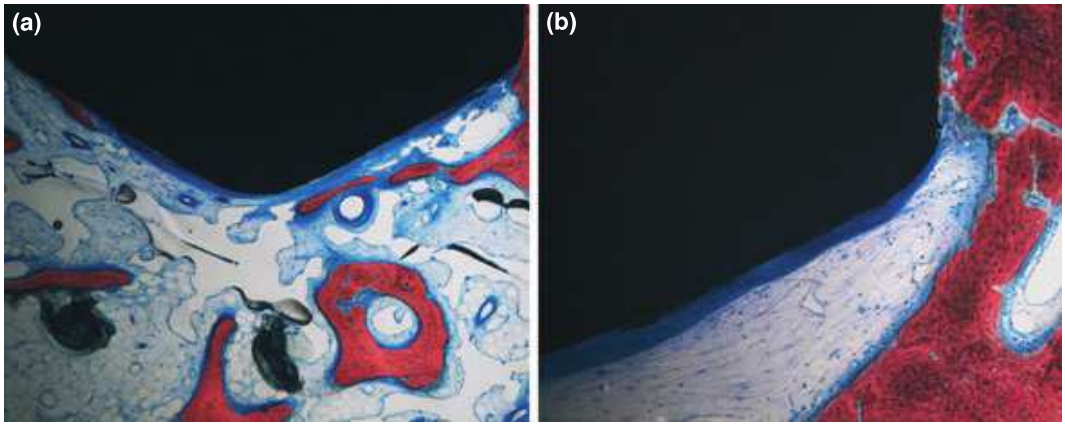

Fig. 3.9. (a) Ground sections (original magnification 940) at a control site illustrating the presence of a DCT layer in the apical region, similar to that found at the defect sites (b; original magnification 9100). Stevenel's blue and aliza- rin red stain.

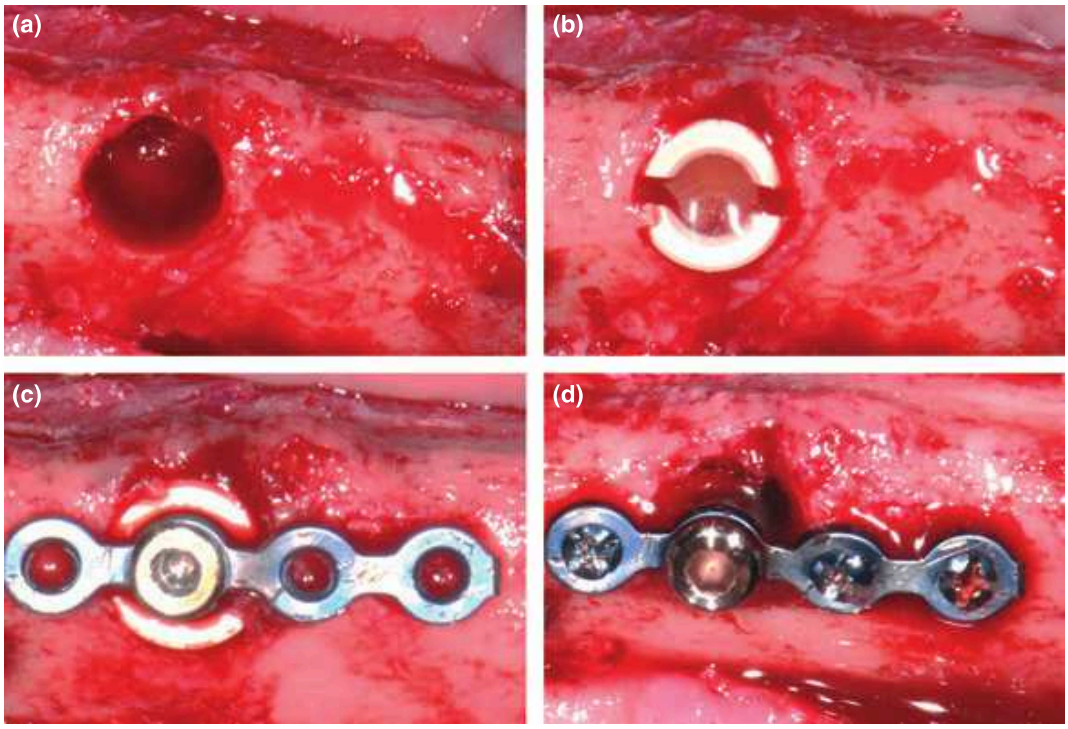

Fig. 4.1. Clinical illustration of the surgical procedures at a control site. (a) Prepared defect (5.2 mm wide and 8.2 mm deep). (b) PEEK basket in place. Note the alignment of the two coronal notches with the mesio-distal plane. (c) After the placement of the implant within the basket, a straight-shaped plate was modeled, adapted to the alveo- lar bony crest, and then attached to the implant with a cover screw. (d) The basket was removed, the implant/plate assembly was repositioned in the recipient defect site, and the plate secured to the alveolar bone using three fixation screws.

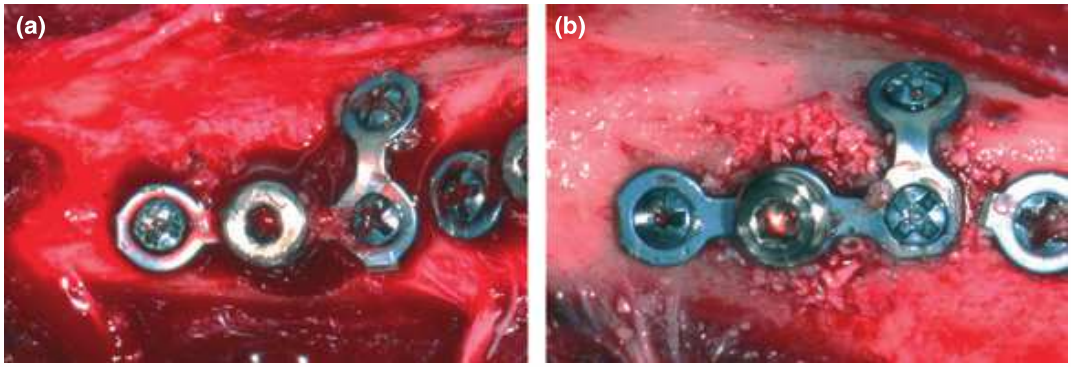

Fig. 4.2 a) Control site: coagulum fills the 1.2-mm-wide gap around the implant. (b) Test site: the gap is grafted with demineralized bovine bone matrix (DBBM).

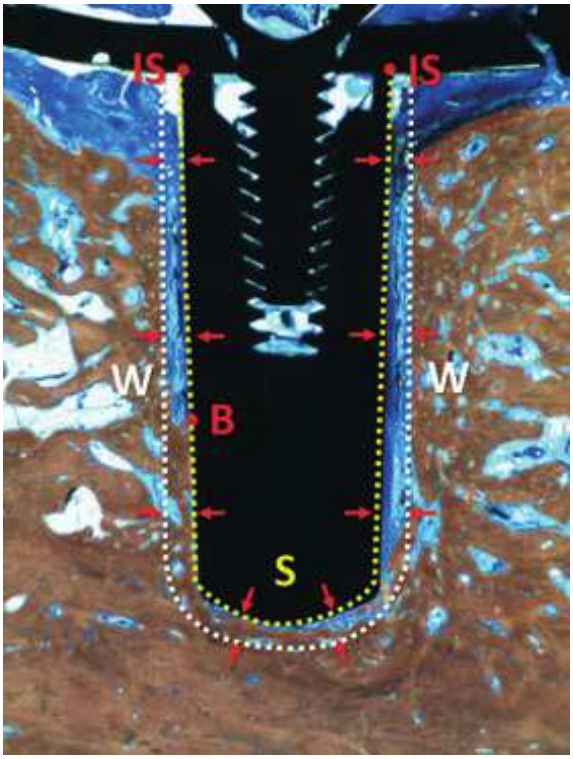

Fig. 4.3. Schematic illustration of landmarks used for histological measurements. (IS) the shoulder of the implant; (b) the most coronal mineralized bone-to- implant contact; (S) the implant surface; (W) the bony walls of the implant bed. The red arrows indicate the zones were the width of the remaining defect (S-W), and the dense connective tissue width (wDCT; see Fig. 5) were measured.

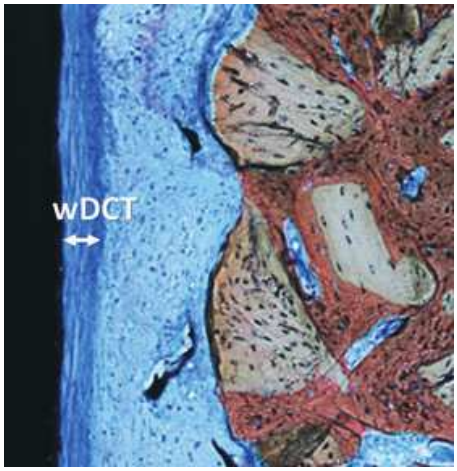

Fig. 4.4. Schematic illustration of the measurement of the width of the layer of dense connective tissue (DCT) adherent to the implant surface at test and control sites. The implant profile is on the left. The picture represents a detail of an histological image of a test site.

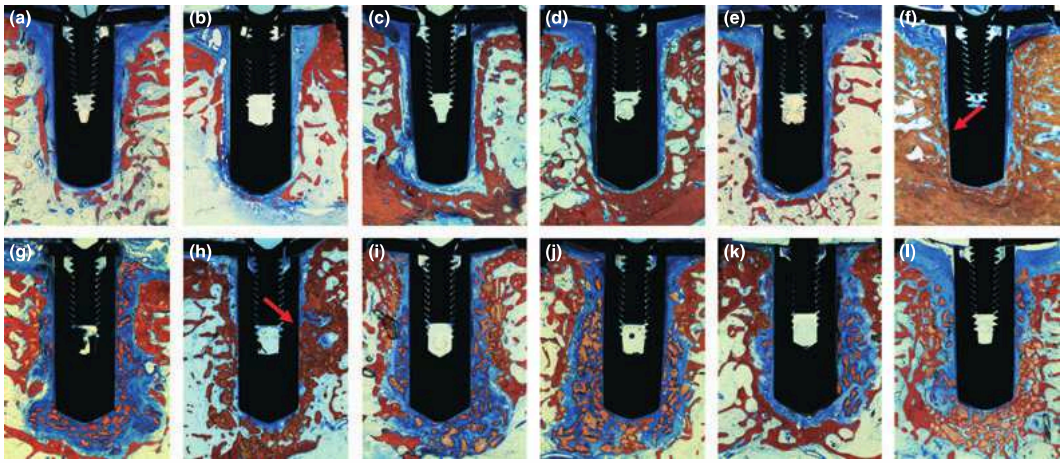

Fig.4.5. Overview of the six control implants (from a to f) and the corresponding six test implants (from g to l). Ground sections, Stevenel's blue and alizarin red stain. Original magnification 912. A small amount of mineralized bone-to-implant contact was found in one control and in one test sites (see arrows indicating the respective B position in fig- ures f and h). No gaps were identifiable between fixation plate, implant shoulder, and cover screw. Two cover screws resulted to be slightly exposed to the oral cavity (e, f), while all the others were still covered by mucosa (including l).

Table 1. **Histological linear measurements after 3 months of healing at the 1.2 mm wide defects**

n = 6	IS-B (mm)	MBIC%	S-W* (mm)	Defect filling*%	IS-D (mm)	DCT%	wDCT (mm)
CTRL							
Mean (SD)	0.96 (2.35)	4.0 (9.8)	0.48 (0.12)	60.0 (9.7)	1.44 (1.84)	84.9 (17.8)	0.12 (0.09)
Min; Max	0.00; 5.76	0.0; 23.9	0.29; 0.62	48.1; 75.8	0.00; 5.10	58.5; 100.0	0.01; 0.23
TEST (DBBM)							
Mean (SD)	0.54 (1.31)	3.9 (9.7)	0.88 (0.41)	26.8 (34.1)	0.36 (0.66)	88.5 (16.7)	0.12 (0.11)
Min; Max	0.00; 3.22	0.0; 23.6	0.17; 1.29	−7.3; 85.9	0.00; 1.64	60.9; 100.0	0.02; 0.30

Mean values, standard deviations (SD) and range (minimum–maximum). IS, Implant shoulder; B: Most coronal bone-to-implant contact; MBIC, mineralized bone-to-implant contact; S: Implant surface; W: Bony walls; D: coronal end of DCT (dense connective tissue); DCT%: DCT% in relation to the length of the implant surface; wDCT, Width of DCT.
*$P < 0.05$ between test and control.

Table 4.1. Histological linear measurements after 3 months of healing at the 1.2 mm wide defects

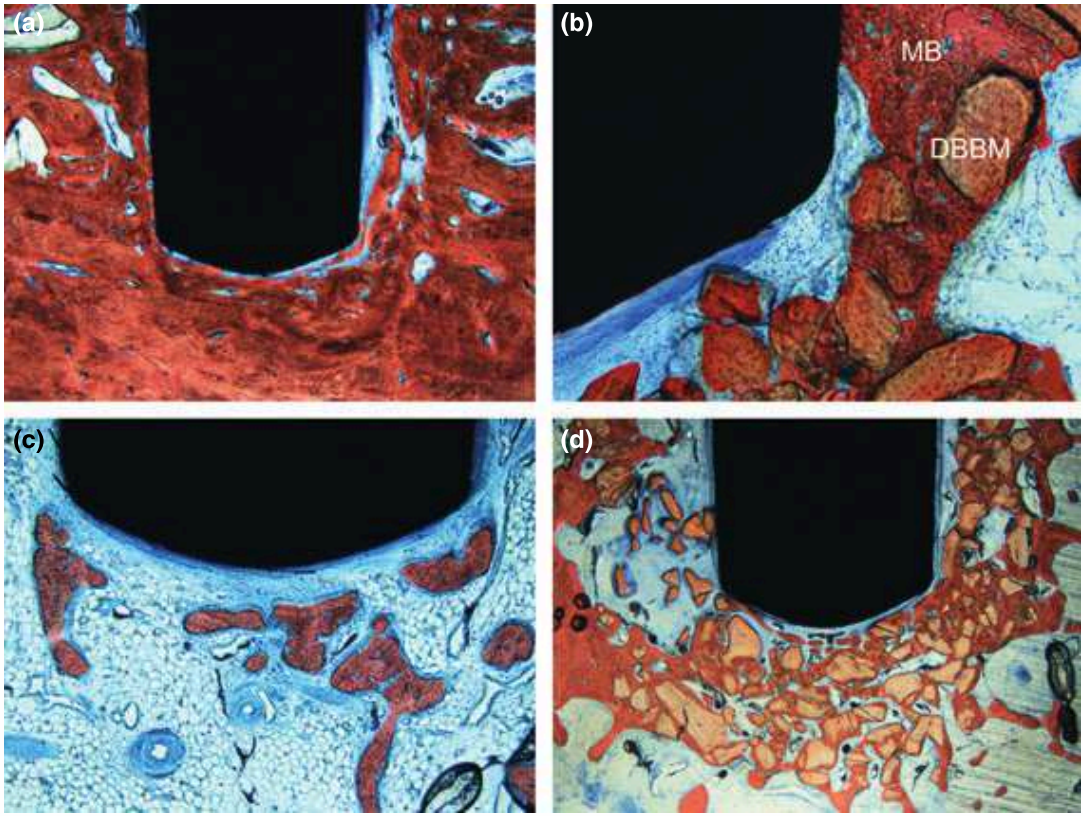

Fig. 4.6. (a) Detail of the control site presenting MBIC (see Fig. 6f), magnification 920. (b) Detail of test site pre- senting MBIC (see Fig. 6h), magnification 9100. MB, Mineralized bone; DBBM, deproteinized bovine bone matrix. (c) Detail of the apical area of the control implant represented in Fig. 6a. DCT is lining the implant surface. No MBIC is observable. Mature bone resides in proximity of the implant surface, surrounded by bone marrow. Original magnification 940. (d) Detail of the apical area of the test implant represented in Fig. 6l. Original magnification 920.

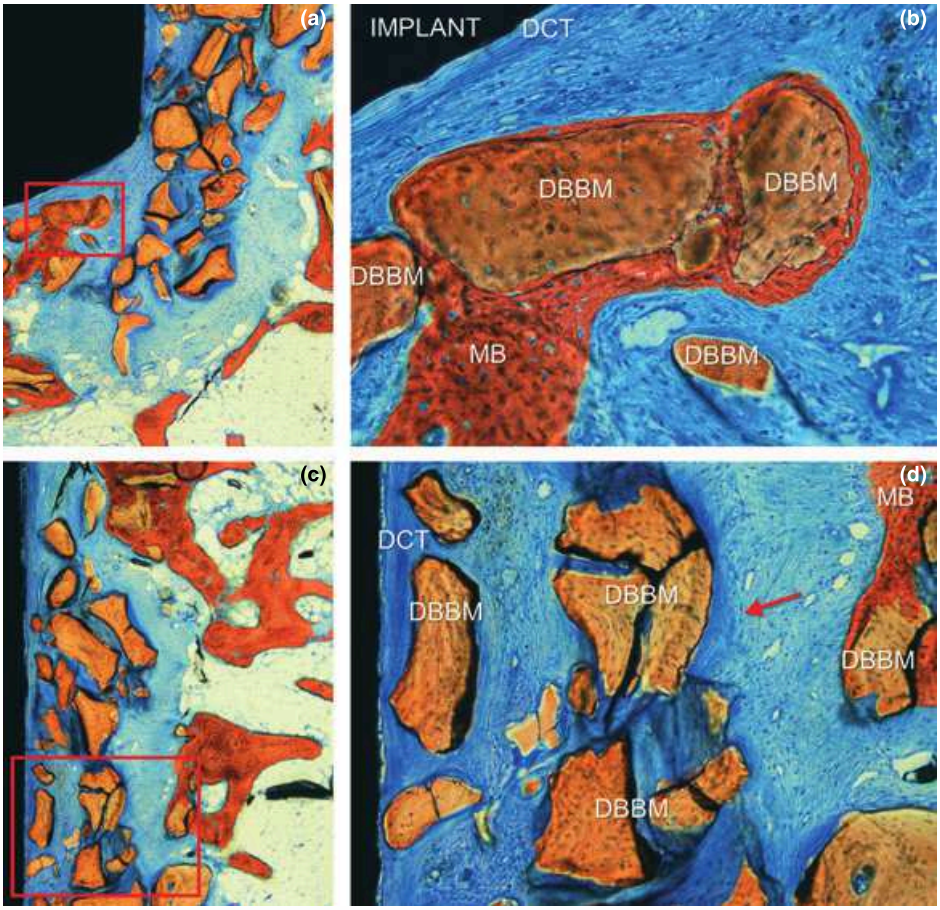

Fig. 4.7. Details of a test implant. DCT, dense connective tissue; DBBM, deproteinized bovine bone matrix; MB, min- eralized bone. (a) DBBM particles reside laterally to the implant without any contact with the implant surface. Mag- nification 940. Inset: (b) Larger magnification (9200). Only few DBBM particles are embedded in mature bone without any evidence of MBIC. DCT lines the implant surface. (c) Magnification 940. Inset: (d) DBBM particles sur- rounded by connective tissue and separated from the implant surface only by a ~0.1 mm of DCT layer. The arrow indicates a dense connective tissue lining the graft surface. Magnification 9100.

$n = 6$	Mineralized bone	Bone marrow*	Connective tissue	DBBM in bone	DBBM in connective tissue
CTRL					
Mean (SD)	35.9 (16.8)	37.2 (12.8)	26.8 (4.1)	–	–
Min; Max	20.3; 66.9	13.3; 48.3	19.8; 31.4	–	–
TEST (DBBM)					
Mean (SD)	20.5 (8.6)	12.9 (9.9)	32.0 (11.8)	13.0 (11.1)	21.6 (16.0)
Min; Max	10.4; 32.0	2.7; 30.7	9.9; 41.4	2.4; 27.4	0.0; 37.8

Mean values, standard deviations (SD) and range (minimum; maximum). DBBM, deproteinized bovine bone mineral.
*$P < 0.05$ between test and control.

Table 4.2. Morphometric measurements within the original dimensions of the defects (1.2 mm). Data expressed in percentage (%)

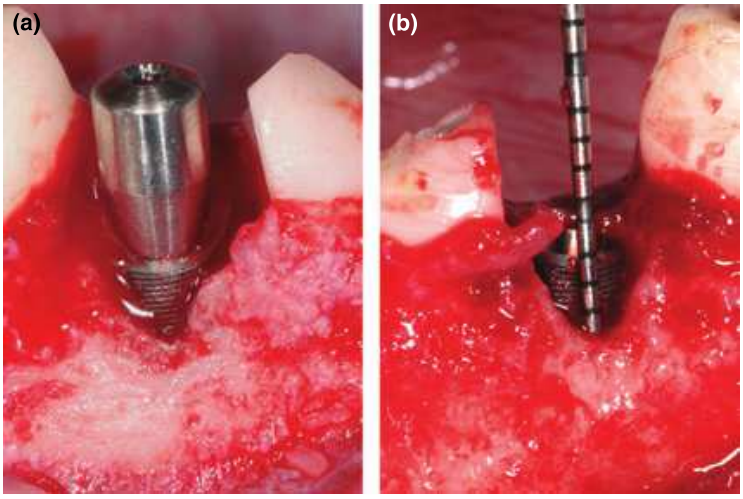

Fig. 5.1. Buccal clinical view of the implants within the distal extraction sockets of the fourth mandibular premolar. A standardized triangular-shaped buccal dehiscence defect, about 12 micro-threads deep (corresponding to about 2.7 mm) and 3.5 mm wide (like the diameter of the implant), was prepared in the coronal region. (a) Implant installed in a buccal position (test site). (b) Implant installed in a lingual position (control site).

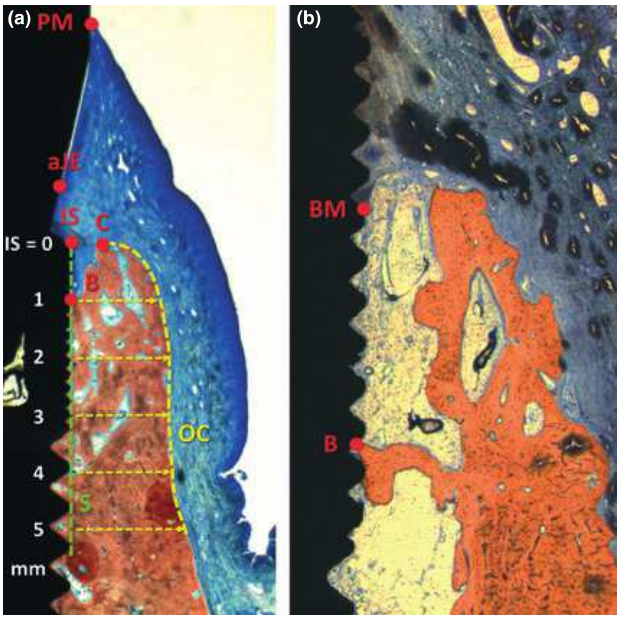

Fig. 5.2. Diagrams depicting the landmarks for the histological evaluation. (a) PM, top of peri-implant mucosa; aJE, apical extension of the junctional epithelium; IS, shoulder of the implant; C, top of the adjacent bony crest; B, coro- nal end of osseointegration. S, implant surface at the top of the threads (dotted green line); OC, outer contour of the alveolar bony ridge (dotted yellow line). (b) BM, coronal extension of the bone-marrow-like tissue; B, coronal end of osseointegration. The measurements performed are reported in the text.

	Coronal diameter		Depth		Width at 1 mm		Width at 3 mm	
	Mesio-distal	Bucco-lingual	Buccal	Lingual	Buccal	Lingual	Buccal	Lingual
Test (buccal positioning)	5.6 (0.5)	4.8 (0.4)	13.7 (1.0)	14.5 (0.9)	0.8 (0.3)	1.3 (0.5)	1.5 (0.3)	2.2 (0.5)
Control (lingual positioning)	5.3 (0.9)	4.9 (0.4)	13.3 (1.4)	14.3 (1.3)	0.7 (0.3)	1.3 (0.6)	1.5 (0.5)	2.5 (0.8)

Mean values and standard deviations (SD) in millimeters.
No statistically significant differences ($P < 0.05$ between test and control) were found for any of the variables.

Table 5.1. Coronal diameter and depth of extraction sockets and width of the buccal and lingual bony walls at 1 and 3 mm apically to the alveolar bony crest

	Coronal diameter		Depth		Width at 1 mm		Width at 3 mm	
	Mesio-distal	Bucco-lingual	Buccal	Lingual	Buccal	Lingual	Buccal	Lingual
Test (buccal positioning)	5.6 (0.5)	4.8 (0.4)	13.7 (1.0)	14.5 (0.9)	0.8 (0.3)	1.3 (0.5)	1.5 (0.3)	2.2 (0.5)
Control (lingual positioning)	5.3 (0.9)	4.9 (0.4)	13.3 (1.4)	14.3 (1.3)	0.7 (0.3)	1.3 (0.6)	1.5 (0.5)	2.5 (0.8)

Mean values and standard deviations (SD) in millimeters.
No statistically significant differences ($P < 0.05$ between test and control) were found for any of the variables.

Table 5.2. Histological measurements of the hard tissue dimensions after 4 months of healing

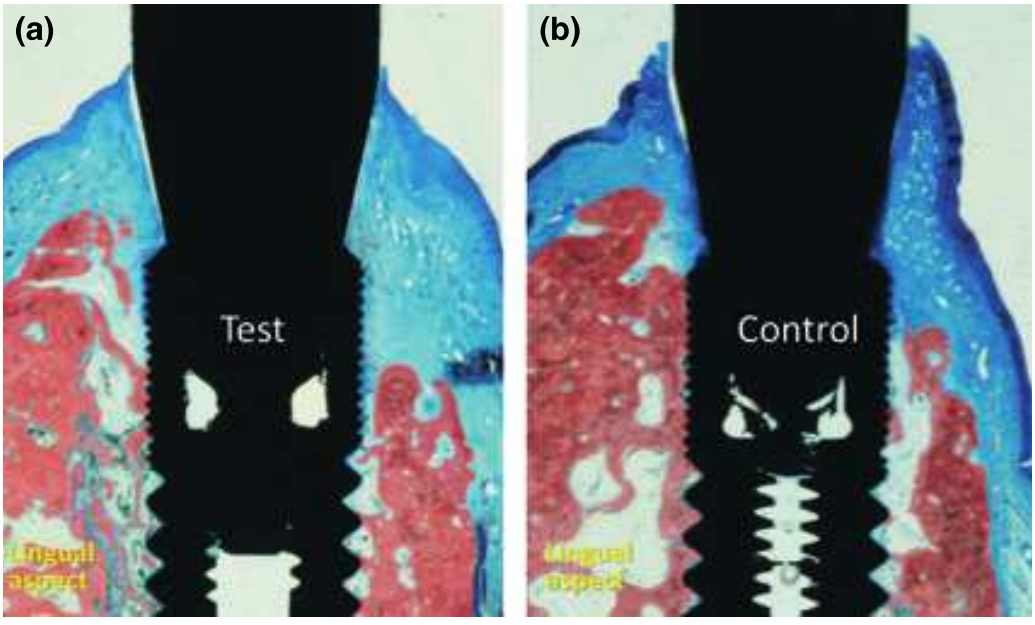

Fig. 5.3. Ground sections illustrating the healing after 4 months at the test (a) and control (b) sites. Stevenel's blue and alizarin red. The implants appeared to be well integrated into mature bone. The buccal bony crest was more apically located at the implant placed more buccally (a, test) compared with that placed more lingually (b, control).

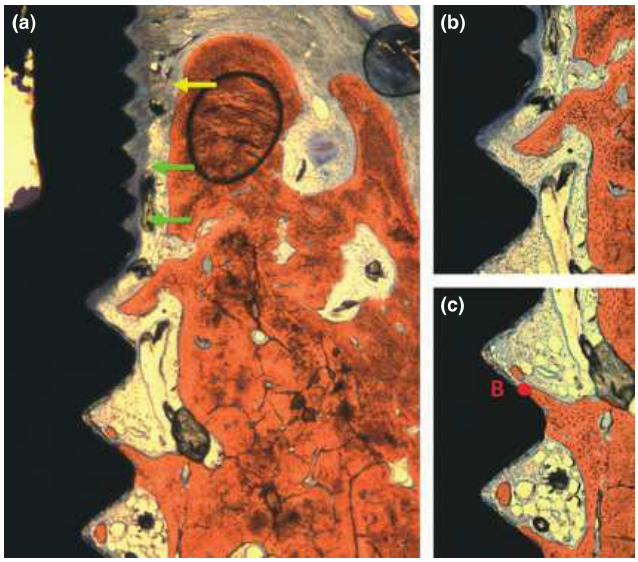

Fig. 5.4. Ground section illustrating a remaining defect. Stevenel's blue and alizarin red. (a) A soft tissue, similar to bone marrow, was often found occupying the apical portion of the defects and in close contact with the implant sur- face. This bone-marrow-like tissue was delimited in the coronal region by the peri-implant soft tissue (yellow arrow). In some specimens, in the coronal region of the defects, a layer of dense connective tissue was found inter- posed between the bone-marrow-like tissue and the implant surface (green arrows). Original magnification 940. (b) Larger magnification of the image in (a) at the level of the dense connective tissue layer. Original magnification 9100. (c) Larger magnification of the image in (a) showing the similarity of the two soft tissues located above or below the coronal end of osseointegration (reference point B). Original magnification 9100.

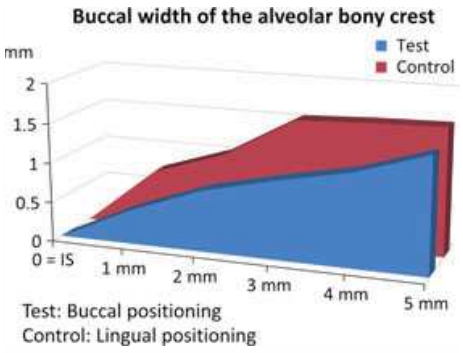

Fig. 5.5. Graphic representing the mean values of S-OC0–5 at the test and control sites after 4 months of healing. A wider width of the bony ridge at the buccal aspect was found at the control than at the test sites. No sta- tistically significant differences were, however, found at any of the levels evaluated.

	PM-C		PM-B		PM-IS	
	b	l	b	l	b	l
Test (buccal)						
Mean (SD)	4.27 (0.39)	2.60 (0.45)	5.05 (1.02)	4.69 (1.20)	2.56 (1.15)	3.00 (0.66)
Percentiles						
25th	4.04	2.40	4.47	3.97	2.35	3.00
50th	4.18	2.62	4.82	4.56	2.94	3.23
75th	4.58	2.84	4.99	5.71	3.30	3.32
Control (lingual positioning)						
Mean (SD)	4.10 (1.00)	3.00 (1.04)	5.11 (1.55)	4.01 (0.68)	3.41 (0.82)	3.53 (0.39)
Percentiles						
25th	3.83	2.43	4.13	3.60	3.04	3.28
50th	4.07	2.96	5.12	3.84	3.77	3.50
75th	4.54	3.54	5.87	4.29	3.87	3.72

Mean values, standard deviations (SD) and 25th, 50th (median) and 75th percentiles in millimeters. PM, peri-implant mucosa; C, top of the bony crest; B, coronal end of osseointegration ; IS, implant shoulder; b, buccal aspect; l, lingual aspect.
$P < 0.05$ between test and control.

Table 5.3. Histological measurements of soft tissue dimensions after 4 months of healing

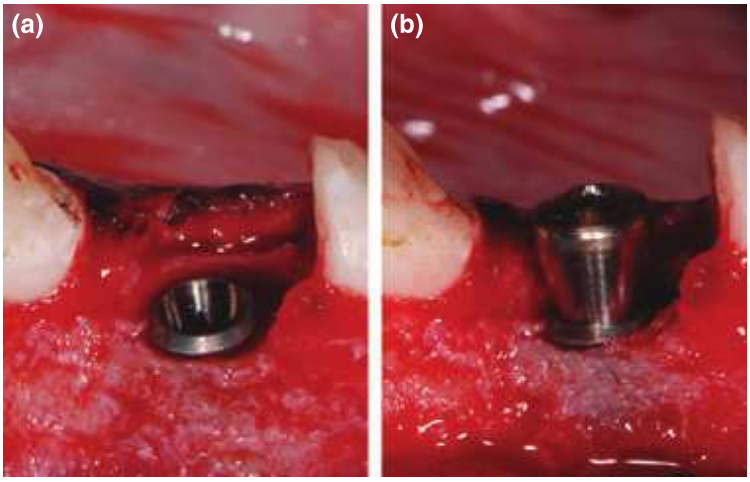

Fig. 6.1. Clinical illustration of the implant positioning. (a) The implant was placed in the center of the alveolus, with the margin of the rough surface placed at the same level of the alveolar buccal bony crest. (b) A healing abut- ment was affixed to the implant.

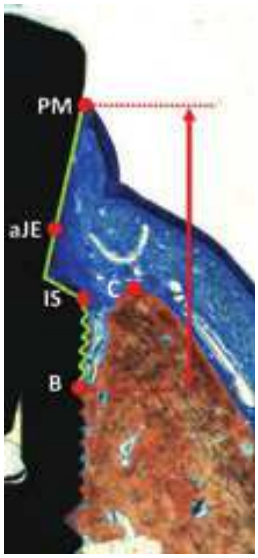

Fig. 6.2. The following landmarks were identified (red circles): the implant shoulder (IS), the most coronal bone-to-implant contact (B), the top of the adjacent bony crest (C), the top of peri-implant mucosa (PM), the apical portion of the barrier (junctional) epithelium (aJE). The red arrow indicates how the vertical measure- ments were performed, parallel to the long axis of the implant (in the example the distance PM-B). The green line indicates the location of the linear measurements made on the surface of the abutment/implant unit.

	Coronal diameter		Depth		Width at 1 mm		Width at 3 mm	
	Mesio-distal	Bucco-lingual	Buccal	Lingual	Buccal	Lingual	Buccal	Lingual
Test	4.8 (0.7)	4.2 (0.3)	11.2 (0.9)	11.8 (1.0)	0.4 (0.3)*	1.3 (0.6)	0.8 (0.5)*	2.5 (0.8)
Control	5.3 (0.9)	4.8 (0.8)	11.6 (1.7)	12.4 (1.8)	0.6 (0.3)	1.1 (0.5)	1.4 (0.4)	1.8 (0.7)

Mean values and standard deviations (SD) in mm.
*$P < 0.05$ between test and control.

Table 6.1. Coronal diameter and depth of extraction sockets and width of the buccal and lingual bony walls at 1 and 3 mm apically to the alveolar bony crest

	IS-C clinical		GAP clinical	
	Buccal	Lingual	Buccal	Lingual
TEST	0.0	−0.6 (0.5)	0.0 (0.0)	0.1 (0.2)
CONTROL	0.0	−0.6 (0.9)	0.3 (0.4)	0.3 (0.4)

Mean values and standard deviations (SD) in mm.

Table 6.2. Clinical measurement after implant installation

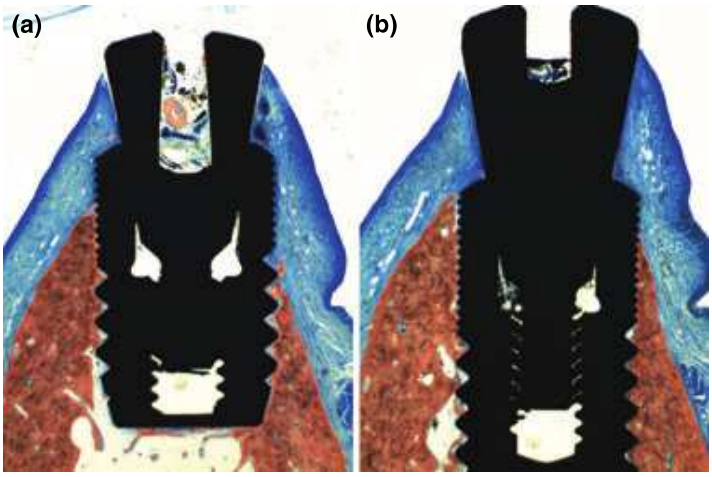

Fig. 6.3. The implants appeared to be well integrated into mature bone. Stevenel's blue and alizarin red stain. Original magnification 916. A higher loss of the buccal alveolar bony crest was observed at the test (a) compared with the control sites (b).

	IS-B		IS-C		GAP		BIC%	
	b	l	b	l	b	l	Total	Apical
Test								
Mean (SD)	2.60 (1.30)	1.07 (0.84)	2.02 (1.44)	0.37 (0.71)	0.11 (0.21)	0.44 (0.66)	54.4 (14.2)	33.1 (26.6)
Percentiles								
25th	1.45	0.50	0.88	−0.05	0.00	0.12	44.2	13.4
50th	2.92	1.12	1.60	0.63	0.01	0.19	51.6	32.2
75th	3.69	1.65	3.30	0.93	0.09	0.35	62.5	52.5
Control								
Mean (SD)	1.67 (1.02)	0.84 (0.65)	1.21 (1.13)	0.21 (0.83)	0.23 (0.34)	0.42 (0.47)	49.0 (20.2)	20.9 (16.6)
Percentiles								
25th	1.02	0.69	0.68	−0.12	0.00	0.17	37.0	14.3
50th	1.79	0.81	1.23	0.22	0.03	0.19	51.2	17.9
75th	2.27	1.04	1.86	0.45	0.43	0.50	63.2	24.2

Mean values, standard deviations (SD) and 25th, 50th (median) and 75th percentiles. b, buccal; l, lingual; IS, implant shoulder; B, coronal end of osseointegration; C, top of alveolar bony crest; S, implant surface; PM, top of the peri-implant mucosa; aJE, apical portion of the junctional epithelium; BIC, bone-to-implant contact.
$P < 0.05$ between test and control.

Table 6.3. Histological measurements of the hard tissue after 4 months of healing

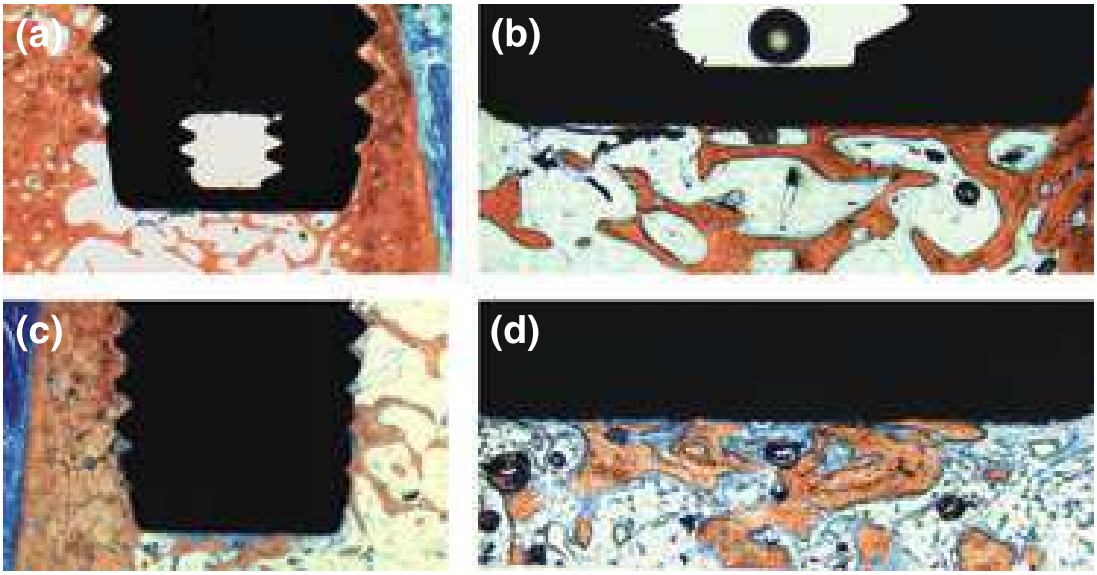

Fig. 6.4. The apical region of the implants presented newly formed bone attached to the surface, both at the test and control sites. Stevenel's blue and alizarin red stain. (a) Apical portion of a test implant (short). Original magnifica- tion about 916. (b) Larger magnification of the apical region (originally 940). (c) Apical portion of a control implant (long). Original magnification about 916. (b) Larger magnification of the apical region (originally 940).

	Vertical no.						Surface no.					
	PM-B		PM-aJE		aJE-B		PM-B		PM-aJE		aJE-B	
	b	l	b	l	b	l	b	l	b	l	b	l
Test												
Mean (SD)	4.97 (1.12)	3.30 (0.69)	2.19 (0.76)	1.68 (0.68)	2.78 (1.02)	1.62 (0.41)	6.48 (1.56)	4.17 (1.05)	2.52 (1.04)	1.88 (0.85)	3.96 (1.54)	2.29 (0.61)
Percentiles												
25th	4.28	2.92	1.62	1.14	2.25	1.30	5.71	3.57	1.78	1.20	3.05	1.81
50th	4.59	3.42	2.14	1.62	2.74	1.79	5.88	4.07	2.35	1.71	3.81	2.32
75th	5.62	3.82	2.77	1.96	3.47	1.84	7.42	4.87	3.20	2.25	5.20	2.51
Control												
Mean (SD)	4.75 (1.10)	3.37 (0.51)	2.39 (0.61)	2.02 (0.54)	2.36 (0.68)	1.35 (0.38)	5.85 (1.44)	4.15 (0.69)	2.62 (0.75)	2.23 (0.79)	3.24 (1.06)	1.92 (0.65)
Percentiles												
25th	4.12	2.95	2.00	1.65	1.91	1.16	4.95	3.65	2.06	1.82	2.50	1.51
50th	4.40	3.55	2.48	1.87	2.29	1.44	5.50	4.39	2.70	1.92	3.14	2.12
75th	5.59	3.67	2.83	2.26	2.96	1.61	7.08	4.64	3.22	2.34	4.20	2.36

Mean values, standard deviations (SD) and 25th, 50th (median) and 75th percentiles. b, buccal; l, lingual; IS, implant shoulder; B, coronal end of osseointegration; C, top of alveolar bony crest; S, implant surface; PM, top of the peri-implant mucosa; aJE, apical portion of the junctional epithelium; BIC, bone-to-implant contact.
$P < 0.05$. No differences statistically significant were found between test and control for any of the variables evaluated.
All differences between vertical and surface measurements were statistically significant ($^{\#}P < 0.05$)

Table 6.4. Histological measurements of the soft tissue after 4 months of healing

Type of Prosthesis	No. of Prostheses*	No. of Supporting Short Implants†
ST	30	30
FPD	7 (4)	20 (12)
FFD	98 (98)	223 (167)
Total	135 (102)	273 (179)

Table 7.1. Prostheses and Short Implants Distributed by Type of Prosthesis.
* Numbers in parentheses indicate prostheses supported by both short and standard implants.
†Numbers in parentheses indicate short implants splinted to longer implants. Unloaded implants (seven) were excluded.

	280 Implants			
	Length (mm)			
	7		8.5	
Diameter (mm)	R	M	R	M
3.75	0	96	65	24
4	0	43	39	13

Table 7. 2 Implant Distribution by Length, Diameter, and Surface Treatment.
M = machined; R = rough.

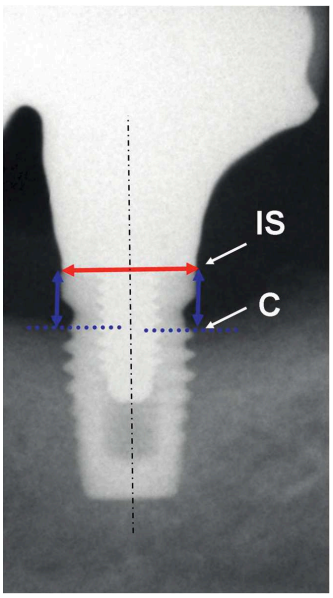

Fig. 7.1. A standardized measurement protocol was used, and the reference measurement was the implant neck diameter, i.e., 3.75 or 4 mm. The measurement system considered the perpendicular distance from the implant shoulder (IS) to the first visible bone-to-implant contact (C) along an ideal line running parallel to the longitudinal axis of the fixture. Measurements were taken on the mesial and distal sides of each implant.

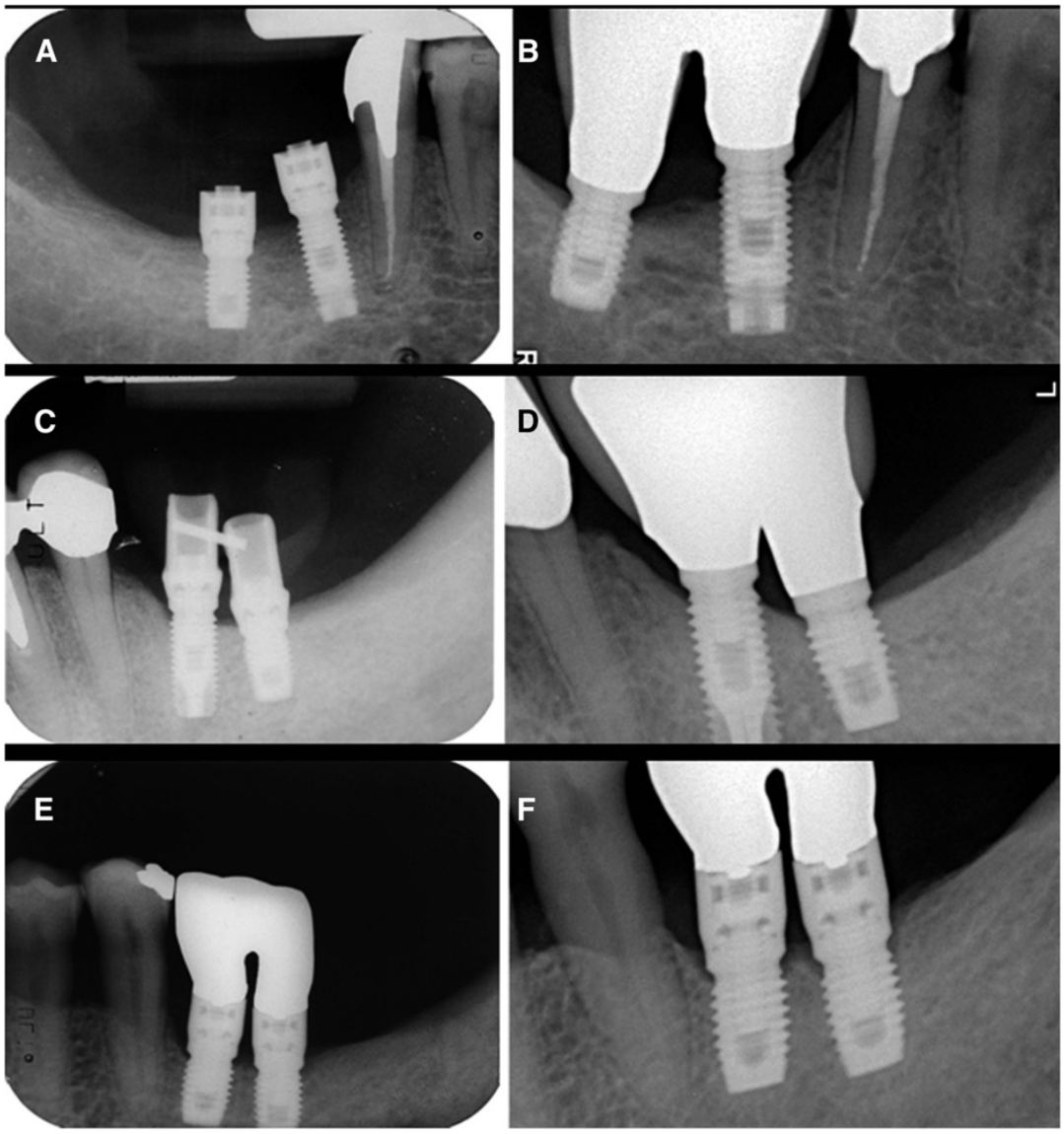

Fig. 7.2. A and B) Standard M, threaded, 3.75 · 7–mm implant in site 31. A) Intraoral radiograph taken
at time of loading (1997). B) Intraoral radiograph taken at the latest follow-up (2010). The short implant was splinted to a standard M, 3.75 · 10.5–mm implant (in site 30). C and D) Standard M, 4 · 7–mm implant in site 19. C) Intraoral radiograph taken at time of loading (1997). D) Intraoral radiograph taken at the latest follow-up (2008). The short implant was splinted to a 4 · 10–mm implant (site 18). E and F) Two standard M, 4 · 7–mm implants in sites 18 and 19. E) Radiograph taken at time of loading (1997). F) Radiograph taken at the latest follow-up (2008).

Site*	Bone Quality[29]	Implant Dimensions (diameter × length, mm)	Implant Surface	Cause	Timing (Months)	Type of Prosthesis (if Loaded)
Left second premolar	II-D	3.75 × 7	M	Pathologic peri-implant bone resorption	50	FFD
Right second molar	IV-D	4 × 7	M	Unstable	12	—
Left second premolar	II-C	3.75 × 8.5	R	Unstable	1	—
Left first molar	III-B	3.75 × 8.5	R	Pathologic peri-implant bone resorption	39	FFD
Right first molar	III-B	4 × 8.5	R	Pathologic peri-implant bone resorption	56	FFD
Right second premolar	II-C	3.75 × 7	M	Unstable	7	—
Left second premolar	III-B	3.75 × 8.5	R	Pathologic peri-implant bone resorption	58	FFD
Left second premolar	III-B	4 × 7	M	Pathologic peri-implant bone resorption	56	FFD
Right first molar	II-C	3.75 × 7	M	Unstable	4	—
Left second premolar	II-B	3.75 × 7	M	Unstable	1	—
Right first molar	II-B	4 × 7	M	Unstable	4	—
Right first molar	III-B	4 × 7	M	Pathologic peri-implant bone resorption	90	FFD
Right first molar	II-C	4 × 7	M	Unstable	2	—
Right first molar	II-B	3.75 × 8.5	R	Pathologic peri-implant bone resorption	72	FFD
Left first molar	III-B	3.75 × 7	M	Pathologic peri-implant bone resorption	136	FFD

Table 7.3. Implant Complications and Failures After Prosthetic Loading

Variable	*P* value (α = 0.05)
Implant length	0.7
Implant diameter	0.41
Surface treatment	0.8

Table 4.

Multilevel Model With MBL as the Dependant Variable

Bone Loss	M	R	All
Mesial	1.41 ± 0.4	1.34 ± 0.58	1.38 ± 0.45
Distal	1.36 ± 0.42	1.35 ± 0.57	1.36 ± 0.5
All	1.39 ± 0.4	1.34 ± 0.58	1.37 ± 0.5

Table 7.5. Mean – SD MBL (in mm) by Surface Treatment. M= machined; R= rough.

Interval (years)	Implants at Baseline	Early Failures	Loaded Implants	Dropouts	Implants at Risk	Survivors During Interval	Failures During Interval	SR (%)	SSR (%)	Cumulative SR (%)	Cumulative SSR (%)
Success of M short implants											
0 to 2	176	6	170	0	170	0		96.2		96.2	
2 to 4	170	0	170	0	170	1		99.5		95.7	
4 to 6	160	0	160	0	160	2		98.8		94.5	
6 to 8	158	0	158	3	156.5	0		100		94.5	
8 to 10	146	0	146	4	144	0		100		94.5	
10 to 12	138	0	138	0	138	1		99.3		93.9	
12 to 14	118	0	118	6	115	0		100		93.9	
14 to 16	85	0	85	11	79.5	0		100		93.9	
Survival of M short implants											
0 to 2	176	6	170	0	170		0		96.2		96.2
2 to 4	170	0	170	0	170		0		100		96.2
4 to 6	161	0	161	0	161		2		98.8		95.7
6 to 8	159	0	159	3	157.5		0		100		95.7
8 to 10	147	0	147	4	145		0		100		95.7
10 to 12	139	0	139	0	139		0		100		95.7
12 to 14	120	0	120	6	117		0		100		95.7
14 to 16	87	0	87	11	81.5		0		100		95.7
Success of R short implants											
0 to 2	104	1	103	0	103	0		99.1		99.1	
2 to 4	103	0	103	0	103	0		100		99.1	
4 to 6	103	0	103	1	102.5	3		97.1		96.2	
6 to 8	93	0	93	0	93	1		99		95.2	
8 to 10	81	0	81	0	81	0		100		95.2	
10 to 12	78	0	78	7	74.5	0		100		95.2	
12 to 14	51	0	51	2	50	0		100		95.2	
14 to 16	29	0	29	4	27	0		100		95.2	
Survival of R short implants											
0 to 2	104	1	103	0	103		0		99.1		99.1
2 to 4	103	0	103	0	103		0		100		99.1
4 to 6	103	0	103	1	102.5		2		98.1		97.2
6 to 8	94	0	94	0	94		0		100		97.2
8 to 10	83	0	83	0	83		0		100		97.2
10 to 12	80	0	80	7	76.5		0		100		97.2
12 to 14	53	0	53	2	52		0		100		97.2
14 to 16	31	0	31	4	29		0		100		97.2

Table 7.6. Short Implant Life Tables

APPENDIX 2 – List of publications related to the thesis

1: Sivolella S, Bressan E, Salata LA, Quiñones ME, Lang NP, Botticelli D. Deproteinized bovine bone mineral particles and osseointegration of implants without primary bone contact: an experimental study in dogs. Clin Oral Implants Res. 2014 Mar;25(3):296-303.

2: Bressan E, Carraro A, Ferroni L, Gardin C, Sbricoli L, Guazzo R, Stellini E,Roman M, Pinton P, Sivolella S, Zavan B. Nanotechnology to drive stem cell commitment. Nanomedicine (Lond). 2013 Mar;8(3):469-86.

3: Gardin C, Ferroni L, Favero L, Stellini E, Stomaci D, Sivolella S, Bressan E, Zavan B. Nanostructured biomaterials for tissue engineered bone tissue reconstruction. Int. J. Mol. Sci. 2012, 13, 737-757.

4: Bressan E, Sbricoli L, Guazzo R, Tocco I, Roman M, Vindigni V, Stellini E, Gardin C, Ferroni L, Sivolella S, Zavan B. Nanostructured surfaces of dental implants. Int J Mol Sci. 2013 Jan 17;14(1):1918-31.

5: Brun P, Scorzeto M, Vassanelli S, Castagliuolo I, Palù G, Ghezzo F, Messina GM, Iucci G, Battaglia V, Sivolella S, Bagno A, Polzonetti G, Marletta G, Dettin M. Mechanisms underlying the attachment and spreading of human osteoblasts: from transient interactions to focal adhesions on vitronectin-grafted bioactivesurfaces. Acta Biomater. 2013 Apr;9(4):6105-15.

6: Bressan E, Ferroni L, Gardin C, Pinton P, Stellini E, Botticelli D, Sivolella S, Zavan B. Donor age-related biological properties of human dental pulp stem cells change in nanostructured scaffolds. PLoS One. 2012;7(11):e49146.

7: Casadei A, Epis R, Ferroni L, Tocco I, Gardin C, Bressan E, Sivolella S, Vindigni V, Pinton P, Mucci G, Zavan B. Adipose tissue regeneration: a state of the art. J Biomed Biotechnol. 2012;2012:462543.

8: Bressan E, Sivolella S, Stellini E, Almagro Urrutia Z, Lang NP, Botticelli D. Healing of buccal dehiscence defects at implants installed immediately into extraction sockets an experimental study in dogs. Clin Oral Implants Res. 2013 Mar;24(3):270-7.

9: Sivolella S, Stellini E, Testori T, Di Fiore A, Berengo M, Lops D. Splinted and unsplinted short implants in mandibles: a retrospective evaluation with 5 to 16 years of follow-up. J Periodontol. 2013 Apr;84(4):502-12.

10: Sivolella S, Bressan E, Salata LA, Urrutia ZA, Lang NP, Botticelli D. Osteogenesis at implants without primary bone contact an experimental study in dogs. Clin Oral Implants Res. 2012 May;23(5):542-9.

11: Bressan E, Sivolella S, Urrutia ZA, Salata LA, Lang NP, Botticelli D. Short implants (6 mm) installed immediately into extraction sockets: an experimentalstudy in dogs. Clin Oral Implants Res. 2012 May;23(5):536-41.

12: Bressan E, Tomasi C, Stellini E, Sivolella S, Favero G, Berglundh T. Implant-supported mandibular overdentures: a cross-sectional study. Clin Oral Implants Res. 2012 Jul;23(7):814-9.

13: Gardin C, Bressan E, Ferroni L, Nalesso E, Vindigni V, Stellini E, Pinton P, Sivolella S, Zavan B. In vitro concurrent endothelial and osteogenic commitment of adipose-derived stem cells and their genomical analyses through comparative genomic hybridization array: novel strategies to increase the successful engraftment of tissue-engineered bone grafts. Stem Cells Dev. 2012 Mar 20;21(5):767-77.

APPENDIX 3 DICHIARAZIONE DI CONFORMITÀ

UNIFE

DOTTORATI DI RICERCA

Il tuo indirizzo e-mail: stefano.sivolella@libero.it
Oggetto: Dichiarazione di conformità della tesi di Dottorato
Io sottoscritto Dott. (Cognome e Nome) SIVOLELLA STEFANO
Nato a: PADOVA
Provincia: PADOVA
Il giorno: 27/01/1971
Avendo frequentato il Dottorato di Ricerca in: FARMACOLOGIA E ONCOLOGIA MOLECOLARE
Ciclo di Dottorato 26
Titolo della tesi: Dental implants osseointegration: in vitro, preclinical and clinical research results.
Titolo della tesi (traduzione): Osteointegrazione degli impianti dentali: risultati della ricerca in vitro, preclinica e clinica.
Tutore: Prof. (Cognome e Nome) Rimessi Alessandro
Settore Scientifico Disciplinare (S.S.D.) MED/04
Parole chiave della tesi (max 10): dental implant; osseointegration

Consapevole, dichiara
CONSAPEVOLE: (1) del fatto che in caso di dichiarazioni mendaci, oltre alle sanzioni previste dal codice penale e dalle Leggi speciali per l'ipotesi di falsità in atti ed uso di atti falsi, decade fin dall'inizio e senza necessità di alcuna formalità dai benefici conseguenti al provvedimento emanato sulla base di tali dichiarazioni; (2) dell'obbligo per l'Università di provvedere al deposito di legge delle tesi di dottorato al fine di assicurarne la conservazione e la consultabilità da parte di terzi; (3) della procedura adottata dall'Università di Ferrara ove si richiede che la tesi sia consegnata dal dottorando in 2 copie di cui una in formato cartaceo e una in formato pdf non modificabile su idonei supporti (CD-ROM, DVD) secondo le istruzioni pubblicate sul sito: http://www.unife.it/studenti/dottorato alla voce ESAME FINALE – disposizioni e modulistica; (4) del fatto che l'Università, sulla base dei dati forniti, archivierà e renderà consultabile in rete il testo completo della tesi di dottorato di cui alla presente dichiarazione attraverso l'Archivio istituzionale ad accesso aperto "EPRINTS.unife.it" oltre che attraverso i Cataloghi delle Biblioteche Nazionali Centrali di Roma e Firenze; DICHIARO SOTTO LA MIA RESPONSABILITA': (1) che la copia della tesi depositata presso l'Università di Ferrara in formato cartaceo è del tutto identica a quella presentata in formato elettronico (CD-ROM, DVD), a quelle da inviare ai Commissari di esame finale e alla copia che produrrò in seduta d'esame finale. Di conseguenza va esclusa qualsiasi responsabilità dell'Ateneo stesso per quanto riguarda eventuali errori, imprecisioni o omissioni nei contenuti della tesi; (2) di prendere atto che la tesi in formato cartaceo è l'unica alla quale farà riferimento l'Università per rilasciare, a mia richiesta, la dichiarazione di conformità di eventuali copie; (3) che il contenuto e l'organizzazione della tesi è opera originale da me realizzata e non compromette in alcun modo i diritti di terzi, ivi compresi quelli relativi alla sicurezza dei dati personali; che pertanto l'Università è in ogni caso esente da responsabilità di qualsivoglia natura civile, amministrativa o penale e sarà da me tenuta indenne da qualsiasi richiesta o rivendicazione da parte di terzi; (4) che la tesi di dottorato non è il risultato di attività rientranti nella normativa sulla proprietà industriale, non è stata prodotta nell'ambito di progetti finanziati da soggetti pubblici o privati con vincoli alla divulgazione dei risultati, non è oggetto di eventuali registrazioni di tipo brevettale o di tutela.

PER ACCETTAZIONE DI QUANTO SOPRA RIPORTATO

Ferrara, li 19/01/2015

Firma del Dottorando _____

Visto: Il Tutore Si approva
Firma del Tutore _____